

QUANTUM EFFECTIVE FIELD THEORIES  
IN HEAVY QUARK PHYSICS  
AND PHASE TRANSITIONS IN COSMOLOGY

Thesis by  
Clarence L. Y. Lee

In Partial Fulfillment of the Requirements  
for the Degree of  
Doctor of Philosophy

California Institute of Technology  
Pasadena, California

1994  
(Submitted May 24, 1994)

## Acknowledgements

It is a privilege and an honor to have undertaken advanced scientific training at an academic institution of higher learning with the eminence of Caltech. The excellence of its research faculty and facilities, the informal atmosphere and pleasant setting fostered in part by its small size, are conducive to productive scholarship.

Over the course of my graduate studies, there a number of people from whom I have benefitted. It is a great pleasure and yet a rather difficult task to thank appropriately all of these people. Since an attempt to acknowledge them one-by-one is likely to result in some unintentional omissions, I would like to take this opportunity to thank them all including those not listed explicitly herein. However, I would also like to point out some individuals who have a particularly important role in my development.

I would like to begin by expressing my gratitude to my advisor, Prof. Mark Wise, for his advice, instruction and insight in physics. His enthusiasm and dedication to research provides a model to be emulated. Prof. John Preskill has provided enlightenment over an incredibly broad range of topics, and especially on quantum field theory. His approach to physics as exemplified by his verbal and written exposition form a standard for clarity of thought and deep intellect. I am also grateful for fruitful interactions with the other outstanding faculty, post-doctoral fellows and, of course, fellow graduate students.

Finally, my fondest thanks go to my family. My siblings provided encouragement. To my parents, I am indebted for their support and sacrifice over the years. It is especially difficult to adequately thank my mother for nurturing my childhood thirst for knowledge to the point that I would eventually pursue doctoral studies in physics at one of the world's finest institution. I am truly saddened that she did not live to see the completion of this thesis, and I dedicate this thesis to her memory.

**Dedicated to the memory of my mother**

## Abstract

This thesis is concerned with aspects of quantum effective field theories, effective actions, and their applications. New spin-flavor symmetries of the strong interactions, which arise in the limit of very large quark masses, can be incorporated into a heavy quark effective field theory (HQEFT). A general method for deriving the effective Lagrangian of this theory to any order in  $1/m_Q$  (where  $m_Q$  is the heavy quark mass) is developed; it is used to calculate terms up to order  $1/m_Q^3$ . The renormalization of terms in the Lagrangian to order  $1/m_Q^2$  is performed. Such operators break these new symmetries and consequently are important corrections to the leading-order predictions. HQEFT can be combined with chiral perturbation theory into a heavy meson chiral perturbation theory (HMChPT) which describes the low-momentum interactions of hadrons containing a heavy quark with pseudo-Goldstone bosons. HMChPT is used to investigate the semi-leptonic four-body decay of  $B$  and  $D$  mesons into final states with at least one Goldstone boson. Such processes may be utilized to test the above heavy quark symmetries. The remainder of this dissertation deals with the evaluation of effective actions and their implications. A method to efficiently compute the one-loop effective action at zero and finite temperatures is elucidated. In a first order cosmological phase transition, the decay rate and the temperature at which it occurs depends on the free energy of a critical bubble configuration. Since this free energy is related to the effective action but is usually approximated with an effective potential, the calculational method developed above is used to study the validity of of this approximation. The corrections are found to be important for quantitative work.

## Table of Contents

<b>Acknowledgments</b> .....	ii
<b>Dedication</b> .....	iii
<b>Abstract</b> .....	iv
<b>Table of Contents</b> .....	v
<b>1. Introduction</b> .....	1
<b>2. Heavy Quark Effective Field Theory</b> .....	6
2.1 New Symmetries in the Strong Interactions of Heavy Quarks .....	6
2.2 Derivation of the Heavy Quark Effective Field Theory Lagrangian .....	8
2.3 Derivation of the HQEFT Feynman Rules .....	13
2.4 Applications of the HQEFT .....	13
2.5 Renormalization in the HQEFT .....	16
2.6 Renormalization of the Operators in the Sub-Leading Terms of the HQEFT Lagrangian .....	18
<b>3. Heavy Quark Symmetry and Chiral Perturbation Theory</b> .....	35
3.1 Chiral Perturbation Theory .....	35
3.2 Heavy Meson Chiral Perturbation Theory .....	36
3.3 Review of the Kinematics .....	39
3.4 Decays to Two Pseudo-Goldstone Bosons .....	43
3.5 $B \rightarrow D\pi\ell\bar{\nu}_\ell$ Decay .....	46
3.6 Validity of Chiral Perturbation Theory .....	51
3.7 Concluding Remarks .....	52
<b>4. Heavy Meson Chiral Perturbation Theory and <math>B \rightarrow D^*X\ell\bar{\nu}_\ell</math></b> .....	54
4.1 Introduction .....	54
4.2 Kinematical Analysis .....	54
4.3 $B \rightarrow D^*X\ell\bar{\nu}_\ell$ Decay .....	60
4.4 Concluding Remarks .....	65
<b>5. One-loop Effective Action at Zero and Finite Temperature</b> .....	66
5.1 Introduction .....	66

5.2 Method of Computation .....	69
5.3 Application and Discussion .....	76
<b>6. Effective Actions and Potentials in First-Order Phase Transitions</b> .....	<b>77</b>
6.1 Introduction .....	77
6.2 The One-Dimensional Kink .....	88
6.3 The Thin-Wall Critical Bubble .....	84
6.4 Thick Wall Critical Bubbles .....	86
6.5 Conclusions: A New Prefactor, and Derivative Corrections .....	88
<b>Appendix A: Calculation of Loop Momentum Integrals in HQEFT</b> .....	<b>90</b>
<b>Appendix B: One-loop Renormalization of the Scalar Field Theory</b> .....	<b>91</b>
<b>References</b> .....	<b>93</b>

## 1. INTRODUCTION

The formulation of the theory of relativity and quantum theory has revolutionized theoretical physics in the twentieth century. The theory of general relativity has been an amazingly successful description of gravitation and astrophysical processes that take place over large scales. On the other hand, the synthesis of the principles of special relativity and quantum theory gave rise to relativistic quantum field theories. Subsequent investigations of quantum field theories have led to a much more profound understanding of microscopic processes and has culminated in a theory known as the standard model of elementary particle physics. The standard model encompasses all known non-gravitational interactions in a quantum field theoretic framework which incorporates gauge symmetry: the strong interactions are described by the theory of quantum chromodynamics (QCD) based on the  $SU(3)_c$  gauge group, and the weak and electromagnetic interactions are unified into an electroweak theory which respects the gauge group  $SU(2)_L \times U(1)_Y$ . This theory has provided a strikingly accurate description of sub-atomic phenomena over the large range of energies explored by experiments. Hence, relativity theory and quantum theory which describe processes ranging from those in the astoundingly large cosmos of the galaxies to the vanishingly small world inside the atom, can be considered a triumph in the human endeavor to understand the Universe.

Although the standard model has been tremendously successful in accounting for an impressively broad variety of phenomena, it is still not wholly satisfactory, nevertheless, because a number of open questions remain. For instance, the generation of quark masses requires a fundamental scalar Higgs particle which has serious theoretical deficiencies. Perhaps more importantly from a pragmatic point of view, there are a large number of undetermined parameters in the theory: the masses of the fundamental particles, the angles in the Cabibbo-Kobayashi-Maskawa (CKM) matrix which determine the mixing of the mass eigenstates of quarks in the weak interactions, as well as the gauge couplings. These problems may be an indication that there exists a more fundamental and complete theory. A better understanding of the underlying physics would clearly require a determination of such quantities. In particular, an obvious way to investigate the quark mixing matrix elements is to study the weak

decays of hadrons. Such processes would not only shed light on the nature of quark mixing but also on a poorly understood aspect of the strong interactions — namely the non-perturbative long-distance forces at low energies which confine quarks and gluons into bound states of hadrons. Indeed, complementary information of this form would be needed to determine the unknown parameters.

There is another reason for studying the weak decays of hadrons. Charge conjugation and parity ( $CP$ ) violation has been observed only in the  $K^0 - \bar{K}^0$  system although it also expected to occur elsewhere. The only source of  $CP$  violation in the minimal standard model is from a complex phase in the CKM matrix. Extensions of this model typically have additional  $CP$  violating complex couplings between the Higgs sector, fermions, and possibly other particles in the theory. Therefore the search for and measurement of  $CP$ -asymmetries in weak decays would allow the possibility of distinguishing between standard and non-standard model physics when the CKM matrix elements have been determined with sufficient accuracy. It would also constrain extensions of the standard model which address the family problem. Finally, the investigation of rare weak processes are also good probes of departures from the standard model because they start at one-loop order.

In order to proceed with this program, it is thus necessary to determine the standard model predictions of weak hadronic processes in terms of standard model parameters. Unfortunately, such an enterprise necessarily entails an evaluation of hadronic matrix elements at low energies where the strong interactions invalidate a perturbative treatment, and thus depriving us of the only analytical tool available for such investigations. While it is possible to calculate hadronic properties using bound state models, such models are based in part on unjustified, often naive, assumptions and consequently are unconnected to the underlying theory of QCD.

There is actually a non-perturbative method available, namely lattice QCD. However, this approach suffers from two major problems: firstly, it does not convey much physical insight, and secondly, current limitations on computing power prevent it from being used in realistic systems involving dynamical fermions. Nonetheless, it provides complementary information unobtainable from perturbative methods which may contribute to a more comprehensive understanding of hadronic systems.

A lack of understanding of the strong interactions dynamics in the low energy

regime makes an analytical approach so intractable that reliable predictions are often only possible through the use of symmetries of the theory. A well-known example is the  $SU(3)_L \times SU(3)_R$  chiral symmetry which arises when the light current quark masses are considerably smaller than the intrinsic mass scale of the strong interactions. By exploiting this symmetry, a significant number of predictions relating processes involving light hadrons have been derived.

A few years ago, analogous symmetries which arise in the opposite limit of large quark masses were discovered.<sup>[1]</sup> The incorporation of these heavy quark symmetries into an heavy quark effective field theory (HQEFT) has allowed model-independent predictions for processes involving hadrons containing a single heavy quark to be made. This formalism may ultimately provide a means of comparing experimental results directly with rigorous QCD-based calculations without recourse to ad hoc models.

In the following chapter, the physical basis of these new heavy quark symmetries and how they are formulated in HQEFT from QCD as a systematic perturbative expansion are elucidated. HQEFT is a valid description of heavy quarks in a low-energy kinematic region. Chapters 3 and 4 extend this formalism to include the low-momentum interactions of hadrons containing a heavy quark with pseudo-Goldstone bosons.

In addition to the inadequacies pointed out above in our understanding of the microworld, another mystifying puzzle is how the great predominance of matter over anti-matter was generated. With the advent of grand unified theories (GUT), baryon number is no longer conserved, which opens up the possibility of generating this asymmetry dynamically. Baryon number violating processes are certainly expected to have been prolific in the early universe. However, such processes could have taken place all the way from the time of the Big Bang, through the GUT era down to the electroweak scale. So a primordial baryon asymmetry created at the GUT scale could have been drastically altered by the subsequent electroweak phase transition. There are also a number of problems associated with GUTs; for instance, while proton decay is predicted by such theories, no positive evidence for this process has been found thus far in spite of extensive efforts. It is then natural to consider the electroweak phase transition and investigate the role it may have played in determining the observed

asymmetry.

There are several conditions which must be satisfied in order for baryogenesis to take place:

- (1) There are baryon-number non-conserving processes.
- (2)  $C$  (charge conjugation symmetry) and  $CP$  (product of charge conjugation symmetry and parity) are violated.
- (3) There must be a departure from thermal equilibrium in the universe, because at thermal equilibrium, the numbers of baryons and anti-baryons are equal.

Since the electroweak interaction within the context of the standard model is relatively well understood (which is not true of physics at the GUT scale), it is important to investigate the prospects of the electroweak phase transition for baryogenesis. The standard model already meets some of the conditions given above. Firstly, there is a known source of baryon number violation in the standard model: baryon number is only a classical symmetry of the Lagrangian; the quantum theory develops an axial vector anomaly which violates baryon number through purely quantum mechanical, non-perturbative effects. Today, at zero temperature, such processes can only occur via instanton-induced barrier tunnelling which suppresses it to such an extent that it essentially never happens. However, the phase transition took place at finite temperature where thermal fluctuations over the barrier could have occurred. Secondly, both  $C$  and  $CP$  non-conservation have been observed to occur. Note that the measurement of  $CP$  violation described above aids in this study as well. (Although the amount of  $CP$  violation expected in the minimal standard model is not expected to be sufficient, additional contributions arise in extended models which can be constrained, conversely, by baryogenesis.) Finally, the standard electroweak theory will involve out-of-equilibrium behavior if the phase transition is first order. In such a transition, the field is trapped in a meta-stable vacuum which is separated from the true vacuum by an energy barrier. The transition proceeds through barrier penetration at zero temperature while thermal fluctuations that carry the field over the barrier are also possible at finite temperature. This mechanism corresponds to the nucleation of true vacuum bubbles in the surrounding false vacuum sea. Some of these bubbles subsequently expand and coalesce, thereby completing the transition. The time scale of the non-equilibrium processes in such a transition is characterized by the

bubble nucleation rate or the decay rate of the meta-stable vacuum. Thus, to better understand this phase transition, it is clear that an accurate determination of this nucleation rate and the temperature at which the transition took place is necessary.

Chapters 5 and 6 of this thesis are devoted to a study of this process. The accurate determination of both the decay rate and the transition temperature involves the calculation of the free energy of an extremal bubble configuration. This procedure requires not just an evaluation of the effective potential for the theory, but rather the effective action which includes derivative corrections as well. In Chapter 5, a general method for evaluating the one-loop effective action of a (scalar) field theory, which may have a non-convex classical potential, at zero and finite temperature is presented. This method involves a one-loop computation about a non-perturbatively determined classical solution. In Chapter 6, this method is utilized in the analysis of the nucleation rate in a generic first-order phase transition. While the motivation for this investigation originates from the electroweak phase transition, this formalism is valid for any first-order transition. In particular, it is applicable to another phase transition of great cosmological interest — the inflationary transition which is thought to be (weakly) first order.

## 2. THE HEAVY QUARK EFFECTIVE FIELD THEORY

### 2.1. NEW SYMMETRIES IN THE STRONG INTERACTIONS OF HEAVY QUARKS

The physical basis for why the strong interactions of systems containing heavy quarks is simpler can be easily understood. QCD, the theory of the strong interactions, is a non-Abelian gauge theory which is asymptotically free. The strong interactions are characterized by a scale  $\Lambda_{\text{QCD}}$  which has a value of approximately a few hundred MeV. This scale divides the strong and weak coupling regimes: at short distances, or equivalently, momenta much greater than  $\Lambda_{\text{QCD}}$ , the effective strong coupling  $g_s$  is small, and the force is weak so that a perturbative analysis is valid; at long distances, or momenta much less than  $\Lambda_{\text{QCD}}$ , the effective coupling becomes strong and is responsible for the confinement of quarks and gluons into hadronic bound states. Hence, it is natural to define a heavy quark to be one with mass  $m_Q \gg \Lambda_{\text{QCD}}$ . In a hadron containing a single heavy quark, its size is determined by the confinement scale  $R \sim 1/\Lambda_{\text{QCD}}$ , and the typical momenta exchanged by the light degrees of freedom (light quarks, anti-quarks or gluons) is of order  $\Lambda_{\text{QCD}}$ . The interaction scale of the heavy quark is given by its Compton wavelength which is much less than the confinement scale:  $\lambda_Q \sim 1/m_Q \ll 1/\Lambda_{\text{QCD}}$ . This relation means that in the heavy quark limit where its mass becomes infinite, the light degrees of freedom cannot resolve the structure of the heavy quark so that their interactions are independent of the heavy mass and consequently flavor. To the light degrees of freedom, the heavy quark will only appear as a static color source which manifests itself as a long-distance confining color force (independent of the mass). Furthermore, the color magnetic force, which arises from relativistic effects, vanishes when the heavy quark mass approaches infinity. Since it is only through the color magnetic field that the spin of the light degrees of freedom couple to the heavy quark spin, this indicates that the heavy spin decouples in the infinite mass limit. As a result, the low-momentum strong interactions of hadrons containing a heavy quark have a spin-flavor symmetry.

It is important to note, however, that this heavy quark symmetry (HQS) is not a symmetry (or even an approximate one) of the QCD Lagrangian, but rather a symmetry of the effective field theory HQEFT which is a very good approximation of

QCD in a certain kinematic region. It is realized when the heavy quark interacts with light degrees of freedom that have momenta less than or on the order of  $\Lambda_{\text{QCD}}$ . (The interaction of heavy quarks with hard gluons can be treated using perturbative QCD, of course.) In this regime, the heavy quark is almost on-shell, and its momentum can be written as  $p_Q^\mu = m_Q v^\mu + k^\mu$ , where  $v^\mu$  is the velocity of the heavy quark and  $k^\mu$  is a “residual” momentum that is of order  $\Lambda_{\text{QCD}}$  and represents the amount by which the quark is off-shell. Changes in  $v^\mu$  are suppressed by  $k^\mu/m_Q \sim \Lambda_{\text{QCD}}/m_Q$  which vanishes as  $m_Q$  goes to infinity. Hence the velocity is no longer a dynamical quantity but satisfies a super-selection rule: in the infinite quark mass limit, the velocity of the heavy quark is conserved in low-momentum strong interactions. In hadrons consisting of more than one heavy quark, the heavy particles can exchange momenta of order the heavy mass and consequently the velocity super-selection rule no longer holds. It is this limitation which restricts most applications of heavy quark symmetry to systems containing a single quark. Indeed, in the remainder of this thesis, the term “heavy hadron” will be restricted to mean a hadron containing a single heavy quark, unless stated otherwise.

For large but finite quark masses, these heavy quark symmetries are approximate, and corrections of order  $\Lambda_{\text{QCD}}/m_Q$  arise. However, the condition  $m_Q \gg \Lambda_{\text{QCD}}$  is both necessary and sufficient for systems containing such a quark to be close to the symmetry limit.

The HQEFT embodies these observations into a field theoretic framework which is especially useful for performing calculations. In particular, it quantifies the large quark mass limit into a systematic perturbative expansion in powers of  $\Lambda_{\text{QCD}}/m_Q$ . At each order in this expansion, QCD is included as an expansion to all orders in the effective strong coupling. Thus, results derived from HQEFT are based on a well-defined limit of QCD and are also model-independent. Furthermore, symmetry-breaking corrections can be investigated systematically. To see how this is done requires the HQEFT Lagrangian which will be derived in the next section.

The six quarks  $u, d, s, c, b, t$  in the standard model can be divided naturally into two triplets based on their masses. The light quarks  $u, d, s$  with masses much less than the QCD scale ( $m_u \approx 0.005 \text{ GeV}$ ,  $m_d \approx 0.01 \text{ GeV}$ ,  $m_s \approx 0.15 \text{ GeV}$ ) which give rise to an approximate  $\text{SU}(3)$  flavor symmetry, and the heavy quarks  $c, b, t$  with masses much

greater than  $\Lambda_{\text{QCD}}$  ( $m_c \approx 1.8 \text{ GeV}$ ,  $m_b \approx 5.2 \text{ GeV}$ ,  $m_t \approx 174 \text{ GeV}$ ). While in principle the applicability of the heavy quark symmetries improve as the quark mass increases above the QCD scale, there is actually a limitation on how heavy the quark can be: very massive quarks are so short-lived that they will likely decay weakly before they can hadronize. So ironically, while the  $t$  quark is the heaviest of all quarks, HQS is not expected to be very useful for describing its properties.

## 2.2. DERIVATION OF THE HEAVY QUARK EFFECTIVE FIELD THEORY LAGRANGIAN

The HQEFT Lagrangian will be derived from the part of the QCD Lagrangian involving the heavy quark fields, and for the moment it suffices to consider only one heavy flavor:<sup>1</sup>

$$\mathcal{L}_{H,\text{QCD}} = \bar{\psi}(i\not{D} - m)\psi, \quad (2.2.1)$$

where  $\psi$  is the QCD quark field, and  $D^\mu$  is the gauge-covariant derivative is defined as

$$D^\mu = \partial^\mu - igA_a^\mu T^a,$$

with

$$[D^\mu, D^\nu] = -igG_a^{\mu\nu} T^a,$$

in which  $G_a^{\mu\nu}$  is the gluon field tensor and  $T^a$  is the color SU(3) generator. Since light quark fields do not arise in this chapter, for notational simplicity, the heavy quark mass will hereafter be denoted by  $m$ . Since the HQEFT velocity superselection rule imposes the condition that the velocity of a heavy quark is conserved unless there is a non-QCD operator, such as a weak current or other source, that creates or annihilates heavy quarks,<sup>[2]</sup> heavy quark fields at different velocities correspond to distinct fields. Hence one introduces the heavy quark field  $h_v$  at a particular velocity  $v_\mu$ :

$$h_v = h_v^+ + h_v^- \quad (2.2.2)$$

where the fields  $h_v^+$  and  $h_v^-$  are defined by

$$\not{v}h_v^\pm = \pm h_v^\pm. \quad (2.2.3)$$

---

<sup>1</sup>Based in part on C.L.Y. Lee, CALT-68-1663.

The heavy quark and heavy anti-quark fields in HQEFT are different distinct fields which are separated by  $2m$  in momentum space. So to leading order in the heavy quark limit ( $m \rightarrow \infty$ ), they are separated infinitely far apart and hence are effectively decoupled. Thus heavy quark and anti-quark production is suppressed in the low-energy regime where HQEFT is valid. Hence heavy quark fields are related to only the positive component of the QCD quark field  $\psi$  by

$$\psi = e^{-imv \cdot x} h_v \quad (2.2.4)$$

while for heavy anti-quark fields the relation is

$$\psi = e^{+imv \cdot x} H_v \quad (2.2.5)$$

with

$$H_v = H_v^+ + H_v^-, \quad (2.2.6)$$

and

$$\not{v} H_v^\pm = \pm H_v^\pm. \quad (2.2.7)$$

Note that since the negative-energy component of  $\psi$  which creates or annihilates anti-quarks has been projected away in eq. (2.2.4), and similarly the positive-energy component has been eliminated in eq. (2.2.5), there is no heavy quark-antiquark-gluon coupling in HQEFT. Furthermore, since only heavy quarks arise in the following discussion, this derivation will be limited to heavy quark fields; however, the extension to include heavy anti-quarks is straightforward and would proceed along parallel lines with eq. (2.2.5,2.2.6,2.2.7) replacing eq. (2.2.4,2.2.2,2.2.3), respectively.

The QCD equation of motion for the field  $\psi$  is

$$(i\not{D} - m)\psi = 0. \quad (2.2.8)$$

Substituting eqs. (2.2.4) and (2.2.2) for  $\psi$  gives

$$h_v^- = \left(1 - \frac{i\not{D}}{2m}\right)^{-1} \frac{i\not{D}}{2m} h_v^+. \quad (2.2.9)$$

Here the  $\frac{i\not{D}}{2m}$  term is small compared to 1 when  $m \gg \Lambda_{\text{QCD}}$  because  $\not{D}$  acts on  $h_v^+$  to give a “residual” momentum of  $\mathcal{O}(\Lambda_{\text{QCD}})$ . So expanding the factor  $(1 - \frac{i\not{D}}{2m})^{-1}$  yields

$$h_v^- = \sum_{j=0}^{\infty} \left(\frac{i\not{D}}{2m}\right)^{j+1} h_v^+. \quad (2.2.10)$$

This shows that  $h_v^-$  is suppressed by  $\Lambda_{\text{QCD}}/m$  relative to  $h_v^+$ . Hence  $h_v^-$  is called the small component and can be regarded as the approximate amount by which the heavy quark field is off-shell, while  $h_v^+$  is known as the large component.

Expanding eq. (2.2.10), and substituting this into eqs. (2.2.2) and (2.2.4) gives

$$\psi = e^{-imv \cdot x} \left[ 1 + \frac{i\not{D}}{2m} + \left( \frac{i\not{D}}{2m} \right)^2 + \left( \frac{i\not{D}}{2m} \right)^3 + \left( \frac{i\not{D}}{2m} \right)^4 + \mathcal{O}\left(\frac{1}{m^5}\right) \right] h_v^+. \quad (2.2.11)$$

For convenience, set

$$Q_v = h_v^+,$$

then substituting eq. (2.2.11) for  $\psi$  yields the HQEFT Lagrangian

$$\mathcal{L}_{\text{HQEFT},v} = \sum_{n=0}^{\infty} \mathcal{L}_{\text{HQEFT},v}^{(n)}, \quad (2.2.12)$$

where the superscript  $n$  denotes the  $n$ th order term in the  $1/m$  expansion of  $\mathcal{L}_{\text{HQEFT},v}$ ; the first four terms are

$$\mathcal{L}_{\text{HQEFT},v}^{(0)} = \bar{Q}_v i(v \cdot D) Q_v, \quad (2.2.13)$$

$$\mathcal{L}_{\text{HQEFT},v}^{(1)} = -\frac{1}{2m} \bar{Q}_v (D^2 - \frac{g}{2} \sigma^{\mu\nu} G_{\mu\nu}) Q_v, \quad (2.2.14)$$

$$\mathcal{L}_{\text{HQEFT},v}^{(2)} = \frac{g}{4m^2} \bar{Q}_v (v^\mu D^\nu G_{\mu\nu} + i\sigma^{\alpha\mu} v^\nu D_\alpha G_{\mu\nu}) Q_v, \quad (2.2.15)$$

$$\mathcal{L}_{\text{HQEFT},v}^{(3)} = \frac{1}{8m^3} \bar{Q}_v \left[ 2(D^2 - \frac{g}{2} \sigma^{\mu\nu} G_{\mu\nu})^2 - \frac{g}{2} \sigma^{\mu\nu} G_{\mu\nu} (v \cdot D) \not{D} \right] Q_v. \quad (2.2.16)$$

This procedure can be continued to obtain higher order terms in  $1/m$ . Note that the different terms have been rearranged so that they have definite transformation properties under the heavy quark spin. In anticipation of the recurrence of some of the above operators in subsequent discussions, we make the following definitions:

the kinetic energy operator

$$\hat{O}_{\text{kin}} = -\frac{1}{2m} \bar{Q}_v D^2 Q_v, \quad (2.2.17)$$

the chromomagnetic moment operator

$$\hat{O}_{\text{mag}} = \frac{g}{4m} \bar{Q}_v \sigma^{\mu\nu} G_{\mu\nu} Q_v, \quad (2.2.18)$$

and the operators occurring at  $\mathcal{O}(1/m^2)$ ,

$$\hat{O}_1 = \frac{g}{4m^2} \bar{Q}_v v^\mu D^\nu (G_{\mu\nu} Q_v), \quad (2.2.19)$$

$$\hat{O}_2 = \frac{ig}{4m^2} \bar{Q}_v \sigma^{\alpha\mu} v^\nu D_\alpha (G_{\mu\nu} Q_v). \quad (2.2.20)$$

The equation of motion for the field  $Q$  is

$$(v \cdot D)Q_v = \mathcal{O}(1/m). \quad (2.2.21)$$

In the above expression for  $\mathcal{L}_{\text{HQEFT},v}^{(n)}$ , terms that vanish by the equations of motion have been omitted from the sub-leading order terms.

## Heavy Quark Spin-Flavor Symmetry

In a theory with  $N_f$  flavors of heavy quarks, each moving at velocity  $v$ , the above expression for  $\mathcal{L}_{\text{HQEFT},v}$  applies to each of these individual flavors, and hence the Lagrangian density generalizes to

$$\mathcal{L}_{\text{HQEFT},v}^{\text{flavor}} = \sum_{j=1}^{N_f} \mathcal{L}_{\text{HQEFT},v,(j)},$$

where  $\mathcal{L}_{\text{HQEFT},v,(j)}$  is the Lagrangian density of the  $j^{\text{th}}$  flavor which is given by eq. (2.2.12) with  $Q_v$  replaced by  $Q_v^{(j)}$  — the heavy quark field of flavor  $j$  at velocity  $v$ . Note that at leading order, the Lagrangian  $\mathcal{L}_{\text{HQEFT},v}^{\text{flavor}}$  neither depends on the heavy quark masses nor does the heavy quark spin couple to the gluon; hence it has a  $\text{SU}(2N_f)$  spin-flavor symmetry which was first observed by Isgur and Wise.<sup>[1]</sup> A curious feature of this property is that it relates heavy quarks of one mass to heavy quarks of another mass with the same velocity, and since the heavy masses can be very different, it relates heavy quarks of possibly very different momenta. Lorentz invariance of the Lagrangian  $\mathcal{L}_{\text{HQEFT},v}^{\text{flavor}}$  can be recovered by summing over all velocities of the heavy quark fields:

$$\mathcal{L}_{\text{HQEFT}} = \sum_{\vec{v}} \sum_{j=1}^{N_f} \mathcal{L}_{\text{HQEFT},v,(j)}.$$

Here, heavy degrees of freedom have been integrated in to incorporate the heavy quark field at each of the infinitely many velocities.

The No-Go theorem<sup>[3]</sup> which forbids the mixing of space-time and internal symmetries is evaded here by using an infinite number of fields, one for each four-velocity.

This derivation of  $\mathcal{L}_{\text{HQEFT}}$  illustrates how the full HQEFT Lagrangian is constructed; however, since subsequent discussions in this chapter only consider heavy

quarks of a given flavor at a particular velocity, it suffices to work with the Lagrangian  $\mathcal{L}_{\text{HQEFT},v}$  rather than  $\mathcal{L}_{\text{HQEFT}}$ .

If one were to determine all of the linearly independent operators that can be constructed at each order in  $1/m$  in this theory subject to the usual constraints of Lorentz invariance, gauge invariance, parity conservation, time reversal invariance, locality and hermiticity, one finds that at each respective order, they can all be expressed in terms of the existing operators in  $\mathcal{L}_{\text{HQEFT},v}^{(n)}$  as given in eqs. (2.2.13 – 2.2.16), with operators that vanish by the equation of motion excluded.<sup>[4]</sup> So it is gratifying to verify that this method of derivation does yield the most general expression for the Lagrangian subject to the constraints imposed on the theory.

The above derivation of  $\mathcal{L}_{\text{HQEFT},v}$  at tree level utilized the QCD equation of motion for the field  $\psi$ , eq. (2.2.8). This approach is equivalent to writing down the action functional for the Lagrangian in eq. (2.2.1), expressing  $\psi$  in terms of  $h_v^+$  and  $h_v^-$  as in eqs. (2.2.2 – 2.2.4) and then performing the functional integral over the small component field  $h_v^-$ ; this would give the  $h_v^-$  field in terms of the  $h_v^+$  as in eq. (2.2.9) above.<sup>[4,5]</sup> Note that the expression for  $h_v^-$  in eq. (2.2.9) involves non-local operators, which corresponds to the non-local expression that results when the heavy degrees of freedom are integrated out in the functional integral. Expanding out this expression in an operator product expansion as in eq. (2.2.10) yields a series of local operators in which each higher order term is suppressed by more powers of the heavy mass. Proceeding in this way using the functional integral verifies the above results in eqs. (2.2.12 – 2.2.16). The expansion in eq. (2.2.10) shows how the short distance physics, which can be incorporated into coefficients that match the effective theory to the full theory, is disentangled from the long distance physics which remains in the HQEFT and is manifest in matrix elements of the effective theory operators. Yet another equivalent method is to determine the most general operators that are allowed in HQEFT at each order in  $1/m$  (up to the order of interest) with arbitrary coupling constants which are then evaluated by matching amplitudes of these operators with the corresponding ones in QCD.

### 2.3. DERIVATION OF THE HQEFT FEYNMAN RULES

In HQEFT, calculations are performed using the Lagrangian  $\mathcal{L}_{\text{HQEFT},v}$  as given by eqs. (2.2.12 – 2.2.16) in the following manner. The propagation of the heavy quark is determined by the leading order Lagrangian  $\mathcal{L}_{\text{HQEFT},v}^{(0)}$ , eq. (2.2.13). All of the non-leading terms,  $\mathcal{L}_{\text{HQEFT},v}^{(n)}$  for  $n \geq 1$ , are treated perturbatively as new interaction vertices — each of these remaining higher order terms is a non-renormalizable operator which is suppressed by powers of  $\Lambda_{\text{QCD}}/m$ , where  $\Lambda_{\text{QCD}}/m$  is the new perturbative small expansion parameter.

The leading piece of the HQEFT Lagrangian  $\mathcal{L}_{\text{HQEFT},v}^{(0)}$  determines the Feynman rules at leading order. Inverting the  $\bar{Q}_v i(v \cdot \partial)Q_v$  part of  $\mathcal{L}_{\text{HQEFT},v}^{(0)}$  gives the heavy quark propagator:

$$\frac{i}{v \cdot k + i\epsilon}. \quad (2.3.1)$$

Here,  $k$  is a residual momentum that does not include the effect of the heavy mass. The remaining piece yields the heavy quark-gluon interaction vertex:

$$igv_\mu T^a. \quad (2.3.2)$$

These HQEFT Feynman rules reproduce the leading order terms of the corresponding QCD rules in the heavy quark limit; the remaining terms are suppressed by powers of  $m$ , and are accounted for by the non-leading operators in  $\mathcal{L}_{\text{HQEFT},v}$  which generate new interaction vertices.

### 2.4. APPLICATIONS OF THE HQEFT

The new spin-flavor symmetries of the HQEFT endow it with considerable predictive power. In addition, now having determined the Feynman rules including the new interaction vertices which break these symmetries, the effective Lagrangian  $\mathcal{L}_{\text{HQEFT},v}$  can be used to calculate perturbative  $\alpha_s$  corrections to the leading-order symmetry predictions; such effects contribute, for example, to matching relations between the HQEFT and QCD as well as to the renormalization of operators in the effective theory. This effective Lagrangian can also be used to determine the effect of the sub-leading (suppressed by powers of  $1/m$ ) symmetry-breaking operators on the predictive power of the HQEFT. Some of the significant applications of the HQEFT are reviewed next.

A large number of predictions can be made based on the  $SU(2N_f)$  heavy quark symmetry manifest in the leading order Lagrangian  $\mathcal{L}_{\text{HQEFT},v}^{(0)}$  given by eq. (2.2.13). These applications can be divided into two broad categories: predictions for the weak decays, and spectroscopic applications.<sup>[6]</sup> Of the many weak processes involving heavy hadrons that have been investigated using HQEFT, some of the most important are semi-leptonic decays of  $B$  mesons into  $D$  and  $D^*$  mesons. As an illustration of the power of HQS, an analysis of these decays is presented in what follows. Later in this chapter, an example of the predictions of HQS for the spectroscopy of heavy hadron is considered.

Perhaps the most well known application of HQS is to the exclusive semileptonic meson decays  $\bar{B} \rightarrow D\ell\bar{\nu}_\ell$  and  $\bar{B} \rightarrow D^*\ell\bar{\nu}_\ell$ .<sup>[1]</sup> For the purpose of this analysis, it is convenient to use a mass-independent normalization of meson states

$$\langle M(p')|M(p)\rangle = \frac{2p^0}{m_M}(2\pi)^3\delta^3(\vec{p}-\vec{p}'), \quad (2.4.1)$$

rather than the more conventional relativistic normalization

$$\langle \tilde{M}(p')|\tilde{M}(p)\rangle = 2p^0(2\pi)^3\delta^3(\vec{p}-\vec{p}'). \quad (2.4.2)$$

However, since  $p^0/m_M = v^0$ , eq. (2.4.1) depends only on the velocity and in the heavy quark limit, it is more appropriate to label heavy hadron states by their velocity so that  $|M(v)\rangle = |M(p)\rangle = |\tilde{M}(p)\rangle/\sqrt{m_M}$ . The invariance of QCD under Lorentz and parity transformations allows the hadronic amplitudes of these decays under the vector current  $V_\mu = \bar{c}\gamma_\mu b$  and the axial current  $A_\mu = \bar{c}\gamma_\mu\gamma_5 b$  to be written as

$$\langle D(v')|V_\mu|\bar{B}(v)\rangle = \tilde{f}_+(v+v')_\mu + \tilde{f}_-(v-v')_\mu, \quad (2.4.3a)$$

$$\langle D^*(v',\epsilon)|V_\mu|\bar{B}(v)\rangle = i\tilde{g}\epsilon_{\mu\alpha\beta\gamma}v^\alpha v'^\beta \epsilon^{*\gamma}, \quad (2.4.3b)$$

$$\langle D^*(v',\epsilon)|A_\mu|\bar{B}(v)\rangle = \tilde{f}_\mu^* + \tilde{a}_+(\epsilon^* \cdot v)(v+v')_\mu + \tilde{a}_-(\epsilon^* \cdot v)(v-v')_\mu, \quad (2.4.3c)$$

where  $\tilde{a}_\pm, \tilde{f}_\pm$ , and  $\tilde{g}$  are Lorentz invariant form factors which are functions of the velocity transfer  $v \cdot v'$  and the heavy quark masses. Heavy quark spin symmetry indicates that all of these functions can be expressed in terms of a single universal form factor  $\xi(v \cdot v')$  which depend only on  $v \cdot v'$  and is known as the Isgur-Wise function:

$$\tilde{f}_+ = \tilde{g} = \left[ \frac{\alpha_s(m_b)}{\alpha_s(m_c)} \right]^{-6/25} \xi(v \cdot v'), \quad \tilde{f}_- = 0, \quad (2.4.4a)$$

$$\tilde{f} = \left[ \frac{\alpha_s(m_b)}{\alpha_s(m_c)} \right]^{-6/25} (1 + v \cdot v') \xi(v \cdot v'), \quad (2.4.4b)$$

$$\tilde{a}_+ - \tilde{a}_- = - \left[ \frac{\alpha_s(m_b)}{\alpha_s(m_c)} \right]^{-6/25} \xi(v \cdot v'), \quad \tilde{a}_+ + \tilde{a}_- = 0. \quad (2.4.4c)$$

Furthermore, heavy quark flavor symmetry determines the normalization of  $\xi$  at the zero recoil point,  $v = v'$ :

$$\xi(v \cdot v' = 1) = 1. \quad (2.4.5)$$

Predictive power is retained when order  $\alpha_s(m_{c,b})$  and corrections are calculated. However, when order  $\Lambda_{\text{QCD}}/m_{c,b}$  contributions are included, considerable predictive power is lost because new universal functions arise in the form factors. In spite of this, these semi-leptonic decays will likely still be a very accurate means for determining  $|V_{cb}|$  because there are no  $\Lambda_{\text{QCD}}/m_{c,b}$  corrections at zero recoil  $v \cdot v' = 1$ .<sup>[7]</sup>

Another particularly elegant application of HQEFT is to the semi-leptonic decays of spin- $\frac{1}{2}$  baryons in which the light degrees of freedom have spin  $s_\ell = 0$  so that all of the spin is carried by the heavy quark  $Q$ . These are the  $\Lambda_Q$  and  $\Xi_Q$  states which decay as  $\Lambda_b \rightarrow \Lambda_c \ell \bar{\nu}_\ell$  and  $\Xi_b \rightarrow \Xi_c \ell \bar{\nu}_\ell$ , respectively. Consider  $\Lambda_b$  decay for concreteness, and adopt the conventional normalization for the baryon states:

$$\langle B(v', s') | B(v, s) \rangle = \frac{p^0}{m_B} (2\pi)^3 \delta_{ss'} \delta(\vec{p} - \vec{p}'). \quad (2.4.6)$$

These heavy baryon states have been labeled by their velocity rather than their momenta because heavy quark flavor symmetry relates states of equal velocity but different momenta. ( $s^\mu$  is the spin-polarization four-vector.) The hadronic matrix element for the above  $\Lambda_b$  decay can be expressed in its most general form in terms of six functions (with the spinor normalization  $\bar{u}u = 1$ ):

$$\langle \Lambda_c(v', s') | V_\mu | \Lambda_b(v, s) \rangle = \bar{u}^{(s')}(v') (F_1 \gamma_\mu + F_2 v_\mu + F_3 v'_\mu) u^{(s)}(v), \quad (2.4.7)$$

$$\langle \Lambda_c(v', s') | A_\mu | \Lambda_b(v, s) \rangle = \bar{u}^{(s')}(v') (G_1 \gamma_\mu \gamma_5 + F_2 v_\mu \gamma_5 + F_3 v'_\mu \gamma_5) u^{(s)}(v). \quad (2.4.8)$$

Heavy quark spin transformations relate the spin up and spin down states of a baryon and hence these baryon form factors amongst themselves. At leading-order, the HQS imply that all six form factors are determined by a single universal (baryon Isgur-Wise) function,  $\zeta(v \cdot v')$ :<sup>[8]</sup>

$$F_1 = G_1 = \left[ \frac{\alpha_s(m_b)}{\alpha_s(m_c)} \right]^{-6/25} \zeta(v \cdot v'),$$

$$F_2 = F_3 = G_2 = G_3 = 0,$$

where, once again, the normalization of this universal function is fixed at zero recoil by HQS:  $\zeta(v \cdot v' = 1) = 1$ . Unlike the meson case, however, no new unknown functions of  $v \cdot v'$  appear when  $\Lambda_{\text{QCD}}/m$  corrections are included and five relations remain amongst the six form factors to all orders in the strong coupling, so that most of the predictive power in the HQEFT is retained.

There are a myriad of other applications of the HQEFT besides those given above, so only some of the more important ones which relate to the work presented in this thesis are described.

In the next section, one of the corrections to the leading order predictions is analyzed in detail: the renormalization of the new sub-leading order operators that appear in  $\mathcal{L}_{\text{HQEFT},v}$  is examined, and new features that arise in the effective theory calculation are explored.

## 2.5. RENORMALIZATION IN THE HQEFT

The renormalization of an operator in HQEFT is different from that of the corresponding operator in QCD (that is, the analogous operator with the heavy quark fields replaced by conventional QCD quark fields having an arbitrary but finite mass) because matrix elements, or equivalently, their corresponding Green functions, of the operators in QCD can, in general, have terms of the form  $\ln(m/\mu)$  in their finite parts; here,  $\mu$  is the subtraction point introduced by renormalization. In processes involving heavy quarks, matrix elements are typically formed from a QCD operator sandwiched between hadronic states which have characteristic momenta of  $\mathcal{O}(\Lambda_{\text{QCD}})$ , so that it is appropriate to take  $\mu \sim \mathcal{O}(\Lambda_{\text{QCD}}) \ll m$ , which gives rise to large logarithms that must be taken into account. Since the heavy mass  $m$  is taken to infinity in HQEFT such logarithms become ultra-violet divergences which contribute to the renormalization of the HQEFT operator. Thus, the new divergences in HQEFT mean that the operator in HQEFT,  $\hat{O}_{\text{bare}}^{\text{HQEFT}}$ , requires renormalization even when the analogous operator in QCD,  $\hat{O}_{\text{bare}}^{\text{QCD}}$ , is not renormalized.

Now consider a generic operator  $\hat{O}^{\text{QCD}}$  in QCD which may be renormalized:

$$\hat{O}^{\text{QCD}}(\mu) = Z_{\hat{O}}^{\text{QCD}}(\mu) \hat{O}_{\text{bare}}^{\text{QCD}} \quad (2.5.1)$$

The renormalized operator evaluated at scale  $m$  is related to the operator in HQEFT through

$$\hat{O}^{\text{QCD}}(m) = C(\mu)\hat{O}^{\text{HQEFT}}(\mu) \quad (2.5.2)$$

where  $\mu$  is the subtraction point in the renormalization of the effective theory (which is generally different from the one in eq. (2.5.1)):

$$\hat{O}^{\text{HQEFT}}(\mu) = Z_{\hat{O}}^{\text{HQEFT}}(\mu)\hat{O}_{\text{bare}}^{\text{HQEFT}}. \quad (2.5.3)$$

Combining eqs. (2.5.2) and (2.5.3) relates the operator in the full theory to the bare one in the effective theory:

$$\hat{O}^{\text{QCD}}(m) = Z_{\hat{O}}^{\text{HQEFT}}(\mu)C(\mu)\hat{O}_{\text{bare}}^{\text{HQEFT}}. \quad (2.5.4)$$

$C(\mu)$  is the factor that will account for the large logarithms that arise in the QCD Green functions or matrix elements.

Since the operators  $\hat{O}^{\text{QCD}}(m)$  and  $\hat{O}_{\text{bare}}^{\text{HQEFT}}$  are independent of  $\mu$ , they give rise to a renormalization group equation for  $C$ :

$$\left[ \mu \frac{d}{d\mu} - \gamma_{\hat{O}} \right] C(\mu) = 0, \quad (2.5.5)$$

where  $\gamma_{\hat{O}}$ , the anomalous dimension of the operator  $\hat{O}^{\text{HQEFT}}$ , is defined as

$$\gamma_{\hat{O}} = -\frac{1}{Z_{\hat{O}}^{\text{HQEFT}}} \mu \frac{d}{d\mu} Z_{\hat{O}}^{\text{HQEFT}}(\mu). \quad (2.5.6)$$

Generally the  $\mu$ -independence of physical quantities such as S-matrix elements or scattering amplitudes will yield similar renormalization group equations. Once the renormalization constant and thence the anomalous dimension of the operator have been calculated, the solution of this renormalization group equation determines the scaling behavior of  $C$ :

$$C(\mu) = C(m) \exp \left[ - \int_{g(\mu)}^{g(m)} \frac{\gamma_{\hat{O}}(\bar{g})}{\beta(\bar{g})} d\bar{g} \right], \quad (2.5.7)$$

where  $\beta(g)$  is the  $\beta$ -function that describes the running of the coupling. The initial condition required to complete the solution of the running of the coefficient function

$C$  is determined by noting that there are no large logarithms in the QCD matrix elements at  $\mu = m$  so that matching the full and effective theories at this point gives

$$C(\mu = m) = 1 + \mathcal{O}(\alpha_s(m)/\pi). \quad (2.5.8)$$

Thus by introducing the matching coefficient  $C$  and solving its renormalization group equation, we have summed to all orders the leading logarithms that arise in perturbation theory, which are of the form  $[\alpha_s(\mu) \ln(m/\mu)]^n$  at order  $n$ . This illustrates how the effects of excitations due to the heavy degrees of freedom are included in the low energy effective theory through the running coefficient  $C$ . The operator  $\hat{O}(\mu)$  no longer depends on the heavy mass  $m$ ; the full mass dependence is now contained in  $C$ .

## 2.6. RENORMALIZATION OF THE OPERATORS IN THE SUB-LEADING TERMS OF THE HQEFT LAGRANGIAN

The renormalization of the operators in  $\mathcal{L}_{\text{HQEFT},v}$  in eqs. (2.2.14 – 2.2.16) can be conveniently achieved by calculating Green functions of each individual operator with the external states consisting of an incoming and an outgoing heavy quark and a gluon. For example, the bare one-particle irreducible (1PI) Green function of an operator  $\hat{O}^{\text{HQEFT}}$  with these external states

$$\Gamma_{\alpha\beta\zeta,\text{bare}}^h(w, x, y, z) = \langle 0 | \text{T} \{ Q_{\alpha,\text{bare}}(x) A_{\zeta,\text{bare}}^h(w) \hat{O}_{\text{bare}}^{\text{HQEFT}}(y) \bar{Q}_{\beta,\text{bare}}(z) \} | 0 \rangle,$$

is renormalized as

$$\Gamma_{\alpha\beta\zeta}^h(w, x, y, z; \mu) = Z_{\Gamma}(\mu) \Gamma_{\alpha\beta\zeta,\text{bare}}^h(w, x, y, z),$$

where

$$Z_{\Gamma} = Z_Q Z_A Z_{\hat{O}}, \quad (2.6.1)$$

and

$$Q_{\alpha,\text{bare}} = \sqrt{Z_Q} Q_{\alpha},$$

$$A_{\zeta,\text{bare}}^h = \sqrt{Z_A} A_{\zeta}^h.$$

The renormalization of the  $\hat{O}_{\text{kin}}$  operator in eq. (2.2.14) can be performed more simply by considering a Green function whose external states are only an incoming and an outgoing heavy quark.

Note that if  $v$  and  $v'$  are the velocities of heavy quark fields  $Q$  and  $\bar{Q}$ , and only HQEFT operators are involved in the process, as is the case here, then  $v' = v$  at leading order so that the velocity is conserved as required by the super-selection rule. Corrections to this rule can be taken into account by including higher order operators which are suppressed by powers of the heavy mass  $m$ . Such operators change the momentum of a heavy quark by an amount of order  $\Lambda_{\text{QCD}}$ , and as a result the velocity of the quark changes by approximately  $\Lambda_{\text{QCD}}/m$ .

## Method of Calculating the Green Functions

The Green functions that arise in the renormalization of the operators  $\hat{O}_{\text{mag}}$ ,  $\hat{O}_1$ , and  $\hat{O}_2$  are calculated using the background field method,<sup>[9]</sup> with dimensional regularization applied to the ultraviolet divergences, and the  $\overline{\text{MS}}$  subtraction scheme. The background field method has the desirable feature of maintaining explicit gauge invariance in calculations of quantum effects so that there is no mixing of gauge-invariant operators considered here with gauge non-invariant ones. It is also an efficient way of performing the calculation because the gluon field is not renormalized. The method used to treat the loop momentum integrals that arise in these Green functions is described in Appendix A.<sup>[10]</sup>

## Mixing of HQEFT operators under Renormalization

When one calculates the Green functions at one-loop to renormalize the operators  $\hat{O}_1$  and  $\hat{O}_2$ , one finds that they mix with operators that vanish by the equations of motion. Since matrix elements of the latter operators vanish, such contributions should be isolated from the other terms and then eliminated. There are also additional contributions to the renormalization of these operators coming from double insertions of  $\hat{O}_{\text{kin}}$  and  $\hat{O}_{\text{mag}}$  in one-loop graphs. These effects will be analyzed as they arise in the following discussion.

For operators which mix under renormalization as

$$\hat{O}_i = Z_{ij} \hat{O}_{j,\text{bare}}, \quad (2.6.2)$$

eqs.(2.5.5) and (2.5.6) are generalized to

$$\mu \frac{d}{d\mu} C_j(\mu) - \gamma_{ij} C_i(\mu) = 0 \quad (2.6.3)$$

and

$$\gamma_{ik} = - \left( \mu \frac{d}{d\mu} Z_{ij} \right) Z_{jk}^{-1}, \quad (2.6.4)$$

respectively.

### Renormalization of the Operator $\hat{O}_{\text{kin}}$

The renormalization of the operator  $\hat{O}_{\text{kin}}$  at one-loop is determined by the diagrams shown in Fig. 1. Using the background field method and dimensional regularization, one finds that the first two graphs do not contribute to the renormalization of  $\hat{O}_{\text{kin}}$ , but rather to that of  $(1/m)\bar{Q}(v \cdot D)^2 Q$ , an operator which vanishes by the equations of motion. The last graph contributes a divergence of  $-16g^2/3(4\pi)^2\epsilon$  to the renormalization of  $\hat{O}_{\text{kin}}$ . However, since the field renormalization of the heavy quark [4] is

$$\sqrt{Z_Q} = 1 + \frac{8g^2}{3(4\pi)^2\epsilon}, \quad (2.6.5)$$

the renormalization of the external heavy quark fields cancels this divergence so that  $\hat{O}_{\text{kin}}$  is not renormalized:[11]

$$Z_{\hat{O}_{\text{kin}}} = 1. \quad (2.6.6)$$

Thus

$$\gamma_{\hat{O}_{\text{kin}}} = 0 \quad (2.6.7)$$

and the matching coefficient does not run:

$$C_{\text{kin}}(\mu) = 1. \quad (2.6.8)$$

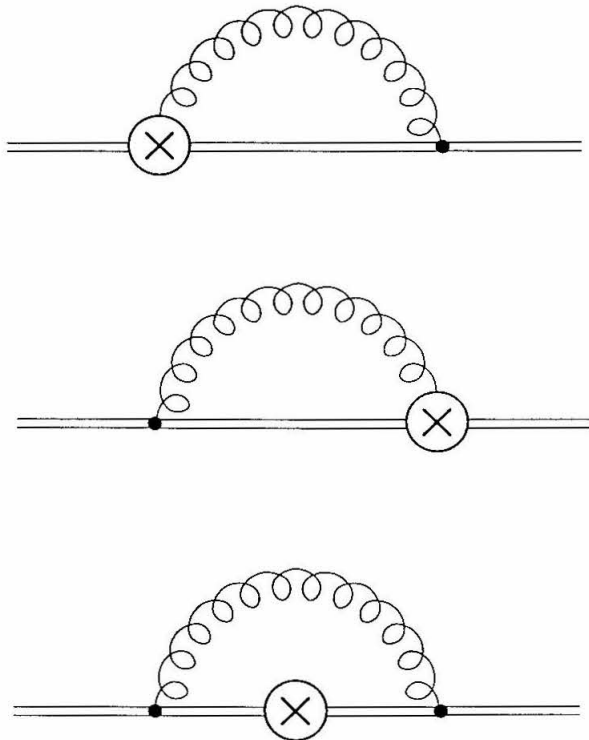


Fig. 1: One-particle irreducible (1PI) diagrams contributing to the one-loop renormalization of the operator  $\hat{O}_{\text{kin}}$ . Here and in all subsequent diagrams within this chapter, double lines and curly lines denote heavy quarks and gluons, respectively, while a circle with an enclosed cross denotes an insertion of  $\hat{O}_{\text{kin}}$ .

### Renormalization of the Operator $\hat{O}_{\text{mag}}$

The diagrams which are relevant to the one-loop renormalization of the operator  $\hat{O}_{\text{mag}}$  are shown in Fig. 2. Figures 2(a) and 2(d) contribute divergences of  $\frac{2g^2}{3(4\pi)^2\epsilon}$  and  $-\frac{12g^2}{(4\pi)^2\epsilon}$ , respectively, to the renormalization of  $\hat{O}_{\text{mag}}$ . The remaining diagrams do not renormalize  $\hat{O}_{\text{mag}}$ . Using this result and eq. (2.6.5) in eq. (2.6.1) gives

$$Z_{\hat{O}_{\text{mag}}} = 1 + \frac{6g^2}{(4\pi)^2\epsilon}, \quad (2.6.9)$$

and an anomalous dimension of

$$\gamma_{\hat{O}_{\text{mag}}} = \frac{6g^2}{(4\pi)^2}, \quad (2.6.10)$$

which is in agreement with previous results <sup>[11,12,10]</sup>. This gives a running coefficient of

$$C_{\text{mag}}(\mu) = \left[ \frac{\alpha_s(\mu)}{\alpha_s(m)} \right]^{\frac{-9}{33-2n_f}}. \quad (2.6.11)$$

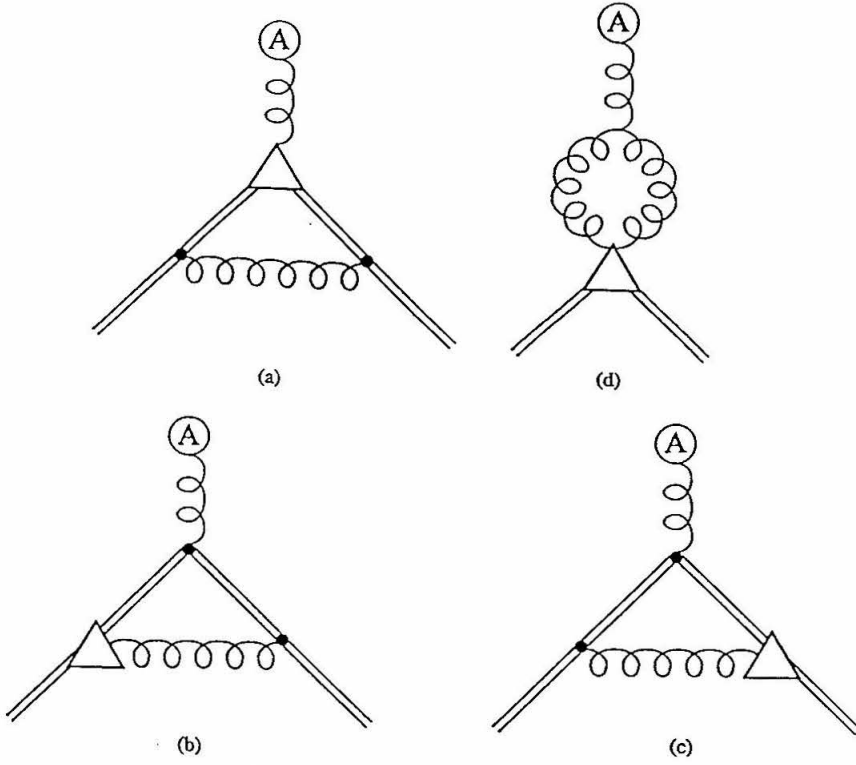


Fig. 2 (Part 1 of 2): 1PI diagrams contributing to the one-loop renormalization of the operator  $\hat{O}_{\text{mag}}$ . A triangle indicates the insertion of  $\hat{O}_{\text{mag}}$  in these and in all following figures in this chapter.

## Renormalization of the Operator $\hat{O}_1$

The diagrams involving  $\hat{O}_1$  that contribute to the renormalization of  $\hat{O}_1$  at one-loop are shown in Fig. 3. As alluded to above, there are two additional sources of contributions that mix into this:

- (1) There is a  $\mathcal{O}(1/m^2)$  effective theory operator, that transforms as a scalar under spin like  $\hat{O}_1$ , which arises at one-loop from double insertions of the kinetic energy operator  $\hat{O}_{\text{kin}}$ :

$$\hat{O}_{\text{kin-kin}}(x) = -\frac{1}{2} \int \text{T}[\hat{O}_{\text{kin}}(x)\hat{O}_{\text{kin}}(y)]d^4y. \quad (2.6.12)$$

Such contributions are not included in the graphs in Fig. 3. They must be taken into account by calculating the diagrams in Fig. 4.

Another such operator which could mix with  $\hat{O}_1$  is  $\hat{O}_{\text{mag-mag}}$  defined in the next section which has a piece that transforms as a scalar. However, on renormalizing it as described in the following section, one finds that it does not mix with  $\hat{O}_1$ .

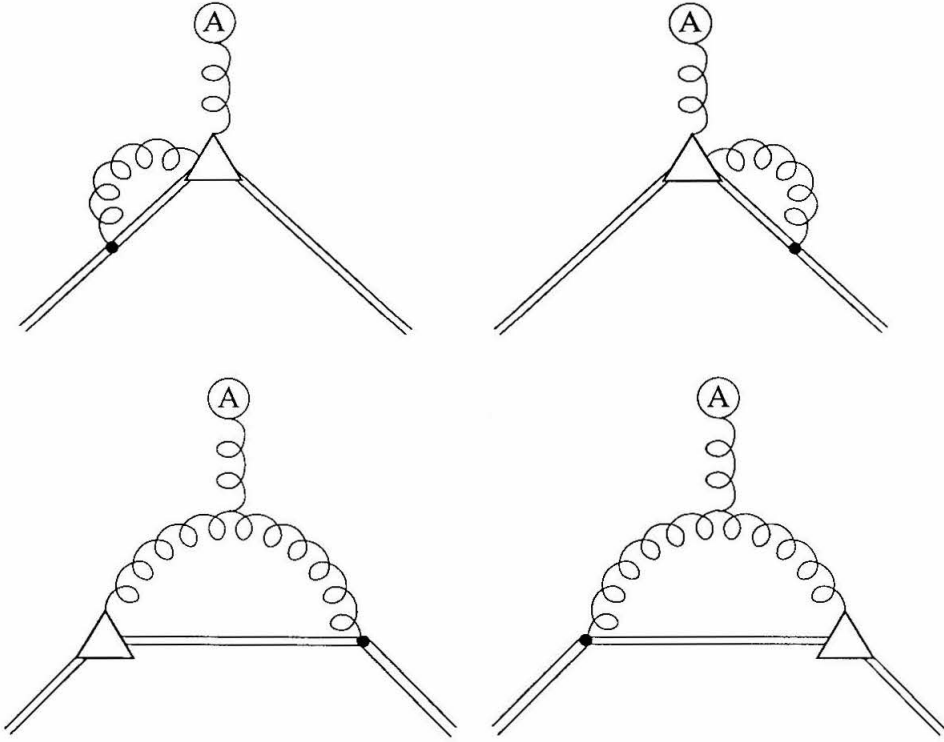


Fig. 2 (Part 2 of 2)

- (2) Effective  $\mathcal{O}(1/m^2)$  operators with the same symmetry which vanish by the equations of motion can mix into the calculation of any of the amplitudes in Figs. 1 and 3. Hence such contributions must be isolated and removed. Operators that generate such terms are  $(1/m^2)\bar{Q}D^2(v \cdot D)Q$ ,  $(1/m^2)\bar{Q}(v \cdot D)D^2Q$ , and  $(1/m^2)\bar{Q}(v \cdot D)^3Q$ .

Evaluating the diagrams in Fig. 3, removing the contributions coming from operators that vanish by the equations of motion as outlined above and removing the field renormalization factors for the external lines leaves a divergence of

$$-\frac{4g^2}{(4\pi)^2\epsilon}.$$

Similarly, calculating and summing the graphs in Fig. 4 by the same method yields a divergence of

$$\frac{220g^2}{9(4\pi)^2\epsilon}.$$

If one defines

$$\hat{\mathbf{O}}^{(1)} = \begin{pmatrix} i\hat{\mathcal{O}}_1 \\ \hat{\mathcal{O}}_{\text{kin-kin}} \end{pmatrix}, \quad (2.6.13)$$

then the mixing of these two operators under renormalization is given by

$$\hat{\mathcal{O}}^{(1)} = \mathbf{Z}^{(1)} \hat{\mathcal{O}}_{\text{bare}}^{(1)}, \quad (2.6.14)$$

where

$$\mathbf{Z}^{(1)} = \begin{pmatrix} 1 + \frac{4g^2}{(4\pi)^2\epsilon} & 0 \\ -\frac{220g^2}{9(4\pi)^2\epsilon} & 1 \end{pmatrix}. \quad (2.6.15)$$

The anomalous dimension matrix is then

$$\gamma^{(1)} = \frac{g^2}{(4\pi)^2} \begin{pmatrix} 4 & 0 \\ -220/9 & 0 \end{pmatrix}. \quad (2.6.16)$$

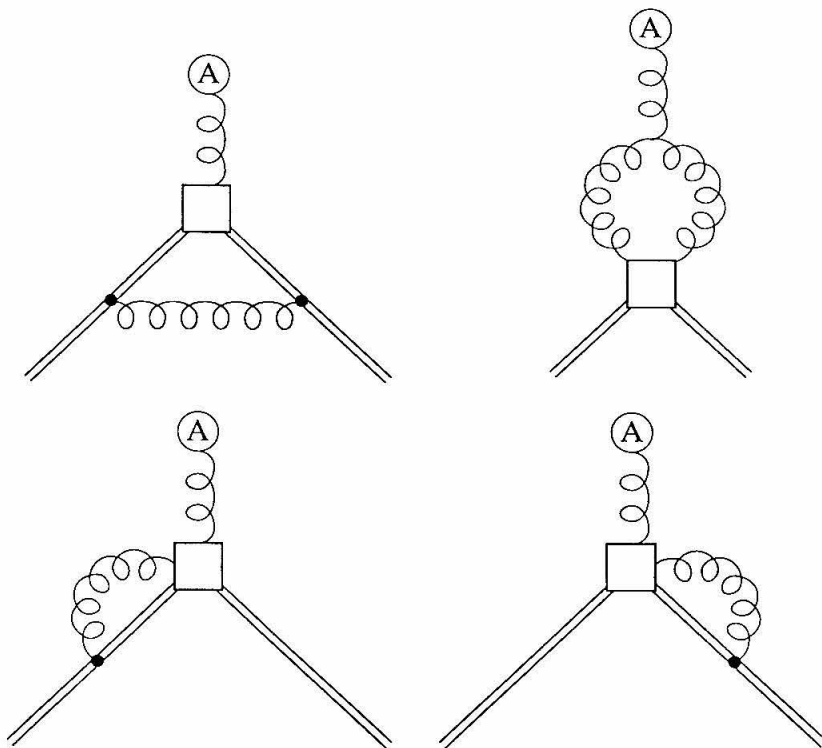


Fig. 3 (Part 1 of 2): One-loop 1PI graphs which renormalize the operators  $\hat{\mathcal{O}}_1$  or  $\hat{\mathcal{O}}_2$  when the square box denotes an insertion of  $\hat{\mathcal{O}}_1$  or  $\hat{\mathcal{O}}_2$ , respectively.

Having calculated the anomalous dimension of the operators that mix under renormalization, eq. (2.6.3) then determines the complete scaling behavior of the matching coefficients  $C_1$  and  $C_{\text{kin-kin}}$  associated with these effective theory operators

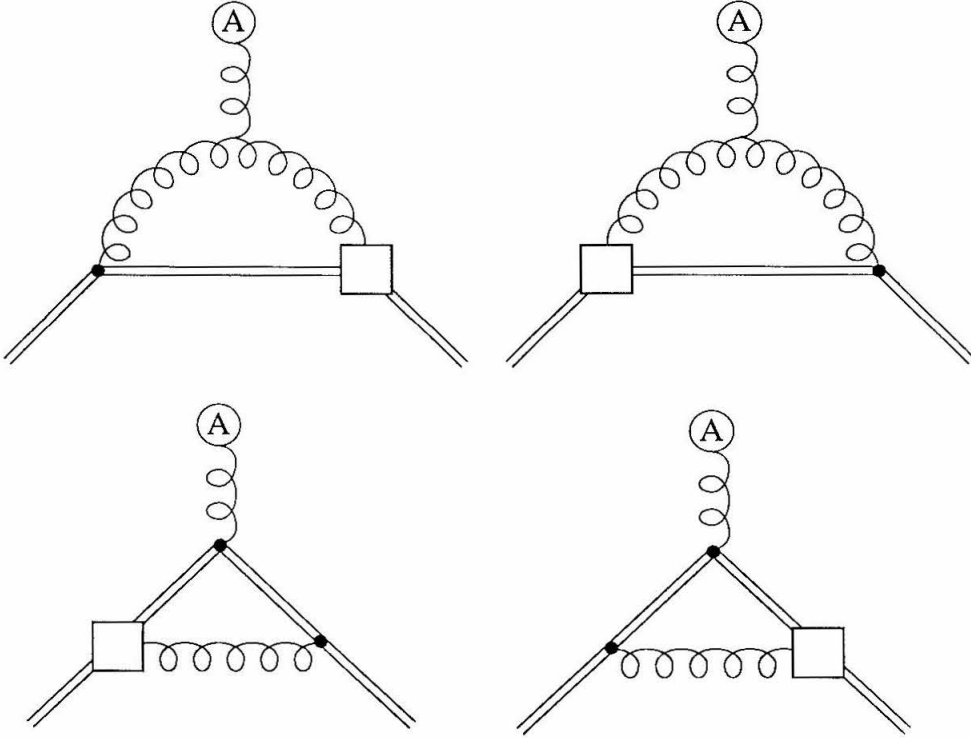


Fig. 3 (Part 2 of 2)

once the initial conditions are specified. Solving eq. (2.6.3), with the anomalous dimension matrix  $\gamma^{(1)}$  given by eq. (2.6.16), and  $C_1(m) = C_{\text{kin-kin}}(m) = 1$ , yields

$$C_1(\mu) = \frac{55}{9} - \frac{46}{9} \left[ \frac{\alpha_s(\mu)}{\alpha_s(m)} \right]^{\frac{-6}{33-2n_f}}, \quad (2.6.17)$$

where  $n_f$  is the number of light quark flavors appropriate to the momentum interval between  $\mu$  and  $m$ , and

$$C_{\text{kin-kin}}(\mu) = 1. \quad (2.6.18)$$

## Renormalization of the Operator $\hat{O}_2$

This analysis proceeds along similar lines as that for  $\hat{O}_1$ . In Fig. 3 diagrams involving  $\hat{O}_2$  which can contribute to the one-loop renormalization of  $\hat{O}_2$  are shown. Also as above, there are two similar additional sources of contributions:

- (1) Diagrams involving the operator formed from double insertions of  $\hat{O}_{\text{mag}}$  defined as

$$\hat{O}_{\text{mag-mag}}(x) = -\frac{1}{2} \int \text{T}[\hat{O}_{\text{mag}}(x)\hat{O}_{\text{mag}}(y)] d^4y, \quad (2.6.19)$$

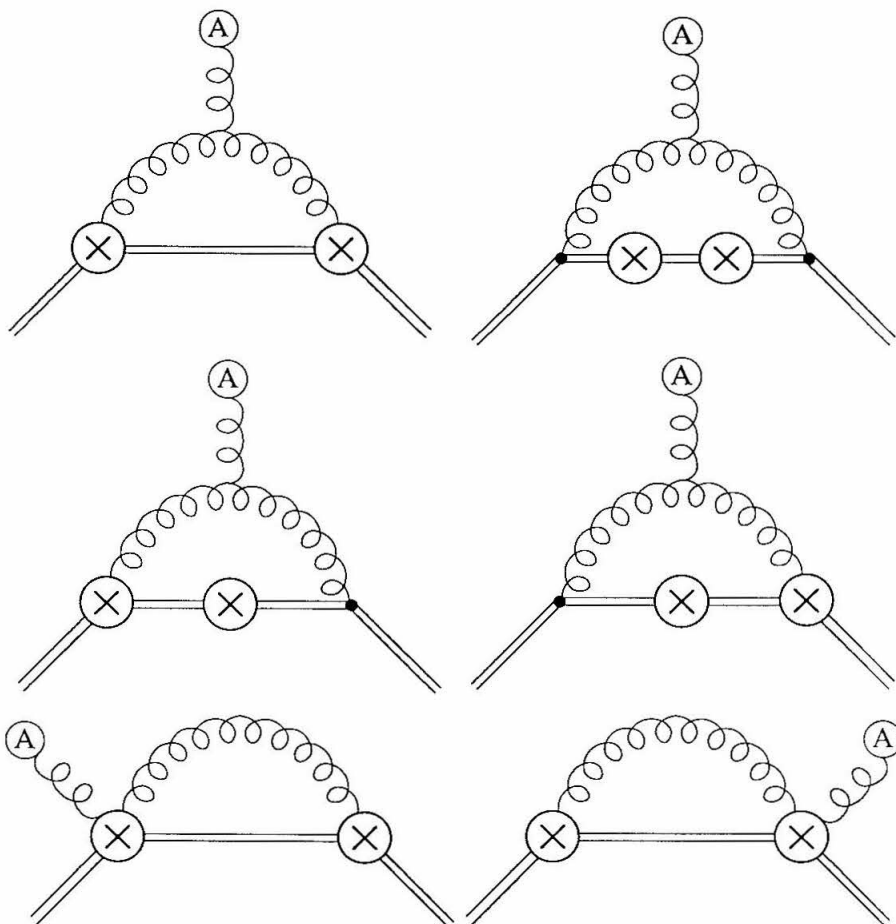


Fig. 4 (Part 1 of 4): One-loop 1PI graphs which renormalize  $\hat{O}_1$  and involve double insertions of  $\hat{O}_{\text{kin}}$ .

and ones involving the operator consisting of a  $\hat{O}_{\text{kin}}$  and a  $\hat{O}_{\text{mag}}$  operator defined by

$$\hat{O}_{\text{kin-mag}}(x) = - \int \text{T}[\hat{O}_{\text{kin}}(x)\hat{O}_{\text{mag}}(y)]d^4y \quad (2.6.20)$$

also contribute to the renormalization of  $\hat{O}_2$ ; such diagrams are displayed in Figs. 5 and 6, respectively.

- (2) Terms coming from operators which vanish by the equations of motion must be identified and removed. These operators are  $(1/m^2)\bar{Q}\sigma^{\mu\nu}G_{\mu\nu}(v \cdot D)Q$ , and  $(1/m^2)\bar{Q}(v \cdot D)\sigma^{\mu\nu}G_{\mu\nu}Q$ .

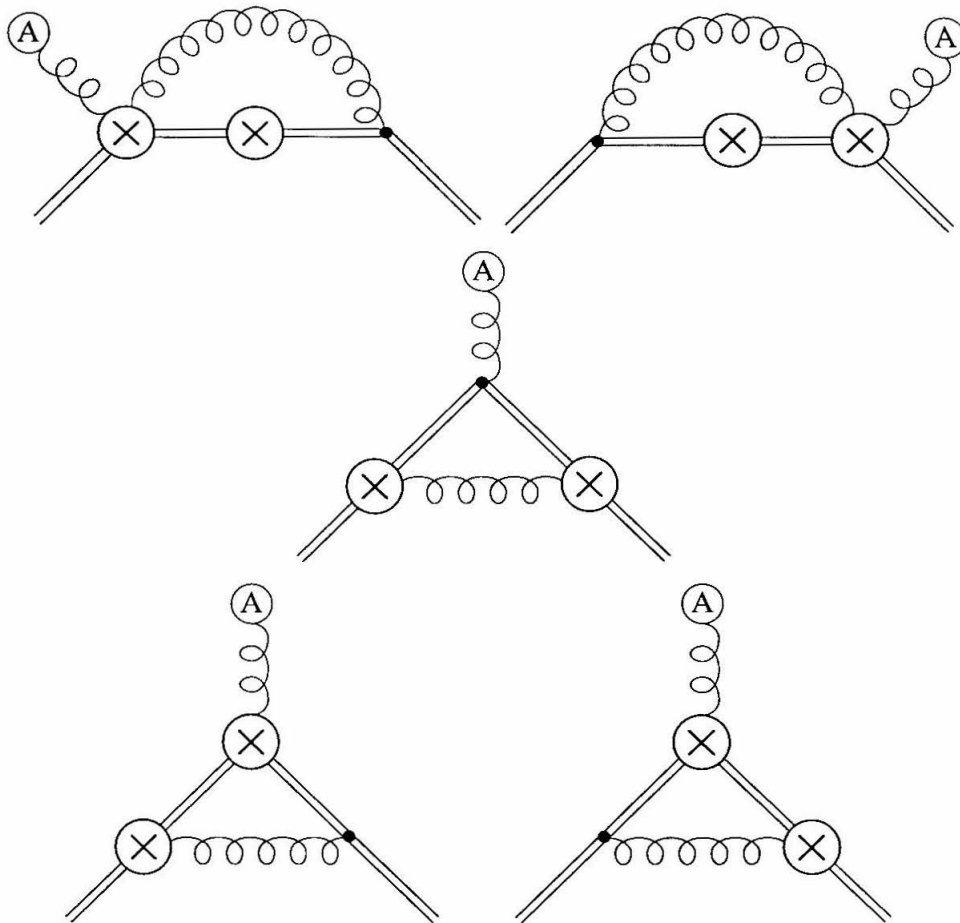


Fig. 4 (Part 2 of 4)

If we write the operators that mix as

$$\hat{\mathbf{O}}^{(2)} = \begin{pmatrix} i\hat{\mathcal{O}}_2 \\ \hat{\mathcal{O}}_{\text{mag-mag}} \\ \hat{\mathcal{O}}_{\text{kin-mag}} \end{pmatrix}, \quad (2.6.21)$$

and their renormalization as

$$\hat{\mathbf{O}}^{(2)} = \mathbf{Z}^{(2)} \hat{\mathbf{O}}_{\text{bare}}^{(2)}, \quad (2.6.22)$$

then calculating the graphs in Figs. 3, 5, and 6 yields

$$\mathbf{Z}^{(2)} = \begin{pmatrix} 1 & 0 & 0 \\ 0 & 1 + \frac{12g^2}{(4\pi)^2\epsilon} & 0 \\ -\frac{20g^2}{3(4\pi)^2\epsilon} & 0 & 1 + \frac{6g^2}{(4\pi)^2\epsilon} \end{pmatrix}, \quad (2.6.23)$$

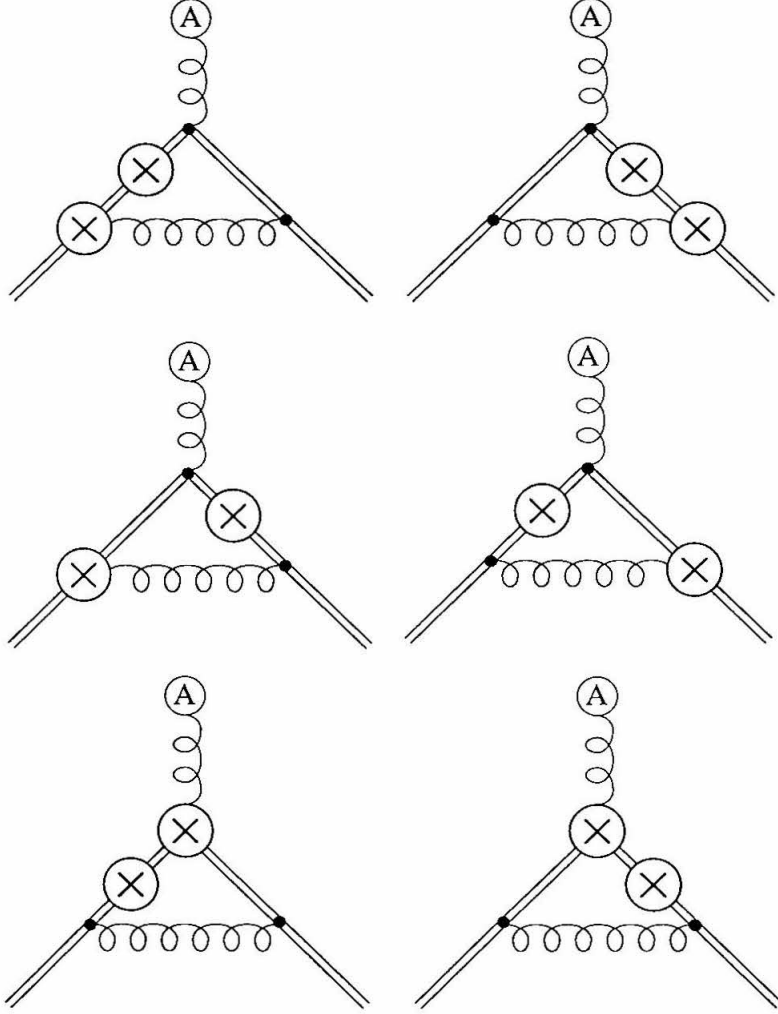


Fig. 4 (Part 3 of 4)

with the corresponding anomalous dimension matrix

$$\gamma^{(2)} = \frac{g^2}{(4\pi)^2} \begin{pmatrix} 0 & 0 & 0 \\ 0 & 12 & 0 \\ -20/3 & 0 & 6 \end{pmatrix}. \quad (2.6.24)$$

The running of the coefficients  $C_2, C_{\text{mag-mag}}, C_{\text{kin-mag}}$  with the matching conditions  $C_2(m) = C_{\text{mag-mag}}(m) = C_{\text{kin-mag}}(m) = 1$  is given by

$$C_2(\mu) = \frac{19}{9} - \frac{10}{9} \left[ \frac{\alpha_s(\mu)}{\alpha_s(m)} \right]^{\frac{-9}{33-2n_f}}, \quad (2.6.25)$$

$$C_{\text{mag-mag}}(\mu) = \left[ \frac{\alpha_s(\mu)}{\alpha_s(m)} \right]^{\frac{-18}{33-2n_f}}, \quad (2.6.26)$$

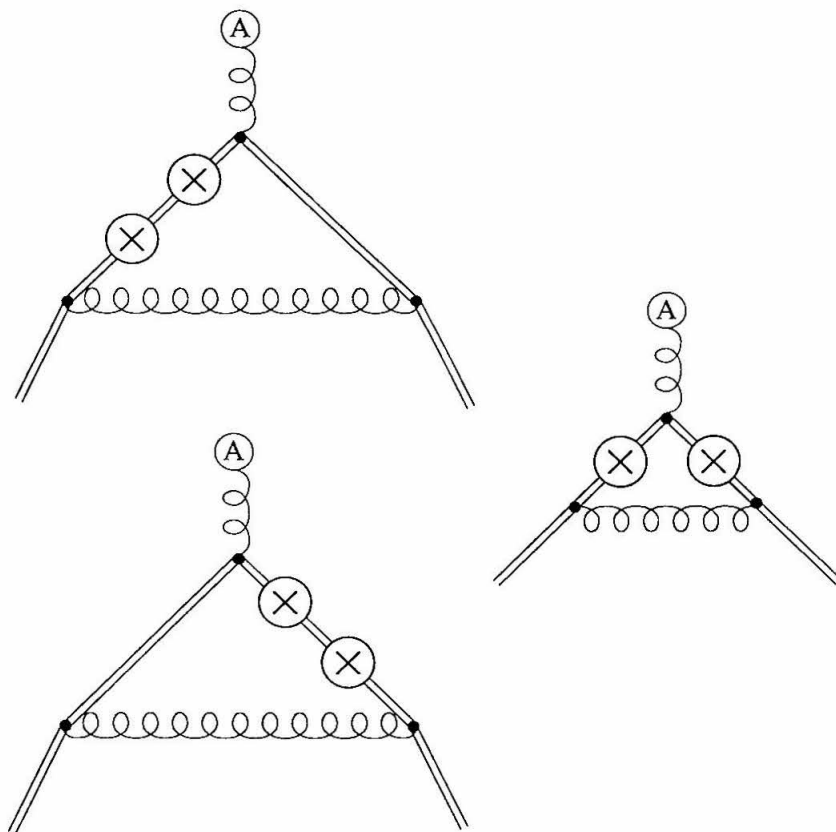


Fig. 4 (Part 4 of 4)

and

$$C_{\text{kin-mag}}(\mu) = \left[ \frac{\alpha_s(\mu)}{\alpha_s(m)} \right]^{\frac{-9}{33-2n_f}}. \quad (2.6.27)$$

## 2.7. A SPECTROSCOPIC APPLICATION

An important spectroscopic application of these results is to the mass splitting observed in hadrons containing a quark of a particular flavor. In the infinite mass limit of a heavy quark with spin  $\vec{S}_Q$  in a hadron with total angular momentum  $\vec{S}$ , the angular momentum of the light degrees of freedom

$$\vec{S}_\ell = \vec{S} - \vec{S}_Q$$

commutes with the Hamiltonian. Hence  $s_\ell$ , the eigenvalue  $\vec{S}_\ell$ , is a conserved quantity in the rest frame of the hadron. As a result, such hadrons will occur in degenerate doublets of total spin

$$s_\pm = s_\ell \pm \frac{1}{2}$$

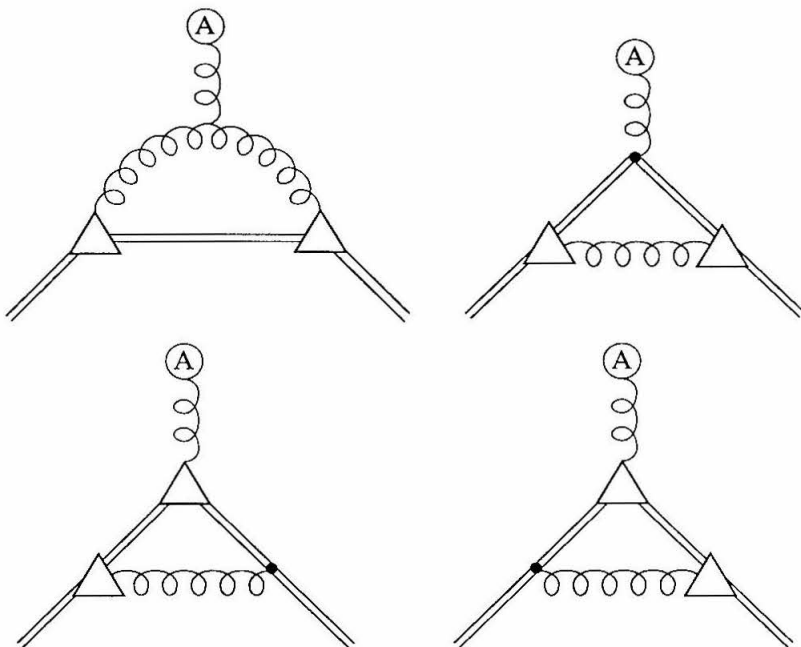


Fig. 5: 1PI graphs with an insertion of the time-ordered operator  $\hat{O}_{\text{mag-mag}}$  which can effect a renormalization of  $\hat{O}_1$  or  $\hat{O}_2$  at one-loop.

provided that  $s_\ell \neq 0$ . For instance, the low-lying heavy mesons will consist of a pseudoscalar state  $P$  and vector state  $P_\mu$ , such as the  $B$  and  $B^*$ . Since these states are related by the heavy quark spin which commutes with the Hamiltonian, they are degenerate at leading order in the HQEFT. Furthermore, because  $\hat{O}_{\text{mag}}$  and  $\hat{O}_2$  are the only operators that transform non-trivially under heavy quark spin transformations to  $\mathcal{O}(1/m^2)$ , they are the leading and next-to-leading order operators, respectively, in the effective theory responsible for the mass splitting. For definiteness, consider again the  $B - B^*$  system; the mass difference is

$$\begin{aligned}
 \Delta m_B &= m_{B^*} - m_B \\
 &= \frac{1}{\langle B|B \rangle} \left\{ \langle B^* | [C_{\text{mag}}(\mu) \hat{O}_{\text{mag}}(\mu) + C_2(\mu) \hat{O}_2(\mu) - iC_{\text{mag-mag}}(\mu) \hat{O}_{\text{mag-mag}}(\mu) \right. \\
 &\quad \left. - iC_{\text{kin-mag}}(\mu) \hat{O}_{\text{kin-mag}}(\mu)] | B^* \rangle \right. \\
 &\quad \left. - \langle B | [C_{\text{mag}}(\mu) \hat{O}_{\text{mag}}(\mu) + C_2(\mu) \hat{O}_2(\mu) - iC_{\text{mag-mag}}(\mu) \hat{O}_{\text{mag-mag}}(\mu) \right. \\
 &\quad \left. - iC_{\text{kin-mag}}(\mu) \hat{O}_{\text{kin-mag}}(\mu)] | B \rangle \right\}.
 \end{aligned} \tag{2.7.1}$$

Note that the full mass dependence has been extracted from the operators and now resides in the coefficient functions; the above matrix elements, which do not involve

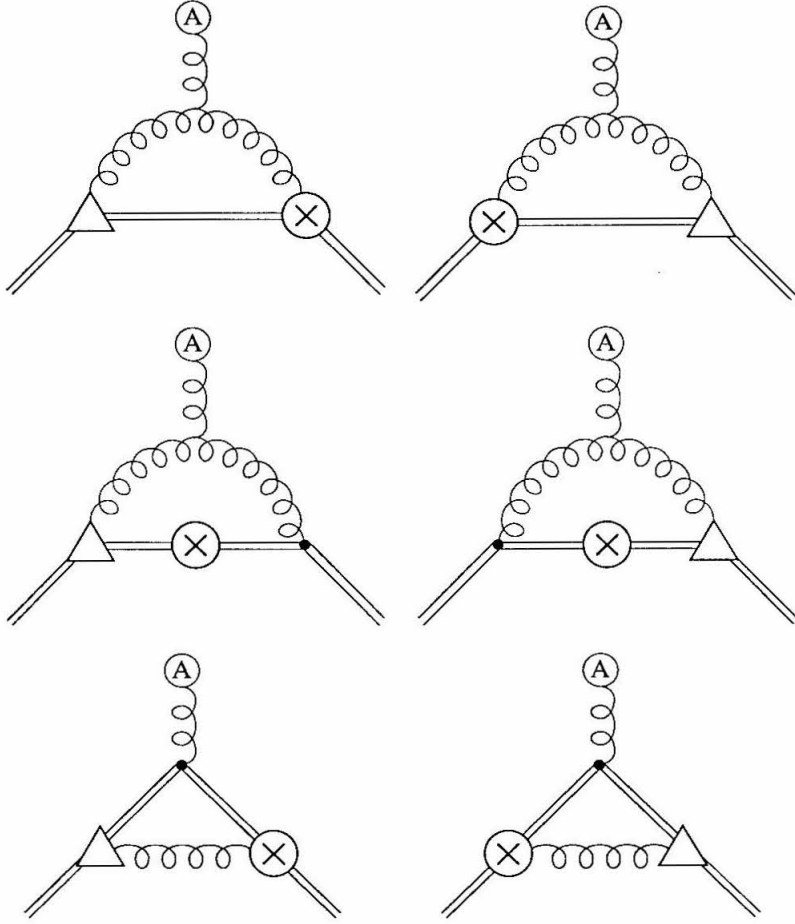


Fig. 6 (Part 1 of 4): 1PI diagrams with an insertion of the time-ordered operator  $\hat{O}_{\text{kin-mag}}$  which give a one-loop contribution to the renormalization of  $\hat{O}_2$ .

the heavy mass, are non-perturbative in nature and cannot be evaluated using the effective theory method presented here. However, they could be tractable using lattice gauge theory, and steps in this direction have already been taken.<sup>[13]</sup>

Since the HQEFT flavor symmetry relates different flavors of heavy quarks, a comparison of these results with experimental values can still be achieved at leading order: eq. (2.7.1) is valid for  $\Delta m_D$  when  $B$  and  $B^*$  are replaced by  $D$  and  $D^*$  respectively, so neglecting the effects at  $\mathcal{O}(1/m_Q^2)$ , one can form a ratio of the mass differences which is independent of the unknown matrix elements: <sup>[10]</sup>

$$\frac{\Delta m_D}{\Delta m_B} = \frac{m_B}{m_D} \left[ \frac{\alpha_s(m_B)}{\alpha_s(m_D)} \right]^{-\frac{9}{33-2n_f}}. \quad (2.7.2)$$

The measured experimental values are  $m_{D^0} = 1864.5$  MeV,  $m_{D^{*0}} = 2007.1$  MeV, and

$m_{B^0} = 5279.4 \text{ MeV}$ .<sup>[14]</sup> Using these values in eq. (2.7.2) and evaluating the anomalous scaling factor with  $\Lambda_{\overline{\text{MS}}}^{(4)} = 230 \text{ MeV}$ <sup>[14]</sup> and  $n_f = 4$  predicts  $\Delta m_B = 46.0 \text{ MeV}$ . This mass-splitting was recently measured to be  $\Delta m_B = 46.4 \pm 0.3 \pm 0.8 \text{ MeV}$ .<sup>[15]</sup>

The good agreement between the result of the  $\mathcal{O}(1/m_Q)$  correction and the experimental data indicates that  $\mathcal{O}(1/m_Q^2)$  effects are small. It would be interesting to see whether this arises from a cancellation between terms or from all of the matrix elements being small. It may be possible to address this issue using lattice QCD.<sup>[16]</sup>

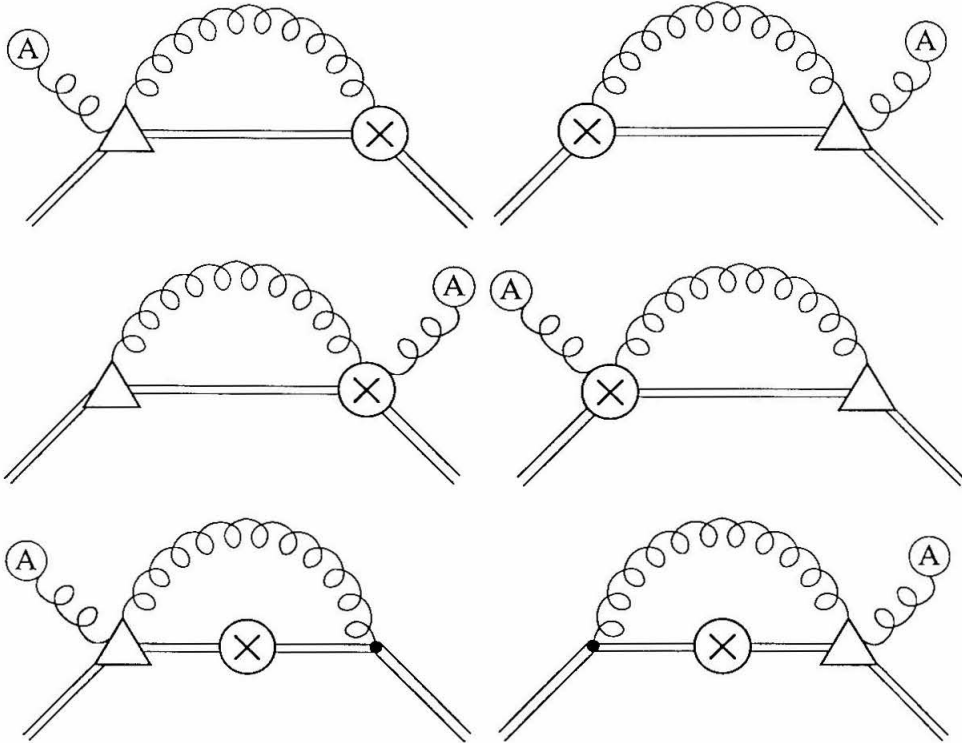


Fig. 6 (Part 2 of 4)

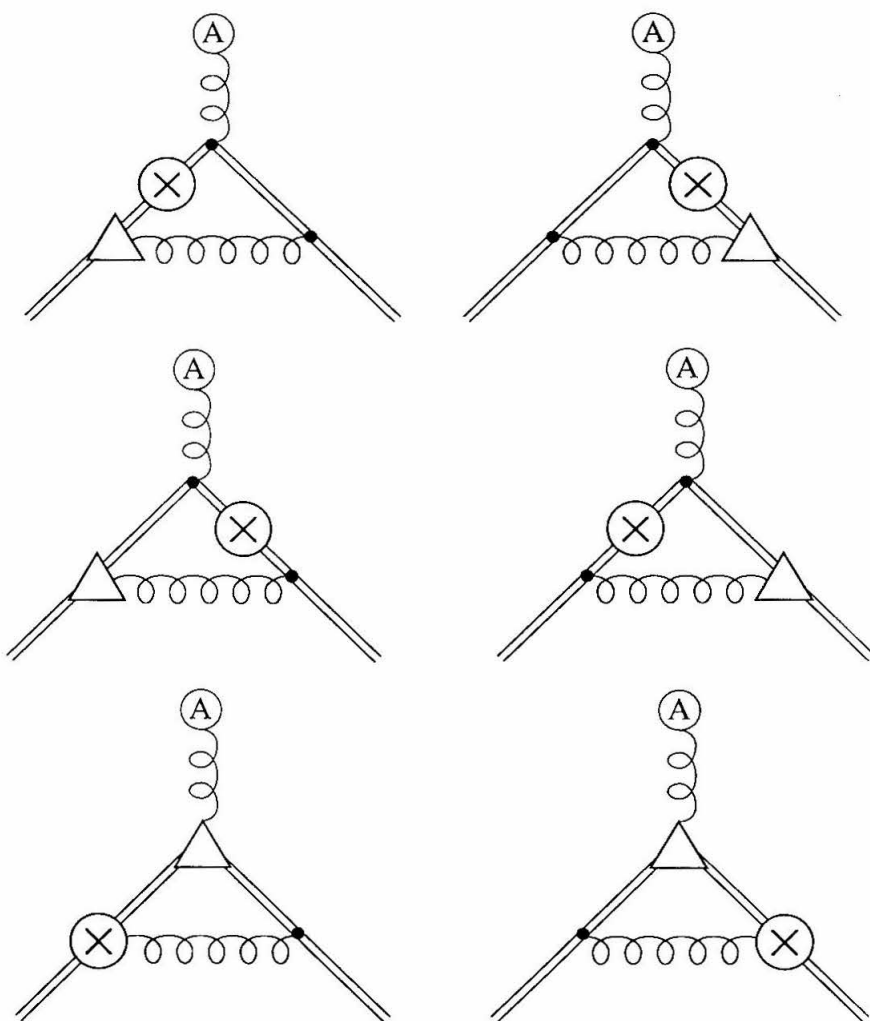


Fig. 6 (Part 3 of 4)

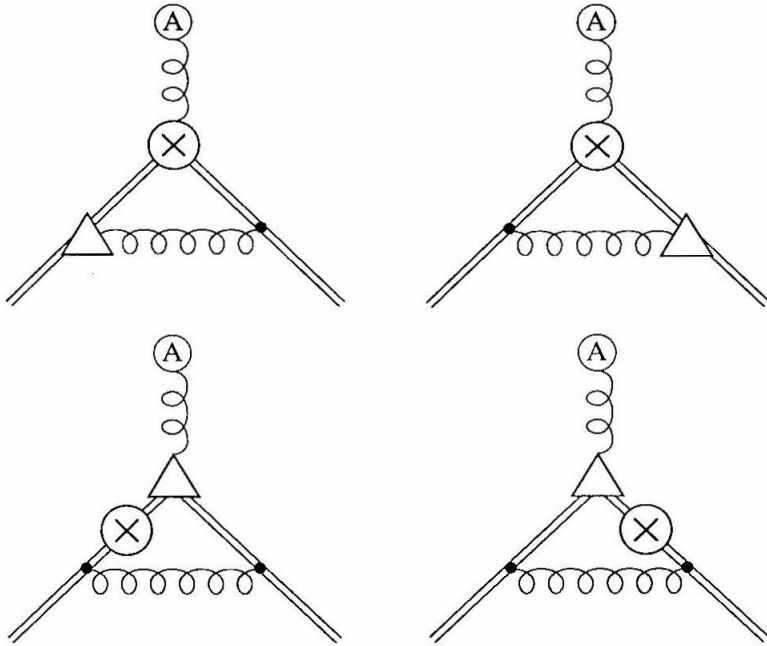


Fig. 6 (Part 4 of 4)

### 3. HEAVY QUARK SYMMETRY AND CHIRAL PERTURBATION THEORY

#### 3.1. CHIRAL PERTURBATION THEORY

In the last chapter, it was observed that the six quarks in the standard model fall naturally into two groups: light quarks and heavy quarks, relative to the scale of the strong interactions. For hadrons containing a heavy quark, the HQEFT was developed. For hadrons consisting of light quarks, chiral perturbation theory plays an analogous role.

The strong interactions have an approximate  $SU(3)_L \times SU(3)_R$  chiral symmetry because the masses of the light  $u, d$  and  $s$  quarks are small compared to  $\Lambda_{\text{QCD}}$ . This global symmetry is spontaneously broken to the vector subgroup  $SU(3)_V$  by chiral condensates. Associated with this spontaneous symmetry breaking is the octet of pseudo-Goldstone bosons consisting of the light mesons  $\pi, K$  and  $\eta$ . The interactions of these particles can be described in terms of a chiral perturbation theory in which the effective Lagrangian contains the most general couplings that respect chiral symmetry. This effective field theory possesses considerable predictive power at low momenta because terms in the Lagrangian with the least numbers of derivatives and insertions of the  $(\bar{3}_L, 3_R) + (3_L, \bar{3}_R)$  symmetry-breaking light quark mass matrix dominate.

The pseudo-Goldstone bosons appear in the Lagrangian density through

$$\xi = \exp(iM/f) , \quad (3.1.1a)$$

and

$$\xi^2 = \Sigma = \exp(2iM/f) . \quad (3.1.1b)$$

In eqs. (3.1.1),  $M$  is the matrix of fields

$$M = \begin{pmatrix} \frac{1}{\sqrt{2}}\pi^0 + \frac{1}{\sqrt{6}}\eta & \pi^+ & K^+ \\ \pi^- & -\frac{1}{\sqrt{2}}\pi^0 + \frac{1}{\sqrt{6}}\eta & K^0 \\ K^- & \bar{K}^0 & -\sqrt{\frac{2}{3}}\eta \end{pmatrix} , \quad (3.1.2)$$

and  $f$  is the pseudoscalar decay constant. At leading order in chiral perturbation theory,  $f$  is the pion decay constant:  $f_\pi \approx 132$  MeV.

Under  $SU(3)_L \times SU(3)_R$  chiral symmetry,

$$\Sigma \rightarrow L\Sigma R^\dagger, \quad (3.1.3a)$$

and

$$\xi \rightarrow L\xi U^\dagger = U\xi R^\dagger, \quad (3.1.3b)$$

where  $L \in SU(3)_L, R \in SU(3)_R$  and  $U$  is a function of  $L, R$  and the meson fields. Typically  $U$  is space-time dependent. However, for  $SU(3)_V$  transformations,  $V = L = R$ , and  $U$  is equal to  $V$ .

### 3.2. HEAVY MESON CHIRAL PERTURBATION THEORY

In this chapter, the low-momentum interactions of the pseudo-Goldstone bosons with the ground-state heavy mesons with flavor quantum numbers  $Q\bar{q}^a$  (where  $a = 1, 2, 3$ , and  $q^1 = u, q^2 = d, q^3 = s$ ) are studied.<sup>2</sup> For such heavy mesons, the spin-parity of the light degrees of freedom is  $s_\ell^{\pi_\ell} = \frac{1}{2}^-$ . It was noted previously that when this spin is combined with that of the heavy quark, the result is pseudoscalar and vector mesons which are degenerate in the limit  $m_Q \rightarrow \infty$ . With three light flavors, there will be a  $SU(3)_V$  anti-triplet of spin-zero mesons denoted by  $P_a$  and a  $SU(3)_V$  anti-triplet of spin-one mesons denoted by  $P_a^*$  from which three degenerate doublets can be formed. For  $Q = c$ ,  $(P_1, P_2, P_3) = (D^0, D^+, D_s)$  and  $(P_1^*, P_2^*, P_3^*) = (D^{*0}, D^{*+}, D_s^*)$  while for  $Q = b$ ,  $(P_1, P_2, P_3) = (B^-, \bar{B}^0, \bar{B}_s)$  and  $(P_1^*, P_2^*, P_3^*) = (B^{*-}, \bar{B}^{*0}, \bar{B}_s^*)$ . Factors of  $\sqrt{m_P}$  and  $\sqrt{m_{P^*}}$  have been absorbed into the  $P$  and  $P^*$  fields. Consequently they have dimension 3/2.

It is important for the effective Lagrangian which describes the interactions of heavy hadrons with the pseudo-Goldstone bosons to be invariant under heavy quark symmetry. Consider, for instance, a process involving only a real  $B$  meson. But then the  $B^*$  meson will contribute as a virtual particle in pole-type Feynman diagrams, and the couplings of the  $B$  to the  $B^*$  are related by heavy quark spin symmetry.

The pseudoscalar and vector meson fields  $P_a$  and  $P_{a\mu}^*$  can be conveniently combined in a  $4 \times 4$  matrix  $H_a$  given by

$$H_a = \frac{1 + \not{v}}{2} (P_{a\mu}^* \gamma^\mu - P_a \gamma_5). \quad (3.2.1)$$

---

<sup>2</sup>Based on C.L.Y. Lee, M. Lu, and M.B. Wise, *Phys. Rev.* **D46**, 5040 (1992)

This is a “shorthand notation.” In cases where the type of heavy quark  $Q$  and its four-velocity  $v$  are important, the  $4 \times 4$  matrix is denoted by  $H_a^{(Q)}(v)$ . The field operators  $P_a$  and  $P_{a\mu}^*$  destroy mesons  $P_a$  and  $P_{a\mu}^*$ , respectively. Since pair creation does not occur in the effective field theory, the corresponding anti-particles are not created. Note that the vector meson field is subject to the constraint  $v^\mu P_{a\mu}^* = 0$ .

The field  $H_a$  is a doublet under heavy quark spin symmetry  $SU(2)_v$  and a  $\bar{3}$  under the unbroken  $SU(3)_V$  light quark flavor symmetry. Under  $SU(2)_v$  and  $SU(3)_L \times SU(3)_R$  it transforms as

$$H_a \rightarrow S(HU^\dagger)_a, \quad (3.2.2a)$$

where  $S \in SU(2)_v$  and  $U$  is the usual space-time dependent  $3 \times 3$  unitary matrix that is introduced to transform matter fields in a chiral Lagrangian. Under Lorentz transformations

$$H_a \rightarrow D(\Lambda)H_a D(\Lambda)^{-1}, \quad (3.2.2b)$$

where  $D(\Lambda)$  is an element of the  $4 \times 4$  matrix representation of the Lorentz group.

It is also useful to introduce the matrix

$$\bar{H}_a = \gamma^0 H_a^\dagger \gamma^0. \quad (3.2.3)$$

The transformations corresponding to eq.(3.2.2a-3.2.2b) for  $\bar{H}_a$  are  $\bar{H}_a \rightarrow U_{ab} \bar{H}_b S^{-1}$ , and  $\bar{H}_a \rightarrow D(\Lambda) \bar{H}_a D(\Lambda)^{-1}$ .

Then the strong interactions of the lowest-lying mesons containing a heavy quark  $Q$  with the pseudo-Goldstone bosons  $\pi, K, \eta$  are determined by the heavy meson chiral Lagrangian density<sup>[17]</sup>

$$\begin{aligned} \mathcal{L} = & \frac{f^2}{8} \text{Tr}(\partial^\mu \Sigma \partial_\mu \Sigma^\dagger) + \lambda_0 \text{Tr}(m_q \Sigma + m_q \Sigma^\dagger) - i \text{Tr} \bar{H}_a v_\mu \partial^\mu H_a \\ & + \frac{i}{2} \text{Tr} \bar{H}_a H_b v_\mu (\xi^\dagger \partial^\mu \xi + \xi \partial^\mu \xi^\dagger)_{ba} + \frac{ig}{2} \text{Tr} \bar{H}_a H_b \gamma_\mu \gamma_5 (\xi^\dagger \partial^\mu \xi - \xi \partial^\mu \xi^\dagger)_{ba} \\ & + \lambda_1 \text{Tr} \bar{H}_a H_b (\xi m_q \xi + \xi^\dagger m_q \xi^\dagger)_{ba} + \lambda'_1 \text{Tr} \bar{H}_a H_a (m_q \Sigma + m_q \Sigma^\dagger)_{bb} \\ & + \frac{\lambda_2}{m_Q} \text{Tr} \bar{H}_a \sigma_{\mu\nu} H_a \sigma^{\mu\nu} + \dots, \end{aligned} \quad (3.2.4)$$

where the ellipsis denotes terms with additional derivatives, factors of the light quark mass matrix

$$m_q = \begin{pmatrix} m_u & 0 & 0 \\ 0 & m_d & 0 \\ 0 & 0 & m_s \end{pmatrix} \quad (3.2.5)$$

associated with explicit violation of  $SU(3)_L \times SU(3)_R$  chiral symmetry, or factors of  $1/m_Q$  associated with violation of heavy quark spin-flavor symmetry. In the Lagrangian density (3.2.4) the light quark flavor indices  $a, b$  run over 1, 2, 3 and repeated indices are summed.

Heavy quark symmetry and chiral symmetry put constraints on  $B_{\ell 4}$  and  $D_{\ell 4}$  semileptonic weak decay amplitudes [17,18,19]. In this chapter we investigate the implications of these symmetries for  $D \rightarrow K\pi\bar{\ell}\nu_\ell$ ,  $D \rightarrow \pi\pi\bar{\ell}\nu_\ell$ ,  $B \rightarrow \pi\pi\ell\bar{\nu}_\ell$  and  $B \rightarrow D\pi\ell\bar{\nu}_\ell$  decays. The decay  $B \rightarrow D^*\pi\ell\bar{\nu}_\ell$  is studied in the next chapter.

Heavy quark flavor symmetry implies that, to leading order in  $\Lambda_{QCD}/m_Q$ , the unknown coupling  $g$  is independent of heavy quark flavor. For  $Q = c$ , the  $D^* \rightarrow D\pi$  decay width is determined by  $g$

$$\Gamma(D^{*+} \rightarrow D^0\pi^+) = \left(\frac{1}{6\pi}\right) \frac{g^2}{f^2} |\vec{p}_\pi|^3. \quad (3.2.6)$$

The present experimental limit<sup>[20]</sup> on this width ( $\Gamma(D^{*+} \rightarrow D^0\pi^+) < 72$  KeV) implies that  $g^2 < 0.4$ . Applying the Noether procedure, the Lagrangian density (3.2.4) gives the following expression for the axial current,

$$\bar{q}_a T_{ab} \gamma_\nu \gamma_5 q_b = -g \text{Tr} \bar{H}_a H_b \gamma_\nu \gamma_5 T_{ba} + \dots \quad (3.2.7)$$

In eq. (3.2.7) the ellipsis represents terms containing the pseudo-Goldstone boson fields and  $T$  is a flavor  $SU(3)$  generator. Treating the quark fields in eq. (3.2.7) as constituent quarks and using the non-relativistic quark model (i.e., static  $SU(6)$ ) to estimate the  $D^*$  matrix element of the l.h.s. of eq. (3.2.7) gives<sup>[19]</sup>  $g = 1$ . (A similar estimate for the pion-nucleon coupling gives  $g_A = 5/3$ .) In the chiral quark model<sup>[21]</sup> there is a constituent-quark pion coupling. Using the measured pion nucleon coupling to determine the constituent-quark pion coupling gives that  $g \approx 0.75$ . The decay  $B^* \rightarrow B\pi$  is kinematically forbidden and so it will not be possible to use it to test the heavy quark flavor independence of  $g$ . The amplitude for the semileptonic decay  $B \rightarrow D\pi\ell\bar{\nu}_\ell$ , in the kinematic region where the pion has low momentum (and the  $D\pi$  mass is greater than that of the  $D^*$ ), can be predicted using chiral perturbation theory. In principle, experimental study of this decay can give information on the flavor dependence of  $g$ .

In the next section we discuss the kinematics of weak semileptonic  $D_{\ell 4}$  and  $B_{\ell 4}$  decay. The fully differential decay rates are expressed in terms of form factors.

The results of section 3.2 are a slight modification of the kinematics of  $K_{\ell 4}$  decay to the situation where the two hadrons in the final state have different masses. The generalization of  $K_{\ell 4}$  decay kinematics to  $D \rightarrow K\pi\bar{\ell}\nu_{\ell}$  decay was previously discussed by Kane *et al.*<sup>[22]</sup> We have included a short review of the kinematics for completeness. Section 3.3 gives the predictions of chiral perturbation theory for  $D \rightarrow K\pi\bar{\ell}\nu_{\ell}$ ,  $D \rightarrow \pi\pi\bar{\ell}\nu_{\ell}$  and  $B \rightarrow \pi\pi\bar{\ell}\nu_{\ell}$  decay form factors. In Section 3.4 the predictions of chiral perturbation theory for  $B \rightarrow D\pi\bar{\ell}\nu_{\ell}$  are given. Section 3.5 contains a brief discussion of the expected kinematic range where chiral perturbation theory for  $B \rightarrow D\pi\bar{\ell}\nu_{\ell}$  is applicable. Concluding remarks are made in Section 3.6.

For  $B_{\ell 4}$  and  $D_{\ell 4}$  decay the kinematic region where chiral perturbation theory is applicable is small. In the kinematic region where chiral perturbation theory is applicable  $\text{Br}(B \rightarrow D\pi\bar{\ell}\nu_{\ell}) \sim (1/16\pi^2) \text{Br}(B \rightarrow D\bar{\ell}\nu_{\ell}) \sim 10^{-4}$ . The situation is worse for the modes with two pseudo-Goldstone bosons in the final state. For example, we expect that  $\text{Br}(D \rightarrow \pi\pi\bar{\ell}\nu_{\ell}) \sim (1/16\pi^2) \sin^2\theta_c (f_D/m_D)^2 \text{Br}(D \rightarrow X_s\bar{\ell}\nu_{\ell})$ , where  $f_D$  is the decay constant for the  $D$ -meson. For  $f_D \sim 200$  MeV this crude order of magnitude estimate gives  $\text{Br}(D \rightarrow \pi\pi\bar{\ell}\nu_{\ell}) \sim 10^{-6}$ . The factor of  $\sin^2\theta_c$  is absent for the Cabibbo allowed decay  $D \rightarrow K\pi\bar{\ell}\nu_{\ell}$ , but the fact that the kaon mass is not very small makes the validity of lowest order chiral perturbation theory dubious. It will be very difficult, in the kinematic region where chiral perturbation theory applies, to observe  $B_{\ell 4}$  and  $D_{\ell 4}$  decay to two pseudo-Goldstone bosons. However, the results of this chapter may still prove useful for these decays. Phenomenological models that predict the form factors over the whole phase space should be constrained to agree with chiral perturbation theory in the kinematic region where it applies.

### 3.3. REVIEW OF THE KINEMATICS

Consider for definiteness the decay  $D \rightarrow K\pi\bar{\ell}\nu_{\ell}$ . At the end of this section we show how to modify the formulae so they apply to the other decays we are considering. It is convenient, following the analysis of  $K_{\ell 4}$  decay by Pais and Treiman<sup>[23]</sup>, to form the following combinations of four-momenta

$$P = p_K + p_{\pi}, \quad Q = p_K - p_{\pi}, \quad L = p_{\ell} + p_{\nu_{\ell}}, \quad N = p_{\ell} - p_{\nu_{\ell}}. \quad (3.3.1)$$

Like  $K_{\ell 4}$  decay,  $D_{\ell 4}$  decay is kinematically parametrized by five variables. For two of

these we take the  $K\pi$  and  $\bar{\ell}\nu_\ell$  squared masses:

$$s_H = P^2, \quad s_L = L^2. \quad (3.3.2)$$

For the remaining three variables we choose:  $\theta_H$ , the angle formed by the kaon three-momentum in the  $K\pi$  rest frame and the line of flight of the  $K\pi$  in the  $D$  rest frame;  $\theta_L$ , the angle formed by the  $\bar{\ell}$  three-momentum in the  $\bar{\ell}\nu_\ell$  rest frame and the line of flight of the  $\bar{\ell}\nu_\ell$  in the  $D$  rest frame;  $\phi$ , the angle between the normals to the planes defined in the  $D$  rest frame by the  $K\pi$  pair and the  $\bar{\ell}\nu_\ell$  pair. (The sense of the angle is from the normal to the  $K\pi$  plane to the normal to the  $\bar{\ell}\nu_\ell$  plane.)

Over most of the available phase space (including the kinematic regime where chiral perturbation theory can be applied) the mass of the lepton can be neglected (i.e.,  $m_\ell^2/s_L \ll 1$ ) and we find that with  $m_\ell = 0$ ;

$$P \cdot L = \frac{m_D^2 - s_H - s_L}{2}, \quad (3.3.3a)$$

$$L \cdot N = 0, \quad P \cdot Q = m_K^2 - m_\pi^2, \quad (3.3.3b)$$

$$Q^2 = 2(m_K^2 + m_\pi^2) - s_H, \quad N^2 = -s_L, \quad (3.3.3c)$$

$$L \cdot Q = \left( \frac{m_K^2 - m_\pi^2}{s_H} \right) P \cdot L + \beta X \cos \theta_H, \quad (3.3.3d)$$

$$P \cdot N = X \cos \theta_L \quad (3.3.3e)$$

$$Q \cdot N = \left( \frac{m_K^2 - m_\pi^2}{s_{K\pi}} \right) X \cos \theta_L + \beta P \cdot L \cos \theta_H \cos \theta_L \\ - \beta (s_L s_H)^{1/2} \sin \theta_H \sin \theta_L \cos \phi, \quad (3.3.3f)$$

$$\epsilon_{\mu\nu\rho\sigma} Q^\mu P^\nu N^\rho L^\sigma = -\beta X (s_L s_H)^{1/2} \sin \theta_H \sin \theta_L \sin \phi. \quad (3.3.3g)$$

In eqs. (3.3.3)

$$X = [(P \cdot L)^2 - s_H s_L]^{1/2}, \quad (3.3.4)$$

and  $\beta$  is  $(2/\sqrt{s_H})$  times the magnitude of the kaon three-momentum in the  $K\pi$  rest frame,

$$\beta = [s_H^2 + m_\pi^4 + m_K^4 - 2m_K^2 m_\pi^2 - 2s_H m_K^2 - 2s_H m_\pi^2]^{1/2} / s_H. \quad (3.3.5)$$

Taking the limit,  $m_K = m_\pi$ , eqs. (3.3.3) agree with the results of Pais and Treiman for  $K_{\ell 4}$  decay.

The invariant matrix element for  $D \rightarrow K\pi\bar{\ell}\nu_\ell$  semileptonic decay is

$$\mathcal{M}_{fi} = \frac{G_F}{\sqrt{2}} V_{cs} \langle \pi(p_\pi), K(p_K) | \bar{s}\gamma_\mu(1 - \gamma_5)c | D(p_D) \rangle \bar{u}(p_\nu)\gamma^\mu(1 - \gamma_5)v(p_\ell), \quad (3.3.6)$$

where  $V_{cs}$  is the  $c \rightarrow s$  element of the Cabibbo-Kobayashi-Maskawa matrix and  $G_F$  is the Fermi constant. The hadronic matrix element can be written in terms of four form factors  $w_\pm, r$  and  $h$  that are defined by

$$\langle \pi(p_\pi), K(p_K) | \bar{s}\gamma_\mu(1 - \gamma_5)c | D(p_D) \rangle = iw_+P_\mu + iw_-Q_\mu + ir(p_D - P)_\mu + h\epsilon_{\mu\alpha\beta\gamma}p_D^\alpha P^\beta Q^\gamma. \quad (3.3.7)$$

The form factors  $w_\pm, r$  and  $h$  are functions of  $s_L, s_H$  and  $\cos\theta_H$ . Summing over the lepton polarizations the absolute value of the square of the matrix element is

$$\sum_{\text{spins}} |\mathcal{M}_{fi}|^2 = 4G_F^2 |V_{cs}|^2 H_{\mu\nu} L^{\mu\nu}, \quad (3.3.8)$$

where

$$H_{\mu\nu} = \langle \pi(p_\pi), K(p_K) | \bar{s}\gamma_\mu(1 - \gamma_5)c | D(p_D) \rangle \cdot \langle \pi(p_\pi), K(p_K) | \bar{s}\gamma_\nu(1 - \gamma_5)c | D(p_D) \rangle^*, \quad (3.3.9a)$$

$$L^{\mu\nu} = \frac{1}{2} [L^\mu L^\nu - N^\mu N^\nu - s_L g^{\mu\nu} - i\epsilon^{\alpha\mu\gamma\nu} L_\alpha N_\gamma], \quad (3.3.9b)$$

with the convention  $\epsilon_{0123} = +1$ . The differential decay rate takes the form

$$d^5\Gamma = \frac{G_F^2 |V_{cs}|^2}{(4\pi)^6 m_D^3} X \beta I(s_H, s_L, \theta_H, \theta_L, \phi) ds_L ds_H d\cos\theta_H d\cos\theta_L d\phi. \quad (3.3.10)$$

The dependence of  $I$  on  $\theta_L$  and  $\phi$  is given by

$$I = I_1 + I_2 \cos 2\theta_L + I_3 \sin^2 \theta_L \cos 2\phi + I_4 \sin 2\theta_L \cos \phi + I_5 \sin \theta_L \cos \phi + I_6 \cos \theta_L + I_7 \sin \theta_L \sin \phi + I_8 \sin 2\theta_L \sin \phi + I_9 \sin^2 \theta_L \sin 2\phi \quad (3.3.11)$$

where  $I_1, \dots, I_9$  depend on  $s_H, s_L$  and  $\theta_H$ .

To display  $I_1, \dots, I_9$  in as compact form as possible it is convenient to introduce the following combinations of kinematic factors and form factors

$$F_1 = Xw_+ + [\beta P \cdot L \cos\theta_H + \left(\frac{m_K^2 - m_\pi^2}{s_H}\right) X]w_- \quad (3.3.12a)$$

$$F_2 = \beta(s_L s_H)^{1/2} w_- \quad (3.3.12b)$$

$$F_3 = \beta X(s_L s_H)^{1/2} h. \quad (3.3.12c)$$

Observe that  $r$  does not appear in eqs. (3.3.12) because its contributions vanish for  $m_\ell = 0$ . In terms of these combinations of form factors

$$I_1 = \frac{1}{4} \left\{ |F_1|^2 + \frac{3}{2} \sin^2 \theta_H (|F_2|^2 + |F_3|^2) \right\} \quad (3.3.13a)$$

$$I_2 = -\frac{1}{4} \left\{ |F_1|^2 - \frac{1}{2} \sin^2 \theta_H (|F_2|^2 + |F_3|^2) \right\} \quad (3.3.13b)$$

$$I_3 = -\frac{1}{4} [ |F_2|^2 - |F_3|^2 ] \sin^2 \theta_H \quad (3.3.13c)$$

$$I_4 = \frac{1}{2} \text{Re}(F_1^* F_2) \sin \theta_H \quad (3.3.13d)$$

$$I_5 = \text{Re}(F_1^* F_3) \sin \theta_H \quad (3.3.13e)$$

$$I_6 = \text{Re}(F_2^* F_3) \sin^2 \theta_H \quad (3.3.13f)$$

$$I_7 = \text{Im}(F_1 F_2^*) \sin \theta_H \quad (3.3.13g)$$

$$I_8 = \frac{1}{2} \text{Im}(F_1 F_3^*) \sin \theta_H \quad (3.3.13h)$$

$$I_9 = -\frac{1}{2} \text{Im}(F_2 F_3^*) \sin^2 \theta_H. \quad (3.3.13i)$$

Eqs. (3.3.11) and (3.3.13) are the same as eqs. (11) of Pais and Treiman. However, the definitions of  $F_1, F_2$  and  $F_3$  are slightly different because  $m_K \neq m_\pi$ .

It is evident from eqs. (3.3.13) that the partial wave expansions for the form factors  $F_1, F_2$  and  $F_3$  are

$$F_1(s_H, s_L, \cos \theta_H) = \sum_{\ell=0}^{\infty} \tilde{F}_{1,\ell}(s_H, s_L) P_\ell(\cos \theta_H), \quad (3.3.14a)$$

$$F_2(s_H, s_L, \cos \theta_H) = \sum_{\ell=1}^{\infty} \frac{1}{[\ell(\ell+1)]^{1/2}} \tilde{F}_{2,\ell}(s_H, s_L) \frac{d}{d \cos \theta_H} P_\ell(\cos \theta_H), \quad (3.3.14b)$$

$$F_3(s_H, s_L, \cos \theta_H) = \sum_{\ell=1}^{\infty} \frac{1}{[\ell(\ell+1)]^{1/2}} \tilde{F}_{3,\ell}(s_H, s_L) \frac{d}{d \cos \theta_H} P_\ell(\cos \theta_H). \quad (3.3.14c)$$

Integrating over the angles gives

$$d^2 \Gamma = \frac{G_F^2 |V_{cs}|^2}{3(4\pi)^5 m_D^3} X \beta \sum_{\ell} \frac{2}{2\ell+1} \left[ |\tilde{F}_{1,\ell}|^2 + |\tilde{F}_{2,\ell}|^2 + |\tilde{F}_{3,\ell}|^2 \right] ds_L ds_H, \quad (3.3.15)$$

and the total decay rate is

$$\Gamma = \int_{(m_K+m_\pi)^2}^{m_D^2} \left[ \int_0^{(m_D-\sqrt{s_H})^2} \left( \frac{d^2 \Gamma}{ds_H ds_L} \right) ds_L \right] ds_H. \quad (3.3.16)$$

$$\Gamma = \int_{(m_K+m_\pi)^2}^{m_D^2} \left[ \int_0^{(m_D-s_H^{1/2})^2} \left( \frac{d^2\Gamma}{ds_L ds_H} \right) ds_L \right] ds_H . \quad (3.3.17)$$

One advantage of the variables  $\theta_H, \theta_L, \phi, s_L$  and  $s_H$  is that in terms of these variables the region of phase space integration is quite simple. The angles are unrestricted and eq. (3.3.17) gives the region for  $s_H$  and  $s_L$ .

Although we have focused on  $D \rightarrow K\pi\bar{\ell}\nu_\ell$  decay the results presented above can be straightforwardly altered to apply to the other decays we discuss in this chapter. For  $D \rightarrow \pi\pi\bar{\ell}\nu_\ell$  decay one simply changes  $V_{cs} \rightarrow V_{cd}$  and  $m_K \rightarrow m_\pi$ . For  $B \rightarrow \pi\pi\bar{\ell}\nu_\ell$  decay one changes  $V_{cs} \rightarrow V_{ub}^*$ ,  $m_D \rightarrow m_B$  and  $m_K \rightarrow m_\pi$ . Also, in eq. (3.3.6)  $p_{\bar{\ell}}$  and  $p_\nu$  are switched. Consequently the term proportional to the alternating tensor in eq. (3.3.9b) and the expressions for  $I_5, I_6$  and  $I_7$  in eqs. (3.3.13e), (3.3.13f) and (3.3.13g) change sign. Finally, for  $B \rightarrow D\pi\bar{\ell}\nu_\ell$  decay the changes  $V_{cs} \rightarrow V_{cb}^*$ ,  $m_D \rightarrow m_B, m_K \rightarrow m_D$  and the same sign changes as for  $B \rightarrow \pi\pi\bar{\ell}\nu_\ell$  decay are made.

### 3.4. DECAYS TO TWO PSEUDO-GOLDSTONE BOSONS

The semileptonic decays  $D \rightarrow K\pi\bar{\ell}\nu_\ell$ ,  $D \rightarrow \pi\pi\bar{\ell}\nu_\ell$  and  $B \rightarrow \pi\pi\bar{\ell}\nu_\ell$  are determined by matrix elements of the left-handed current

$$L_{\nu a} = \bar{q}^a \gamma_\nu (1 - \gamma_5) Q . \quad (3.4.1)$$

This operator transforms under chiral  $SU(3)_L \times SU(3)_R$  as  $(\bar{3}_L, 1_R)$ . In chiral perturbation theory its matrix elements are given by those of

$$L_{\nu a} = \left( \frac{i\alpha}{2} \right) \text{Tr} \gamma_\nu (1 - \gamma_5) H_b \xi_{ba}^\dagger + \dots , \quad (3.4.2)$$

where the ellipsis denotes terms with derivatives, factors of the light quark mass matrix  $m_q$  or factors of  $1/m_Q$ . The constant  $\alpha$  is related to the decay constant of the heavy meson,

$$\langle 0 | \bar{q}^a \gamma^\nu \gamma_5 Q | P_a^{(Q)}(v) \rangle = i f_{P_a^{(Q)}} m_{P_a^{(Q)}} v^\nu . \quad (3.4.3)$$

Taking the  $P_a^{(Q)}$  to vacuum matrix element of eq. (3.4.2) (for this matrix element  $\xi^\dagger$  can be replaced by unity) gives

$$\alpha = f_{P_a^{(Q)}} \sqrt{m_{P_a^{(Q)}}} . \quad (3.4.4)$$

The parameter  $\alpha$  has a calculable logarithmic dependence on the heavy quark<sup>[1,24]</sup> mass from perturbative QCD.

For  $D_{\ell 4}$  and  $B_{\ell 4}$  decay to two pseudo-Goldstone bosons the Feynman diagrams in Fig. 7 determine the required matrix element. In Fig. 7 a solid line represents a heavy meson and a dashed line represents a pseudo-Goldstone boson. The shaded square denotes an insertion of the left handed current. The form factors  $w_{\pm}, r$  and  $h$  that follow from calculation of these Feynman diagrams are given below.

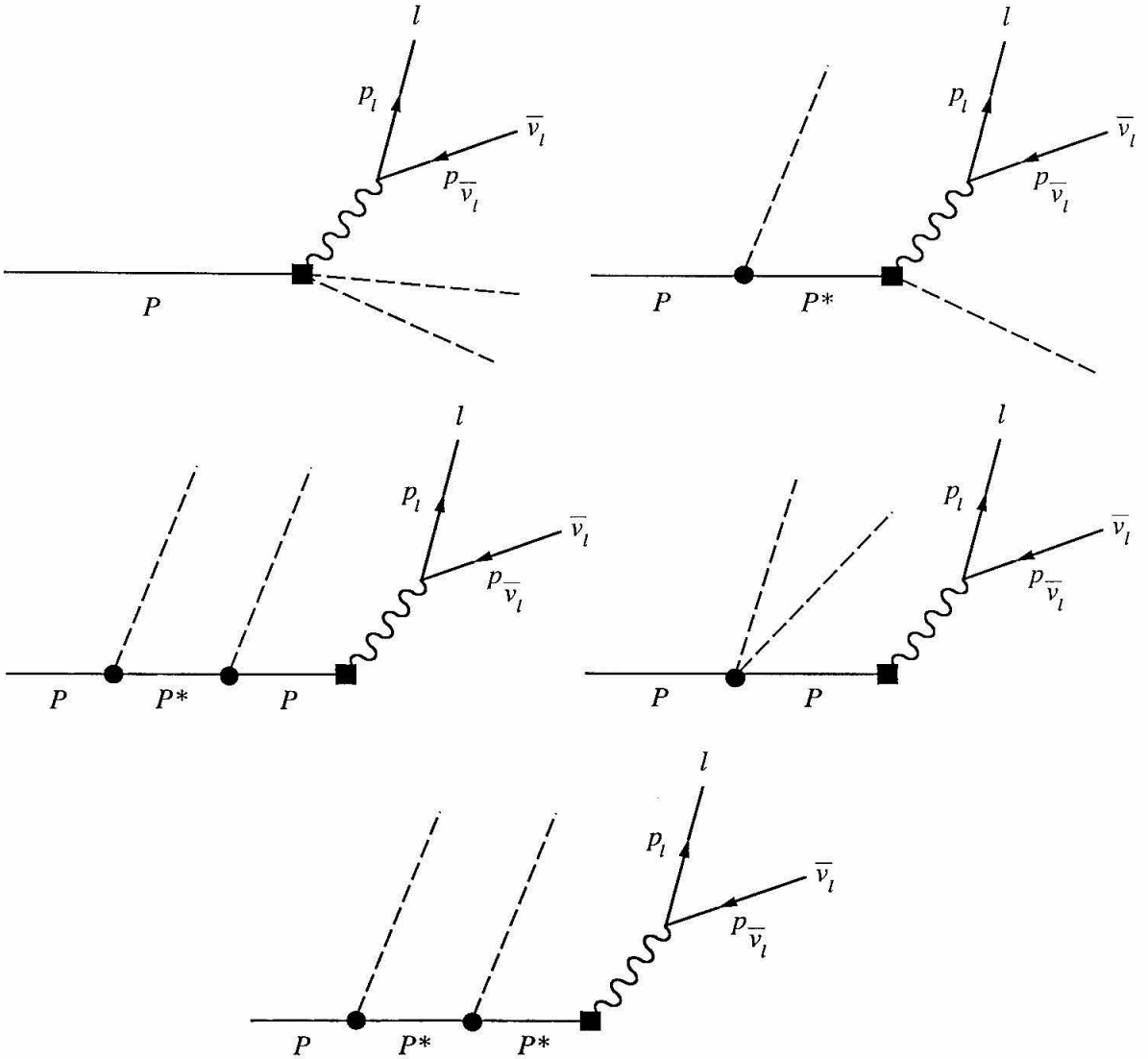


Fig. 7: Feynman diagrams for  $D \rightarrow K\pi, D \rightarrow \pi\pi$  and  $B \rightarrow \pi\pi$  matrix elements of the current  $L_{\nu\alpha}$ . The shaded square denotes an insertion of the current in eq. (3.4.2).

Dashed lines denote pseudo-Goldstone bosons.

(i)  $D \rightarrow K\pi\bar{\ell}\nu_\ell$ 

$D \rightarrow K\pi\bar{\ell}\nu_\ell$  decays are determined by  $Q = c$  matrix elements of  $L_{\nu 3}$ . For the decay  $D^+ \rightarrow K^-\pi^+\bar{\ell}\nu_\ell$ , computation of the Feynman diagrams in Fig. 7 gives

$$w_- = - \left( \frac{f_D m_D g}{2f^2} \right) \frac{1}{[v \cdot p_\pi + \Delta_c]}, \quad w_+ = -w_- + r \quad (3.4.5a)$$

$$r = \left( \frac{f_D}{f^2} \right) \left\{ \frac{1}{2} - \frac{1}{2} \frac{(v \cdot p_K - v \cdot p_\pi)}{[v \cdot (p_K + p_\pi) + \mu]} - \frac{g(v \cdot p_\pi)}{[v \cdot p_\pi + \Delta_c]} \right. \\ \left. - g^2 \frac{[p_\pi \cdot p_K - v \cdot p_K v \cdot p_\pi]}{[v \cdot (p_K + p_\pi) + \mu][v \cdot p_\pi + \Delta_c]} \right\} \quad (3.4.5b)$$

$$h = \left( \frac{f_D g^2}{2f^2} \right) \frac{1}{[v \cdot (p_\pi + p_K) + \Delta_c + \mu]} \frac{1}{[v \cdot p_\pi + \Delta_c]}. \quad (3.4.5c)$$

In eqs. (3.4.5)

$$\Delta_c = m_{D^*} - m_D, \quad (3.4.6)$$

$$\mu = m_{D_s} - m_D, \quad (3.4.7)$$

and  $v^\mu$  is the four velocity of the  $D$ -meson, i.e.,  $p_D^\mu = m_D v^\mu$ . Isospin symmetry implies that the form factors for  $D^0 \rightarrow K^-\pi^0\bar{\ell}\nu_\ell$  are  $1/\sqrt{2}$  times those above, the form factors for  $D^+ \rightarrow \bar{K}^0\pi^0\bar{\ell}\nu_\ell$  are  $-1/\sqrt{2}$  times those above, and the form factors for  $D^0 \rightarrow \bar{K}^0\pi^-\bar{\ell}\nu_\ell$  are equal to those above. It is straightforward using eqs. (3.3.2) and (3.3.3) to express these form factors in terms of  $\theta_H, s_H$  and  $s_L$ .

(ii)  $D^+ \rightarrow \pi^+\pi^-\bar{\ell}\nu_\ell$ 

For this decay a  $Q = c$  matrix element of  $L_{\nu 2}$  is needed. It is straightforward to see that the form factors in this case are given by those in eqs. (3.4.5) if the changes  $p_K \rightarrow p_{\pi^-}$  and  $p_\pi \rightarrow p_{\pi^+}$  are made and  $\mu$  is set to zero. Again using eqs. (3.3.2) and (3.3.3) these form factors can be expressed in terms of  $\theta_H, s_H$  and  $s_L$ .

(iii)  $B^- \rightarrow \pi^+\pi^-\bar{\ell}\nu_\ell$ 

In this case a  $Q = b$  matrix element of  $L_{\nu 1}$  is required. The form factors are given by those in eqs. (3.4.5) if the changes  $f_D \rightarrow f_B, m_D \rightarrow m_B, \Delta_c \rightarrow \Delta_b, p_K \rightarrow p_{\pi^+}$  and  $p_\pi \rightarrow p_{\pi^-}$  are made and  $\mu$  is set to zero. Using eqs. (3.3.2) and (3.3.3) these form factors can be expressed in terms of  $\theta_H, s_H$  and  $s_L$ .

(iv)  $D^0 \rightarrow \pi^- \pi^0 \bar{\ell} \nu_\ell$ 

In this case the  $Q = c$  matrix element of  $L_{\nu 2}$  is required. Computation of the Feynman diagrams in Fig. 7 gives that the form factors are

$$w_- = \left( \frac{g f_D m_D}{2\sqrt{2} f^2} \right) \left( \frac{1}{v \cdot p_{\pi^-} + \Delta_c} + \frac{1}{v \cdot p_{\pi^0} + \Delta_c} \right), \quad (3.4.8a)$$

$$w_+ = \left( \frac{g f_D m_D}{2\sqrt{2} f^2} \right) \left( \frac{1}{v \cdot p_{\pi^-} + \Delta_c} - \frac{1}{v \cdot p_{\pi^0} + \Delta_c} \right) + r, \quad (3.4.8b)$$

$$r = \left( \frac{f_D}{\sqrt{2} f^2} \right) \left\{ \frac{v \cdot (p_{\pi^-} - p_{\pi^0})}{v \cdot (p_{\pi^-} + p_{\pi^0})} + g \frac{(v \cdot p_{\pi^0})}{v \cdot p_{\pi^0} + \Delta_c} - g \frac{(v \cdot p_{\pi^-})}{v \cdot p_{\pi^-} + \Delta_c} - g^2 \frac{[p_{\pi^-} \cdot p_{\pi^0} - (v \cdot p_{\pi^-})(v \cdot p_{\pi^0})]}{v \cdot (p_{\pi^-} + p_{\pi^0})} \cdot \left( \frac{1}{v \cdot p_{\pi^-} + \Delta_c} - \frac{1}{v \cdot p_{\pi^0} + \Delta_c} \right) \right\}, \quad (3.4.8c)$$

$$h = - \left( \frac{f_D g^2}{2\sqrt{2} f^2} \right) \frac{1}{v \cdot (p_{\pi^-} + p_{\pi^0}) + \Delta_c} \cdot \left( \frac{1}{v \cdot p_{\pi^-} + \Delta_c} + \frac{1}{v \cdot p_{\pi^0} + \Delta_c} \right). \quad (3.4.8d)$$

It is straightforward using eqs. (3.3.2) and (3.3.3) to express these form factors in terms of  $\theta_H, s_H$  and  $s_L$ . (Here the difference of four-momenta is  $Q^\mu = p_{\pi^-}^\mu - p_{\pi^0}^\mu$ )

(v)  $B^0 \rightarrow \pi^+ \pi^0 \ell \bar{\nu}_\ell$ 

In this case the  $Q = b$  matrix element of  $L_{\nu 1}$  is needed. The form factors are given by those in eqs. (3.4.8) if the following changes are made:  $f_D \rightarrow f_B, m_D \rightarrow m_B, \Delta_c \rightarrow \Delta_b$ , and  $p_{\pi^-} \rightarrow p_{\pi^+}$ . Using eqs. (3.3.2) and (3.3.3) the form factors can be expressed in terms of  $\theta_H, s_H$  and  $s_L$ .

### 3.5. $B \rightarrow D\pi\ell\bar{\nu}_\ell$ DECAY

In this case matrix elements of the operator  $\bar{c}\gamma_\mu(1 - \gamma_5)b$  are needed. This operator is a singlet under chiral  $SU(3)_L \times SU(3)_R$  and in chiral perturbation theory its matrix elements are equal to those of

$$\bar{c}\gamma_\mu(1 - \gamma_5)b = -\eta(v \cdot v') \text{Tr} \bar{H}_a^{(c)}(v') \gamma_\mu(1 - \gamma_5) H_a^{(b)}(v) + \dots \quad (3.5.1)$$

The ellipsis in eq. (3.5.1) denotes terms with derivatives, insertions of the light quark mass matrix or factors of  $1/m_Q$ . Here the universal form factor is denoted by  $\eta(v \cdot v')$

rather than  $\xi(v \cdot v')$  as in the last chapter to avoid confusion with the use of  $\xi$  in eqs. (3.1.1) which is the conventional notation in chiral perturbation theory. The  $B \rightarrow D$  and  $B \rightarrow D^*$  matrix elements of this current are<sup>[1]</sup>

$$\langle D(v') | \bar{c} \gamma_\mu (1 - \gamma_5) b | B(v) \rangle = \sqrt{m_B m_D} \eta(v \cdot v') (v + v')_\mu \quad (3.5.2a)$$

$$\begin{aligned} \langle D^*(v', \epsilon) | \bar{c} \gamma_\mu (1 - \gamma_5) b | B(v) \rangle &= \sqrt{m_B m_{D^*}} \eta(v \cdot v') [-\epsilon_\mu^* (1 + v \cdot v') \\ &+ (\epsilon^* \cdot v) v'_\mu + i \epsilon_{\alpha\lambda\mu\sigma} \epsilon^{*\alpha} v'^\lambda v^\sigma]. \end{aligned} \quad (3.5.2b)$$

The normalization of  $\eta$  at zero recoil, i.e.,  $v \cdot v' = 1$ , is determined by heavy quark flavor symmetry and by high momentum strong interaction effects that are computable using perturbative QCD methods,<sup>[1,24-27]</sup>

$$\eta(1) \approx \left[ \frac{\alpha_s(m_b)}{\alpha_s(m_c)} \right]^{-6/25}.$$

Since the operator in eq. (3.5.1) does not involve the pseudo-Goldstone boson fields, in the leading order of chiral perturbation theory  $B \rightarrow D\pi$  matrix elements of the current are determined by the pole-type Feynman diagrams in Fig. 8. They give for a charged pion

$$w_+ - w_- = \frac{g}{f} \sqrt{m_B m_D} \eta [v \cdot v' + 1] \left( \frac{1}{v' \cdot p_\pi - \Delta_c} - \frac{1}{v \cdot p_\pi + \Delta_b} \right) + r \quad (3.5.3a)$$

$$w_+ + w_- = -\frac{g}{f} \sqrt{\frac{m_B}{m_D}} \eta \left[ \frac{p_\pi \cdot (v + v')}{v' \cdot p_\pi - \Delta_c} \right] + r \quad (3.5.3b)$$

$$r = \frac{g}{f} \sqrt{\frac{m_D}{m_B}} \eta \left[ \frac{p_\pi \cdot (v + v')}{v \cdot p_\pi + \Delta_b} \right] \quad (3.5.3c)$$

$$h = \frac{g}{2f} \frac{\eta}{\sqrt{m_B m_D}} \left( \frac{1}{v' \cdot p_\pi - \Delta_c} - \frac{1}{v \cdot p_\pi + \Delta_b} \right). \quad (3.5.3d)$$

In eqs. (3.5.3),

$$\Delta_c = m_{D^*} - m_D \approx 140 \text{ MeV} \quad (3.5.4)$$

$$\Delta_b = m_{B^*} - m_B \approx 50 \text{ MeV}. \quad (3.5.5)$$

The form factors for a neutral pion are obtained from the above by multiplying by  $\pm 1/\sqrt{2}$ .

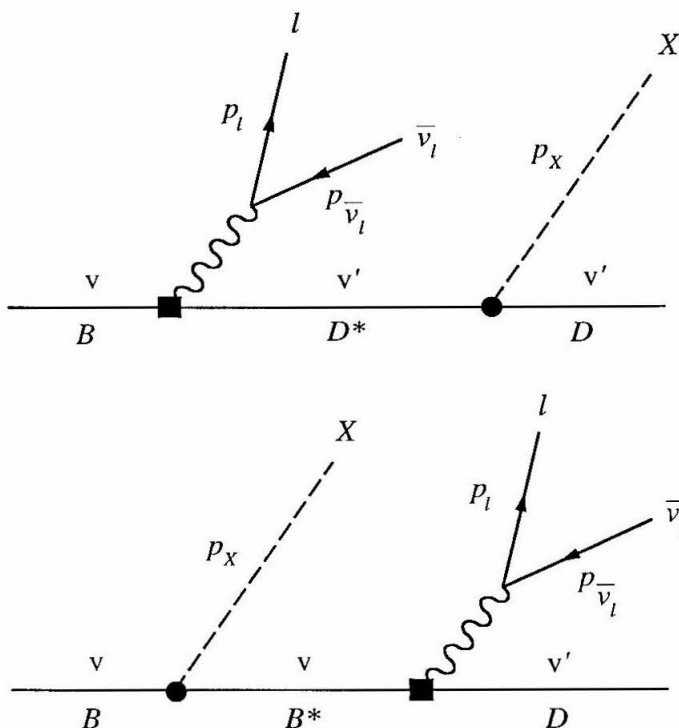


Fig. 8: Feynman diagrams for  $B \rightarrow D\pi$  matrix element of  $\bar{c}\gamma_\nu(1-\gamma_5)b$ . The shaded square denotes an insertion of the current in eq. (3.5.1).

We have assumed in writing eqs. (3.5.3) that the kinematic region is chosen so that  $v' \cdot p_\pi$  is not too close to  $\Delta_c$ . For use of the effective theory propagator to be appropriate it is necessary that

$$v' \cdot p_\pi - \Delta_c \gg m_\pi(m_\pi/2m_D) \approx 5 \text{ MeV} . \quad (3.5.6)$$

This also ensures that the  $D^*$  width can be neglected in the propagator (because it is expected to be only about a hundred KeV).

It is convenient to reexpress some of the formulae of section 3.2 in a way that makes the dependence on the heavy meson masses explicit and neglects terms suppressed by  $m_\pi/m_D$  or  $m_\pi/m_B$ . Introducing the pions four-velocity  $v_\pi^\mu = p_\pi^\mu/m_\pi$  we change integration variables from  $s_H$  and  $s_L$  to  $v' \cdot v_\pi$  and  $v \cdot v'$  using

$$ds_{D\pi} ds_L \approx 4 m_B m_\pi m_D^2 d(v' \cdot v_\pi) d(v \cdot v') . \quad (3.5.7)$$

The form factors  $F_j$  are conveniently written in terms of dimensionless quantities  $\hat{F}_j$ ,

$$F_j = \frac{m_B^{3/2} m_D^{1/2}}{f} g \eta(v \cdot v') \hat{F}_j . \quad (3.5.8)$$

Using  $\beta \approx (2m_\pi/m_D)[(v' \cdot v_\pi)^2 - 1]^{1/2}$  and  $X \approx m_B m_D [(v \cdot v')^2 - 1]^{1/2}$  the differential rate (after integrating over  $\theta_L$  and  $\phi$ ) becomes

$$d^3\Gamma = \frac{8 G_F^2 m_B^2 m_D^3 |V_{cb}|^2}{3(4\pi)^5} \left(\frac{m_\pi}{f}\right)^2 g^2 \eta^2 [(v' \cdot v_\pi)^2 - 1]^{1/2} [(v \cdot v')^2 - 1]^{1/2} \cdot [|\hat{F}_1|^2 + \sin^2 \theta_H (|\hat{F}_2|^2 + |\hat{F}_3|^2)] d(v' \cdot v_\pi) d(v' \cdot v) d \cos \theta_H. \quad (3.5.9)$$

Combining eqs. (3.5.8), (3.5.3) and (3.3.12) the dimensionless form factors  $\hat{F}_j$  are found to be:

$$\begin{aligned} \hat{F}_1 = & [(v \cdot v')^2 - 1]^{1/2} (v + v') \cdot v_\pi \left[ \left(\frac{m_D}{m_B}\right) \frac{1}{v \cdot v_\pi + \hat{\Delta}_b} - \frac{1}{v' \cdot v_\pi - \hat{\Delta}_c} \right] \\ & - v' \cdot v_\pi [v \cdot v' + 1] [(v \cdot v')^2 - 1]^{1/2} \left( \frac{1}{v \cdot v_\pi + \hat{\Delta}_b} - \frac{1}{v' \cdot v_\pi - \hat{\Delta}_c} \right) \\ + \cos \theta_H & [(v' \cdot v_\pi)^2 - 1]^{1/2} [v \cdot v' + 1] [v \cdot v' - m_D/m_B] \left( \frac{1}{v \cdot v_\pi + \hat{\Delta}_b} - \frac{1}{v' \cdot v_\pi - \hat{\Delta}_c} \right) \end{aligned} \quad (3.5.10a)$$

$$\begin{aligned} \hat{F}_2 = & [(v' \cdot v_\pi)^2 - 1]^{1/2} [v \cdot v' + 1] [1 + (m_D/m_B)^2 - 2(m_D/m_B)v \cdot v']^{1/2} \\ & \cdot \left( \frac{1}{v \cdot v_\pi + \hat{\Delta}_b} - \frac{1}{v' \cdot v_\pi - \hat{\Delta}_c} \right) \end{aligned} \quad (3.5.10b)$$

$$\begin{aligned} \hat{F}_3 = & -[(v' \cdot v_\pi)^2 - 1]^{1/2} [(v \cdot v')^2 - 1]^{1/2} [1 + (m_D/m_B)^2 - 2(m_D/m_B)v \cdot v']^{1/2} \\ & \cdot \left( \frac{1}{v \cdot v_\pi + \hat{\Delta}_b} - \frac{1}{v' \cdot v_\pi - \hat{\Delta}_c} \right). \end{aligned} \quad (3.5.10c)$$

In eqs. (3.5.10)

$$v \cdot v_\pi = (v' \cdot v_\pi)(v \cdot v') - [(v' \cdot v_\pi)^2 - 1]^{1/2} [(v \cdot v')^2 - 1]^{1/2} \cos \theta_H \quad (3.5.11)$$

and

$$\hat{\Delta}_c = (m_{D^*} - m_D)/m_\pi, \quad \hat{\Delta}_b = (m_{B^*} - m_B)/m_\pi. \quad (3.5.12)$$

Chiral perturbation theory should be valid for  $v \cdot v_\pi$  and  $v' \cdot v_\pi$  not too much greater than unity. From eq. (3.5.11) it is clear that the kinematic region where  $\cos \theta_H$  is positive yields (for given  $v' \cdot v_\pi$  and  $v \cdot v'$ ) a smaller value for  $v \cdot v_\pi$ . Note that because  $m_\pi$  and  $f$  are comparable, the rate for  $B \rightarrow D\pi\ell\bar{\nu}_\ell$  is not suppressed by factors of  $m_\pi/m_D$  or  $m_\pi/m_B$ . In fact the above formulas indicate that there is

a significant rate for  $B \rightarrow D\pi\ell\bar{\nu}_\ell$  in the kinematic region where chiral perturbation theory is expected to be applicable (and the  $D\pi$  mass is large enough to neglect the width in the virtual  $D^*$  propagator). To illustrate this we write,

$$d^3\Gamma = \frac{G_F^2 m_B^5}{192\pi^3} |V_{cb}|^2 g^2 \eta^2 d^3\hat{\Gamma}. \quad (3.5.13)$$

In Table 1 we give  $d^2\hat{\Gamma}/d(v \cdot v')d(v' \cdot v_\pi)$  for various values of  $v \cdot v'$  and  $v' \cdot v_\pi$ . Provided  $\eta$  does not fall off very rapidly as  $v' \cdot v$  increases, the rate for  $B \rightarrow D\pi\ell\bar{\nu}_\ell$ , in the region where chiral perturbation theory is expected to be applicable (i.e.,  $v \cdot v_\pi$  and  $v' \cdot v_\pi$  around unity) is comparable with what was estimated in the introduction. In Table 1 we used  $\hat{\Delta}_c = 1$ . The rate in the kinematic region where  $v_\pi \cdot v'$  is near one is quite sensitive to the value of  $\hat{\Delta}_c$ . For  $B^+ \rightarrow D^+\pi^-\ell\bar{\nu}_\ell$  decay  $\hat{\Delta}_c = 1$  is consistent with the measured masses, but for  $B^0 \rightarrow D^0\pi^+\ell\bar{\nu}_\ell$  decay  $\hat{\Delta}_c = 1$  is slightly less than the experimental value.

**TABLE 1.** Scaled Decay Rate for  $B \rightarrow D\pi\ell\bar{\nu}_\ell$

$d^2\hat{\Gamma}/d(v \cdot v')d(v' \cdot v_\pi)$  for various values of  $v \cdot v'$  and  $v' \cdot v_\pi$

$d^2\hat{\Gamma}/d(v \cdot v')d(v' \cdot v_\pi)$	$v \cdot v'$	$v' \cdot v_\pi$
0.030	1.2	1.2
0.042	1.4	1.2
0.024	1.2	1.3
0.034	1.4	1.3
0.021	1.2	1.4
0.030	1.4	1.4
0.018	1.2	1.5
0.027	1.4	1.5

### 3.6. VALIDITY OF CHIRAL PERTURBATION THEORY

Chiral perturbation theory is an expansion in momenta so our results are expected to be valid for only a limited kinematic range. For  $B \rightarrow D\pi\ell\bar{\nu}_\ell$  naive dimensional analysis suggests that the expansion parameters are  $(v \cdot p_\pi)/\Lambda$  and  $(v' \cdot p_\pi)/\Lambda$ , where  $\Lambda$  is a nonperturbative strong interaction scale around 1 GeV. However, it is far from clear precisely how small these quantities must be for the  $B \rightarrow D\pi\ell\bar{\nu}_\ell$  differential decay rate given in eqs. (3.5.9) – (3.5.12) to be a good approximation. We do have some experience from comparisons of the predictions of chiral perturbation theory for  $\pi\pi$  scattering, weak kaon decays etc., with experiment. As we shall see shortly, the situation in  $B \rightarrow D\pi\ell\bar{\nu}_\ell$  decay is somewhat different.

For  $B \rightarrow D\pi\ell\bar{\nu}_\ell$  the leading contribution is of order unity. One factor of  $p_\pi$  from the  $D^*D\pi$  (or  $B^*B\pi$ ) vertex is canceled by a factor of  $1/p_\pi$  from the  $D^*$  (or  $B^*$ ) propagator. At the next order of chiral perturbation theory, corrections come from two sources: (i) operators in the chiral Lagrangian for strong  $D^*$  and  $D$  (or  $B^*$  and  $B$ ) interactions with pions containing two derivatives or one factor of the light quark mass matrix; (ii) operators representing the weak current  $\bar{c}\gamma_\mu(1 - \gamma_5)b$  that contain one derivative.

For example, one term in the ellipsis of eq. (3.5.1) is

$$\frac{i\tilde{\eta}(v \cdot v')}{\Lambda} \text{Tr} \left( \bar{H}_a^{(c)}(v') \gamma_\mu (1 - \gamma_5) H_d^{(b)}(v) \gamma^\lambda \gamma_5 \right) [\xi^\dagger \partial_\lambda \xi - \xi \partial_\lambda \xi^\dagger]_{da}, \quad (3.6.1)$$

where  $\tilde{\eta}(v \cdot v')$  is a new universal function of  $v \cdot v'$ . This “higher order” contribution to the current  $\bar{c}\gamma_\mu(1 - \gamma_5)b$  gives rise to the following changes in the form factors  $w_\pm$ ,  $r$  and  $h$

$$\delta(w_+ - w_-) = \frac{2}{\Lambda f} \sqrt{m_B m_D} \tilde{\eta} [v \cdot v' + 1] + r \quad (3.6.2a)$$

$$\delta(w_+ + w_-) = \frac{2}{\Lambda f} \sqrt{\frac{m_B}{m_D}} \tilde{\eta} [p_\pi \cdot v] + r \quad (3.6.2b)$$

$$\delta r = \frac{2}{\Lambda f} \sqrt{\frac{m_D}{m_B}} \tilde{\eta} [p_\pi \cdot v'] \quad (3.6.2c)$$

$$\delta h = -\frac{1}{\Lambda f} \frac{\tilde{\eta}}{\sqrt{m_B m_D}}. \quad (3.6.2d)$$

For the  $\pi\pi$  phase shifts, the first corrections to the leading predictions of chiral perturbation theory are suppressed by  $s/\Lambda^2$  and come from operators in the chiral

Lagrangian with four derivatives and from one-loop diagrams. However, for  $B \rightarrow D\pi\ell\bar{\nu}_\ell$ , loops do not contribute to the leading correction which is only suppressed by  $v \cdot p_\pi/\Lambda$  or  $v' \cdot p_\pi/\Lambda$ .

There are too many higher dimension operators with unknown coefficients to make any predictions for the next order contribution to the form factors for  $B \rightarrow D\pi\ell\bar{\nu}_\ell$ . However, it is certainly possible that our leading prediction for the  $B \rightarrow D\pi\ell\bar{\nu}_\ell$  differential decay rate is valid at the 30% level over the kinematic range displayed in Table 1. Eventually the range of validity of lowest order chiral perturbation theory for  $B \rightarrow D\pi\ell\bar{\nu}_\ell$  may be determined by experiment.

### 3.7. CONCLUDING REMARKS

In this chapter the semileptonic  $B$  and  $D$  meson decays,  $D \rightarrow K\pi\bar{\ell}\nu_\ell$ ,  $D \rightarrow \pi\pi\bar{\ell}\nu_\ell$ ,  $B \rightarrow \pi\pi\bar{\ell}\nu_\ell$  and  $B \rightarrow D\pi\ell\bar{\nu}_\ell$  were considered. Chiral symmetry and heavy quark symmetry were combined to deduce the decay amplitudes in the kinematic region where the pseudo-Goldstone bosons are soft. There was earlier work on these decays that considered the implications of chiral symmetry but it did not implement heavy quark symmetry in a model independent fashion.<sup>[28]</sup>

For  $B \rightarrow D\pi\ell\bar{\nu}_\ell$  decay the rate is large enough that detailed experimental study of the decay (in the kinematic regime where chiral perturbation theory is expected to be applicable) may be possible at a  $B$  factory. Table 1 gives  $d^2\hat{\Gamma}/d(v \cdot v')d(v' \cdot v_\pi)$  for various values of  $v \cdot v'$  and  $v' \cdot v_\pi$  (see eq. (3.5.13)). These indicate that the branching ratio for semileptonic  $B_{\ell 4}$  decay to nonresonant  $D\pi$  (in the kinematic regime where the pion is soft, i.e.,  $v \cdot v_\pi$  and  $v' \cdot v_\pi$  around unity), is about  $10^{-4}$ .

The results of this chapter rely on heavy quark spin and flavor symmetry. There is experimental evidence from semileptonic  $B$  decay<sup>[29]</sup> and from the decays of excited charm mesons<sup>[30]</sup> that (at least in some cases) the charm quark is heavy enough for heavy quark symmetry to be applicable. However, several theoretical analyses suggest that there are large  $\Lambda_{QCD}/m_c$  corrections to the prediction of heavy quark symmetry for the relation between  $B$  and  $D$  meson decay constants.<sup>[31-33]</sup> If this is an isolated case, where the  $\Lambda_{QCD}/m_c$  corrections that break the flavor symmetry are anomalously large, then the results of this chapter can still be used (with  $f_B$  and  $f_D$  in Section 3.3 treated as independent constants).

Semileptonic  $B \rightarrow D\ell\bar{\nu}_\ell$  and  $B \rightarrow D^*\ell\bar{\nu}_\ell$  decay can be utilized to check that there are not large  $\Lambda_{QCD}/m_c$  corrections to the expression for the  $b \rightarrow c$  transition current in eq. (3.5.1). However, our predictions for  $B \rightarrow D\pi\ell\bar{\nu}_\ell$  decay still depend on the validity of heavy quark spin-flavor symmetry for the chiral Lagrangian in eq. (3.2.4). The dependence on the flavor symmetry arises from the equality of the  $B^*B\pi$  and  $D^*D\pi$  couplings. If heavy quark flavor symmetry is *not* used then the form factors for  $B \rightarrow D\pi\ell\bar{\nu}_\ell$  decay given in eqs. (3.5.3) of Section 3.4 become

$$w_+ - w_- = \frac{\sqrt{m_B m_D}}{f} (v \cdot v' + 1) \eta \left( \frac{g_c}{v' \cdot p_\pi - \Delta_c} - \frac{g_b}{v \cdot p_\pi + \Delta_b} \right) + r \quad (3.7.1a)$$

$$w_+ + w_- = -\frac{g_c}{f} \sqrt{\frac{m_B}{m_D}} \eta \left[ \frac{p_\pi \cdot (v + v')}{v' \cdot p_\pi - \Delta_c} \right] + r \quad (3.7.1b)$$

$$r = \frac{g_b}{f} \sqrt{\frac{m_D}{m_B}} \eta \left[ \frac{p_\pi \cdot (v + v')}{v \cdot p_\pi + \Delta_b} \right], \quad (3.7.1c)$$

$$h = \frac{1}{2f} \frac{\eta}{\sqrt{m_B m_D}} \left( \frac{g_c}{v' \cdot p_\pi - \Delta_c} - \frac{g_b}{v \cdot p_\pi + \Delta_b} \right). \quad (3.7.1d)$$

It would be interesting to use  $B \rightarrow D\pi\ell\bar{\nu}_\ell$  decay to test the heavy quark flavor symmetry prediction,  $g_b = g_c$ .

It is not known precisely for what range of  $v \cdot p_\pi$  and  $v' \cdot p_\pi$  chiral perturbation theory will be valid. Our experience with light hadrons suggests that the relevant expansion parameters are roughly  $v \cdot p_\pi/1$  GeV and  $v' \cdot p_\pi/1$  GeV. It may be possible in  $B \rightarrow D\pi\ell\bar{\nu}_\ell$  to study the range of validity of chiral perturbation theory for heavy-meson pion interactions.

A number of extensions and improvements on this work are possible. The decay  $B \rightarrow D^*\pi\ell\bar{\nu}_\ell$  is considered in the following chapter where we will explore to what extent it can also be used to fix  $g$  and to test the heavy quark flavor symmetry prediction  $g = g_b = g_c$ .<sup>[34]</sup> There are computable  $\alpha_s(m_b)$  and  $\alpha_s(m_c)$  corrections to the form factors for the decays discussed in this chapter<sup>[35-37]</sup> and it is worth examining their influence on the rates for  $B_{\ell 4}$  and  $D_{\ell 4}$  decays.

## 4. HEAVY MESON CHIRAL PERTURBATION THEORY and $B \rightarrow D^* X \ell \bar{\nu}_\ell$ DECAY

### 4.1. INTRODUCTION

This chapter investigates the implications of the heavy quark and chiral symmetries for the semi-leptonic decay  $B \rightarrow D^* X \ell \bar{\nu}_\ell$ .<sup>3</sup> The general kinematic analysis for decays of the form

$$\text{pseudoscalar meson} \rightarrow \text{vector meson} + \text{pseudoscalar meson} + \text{lepton} + \text{anti-lepton} \quad (4.1.1)$$

is given in Section 4.2. While the formalism developed here is similar to that in Chapter 3, the presentation here allows for vector mesons in the final state and the notation is also somewhat different. This kinematical framework is applied to the above exclusive decay which allows the differential decay rate to be expressed in a form that is ideally suited for the experimental determination of the different form factors for the process through angular distribution measurements. In Section 4.3, heavy quark and chiral symmetry predictions for the form factors are determined, and the differential decay rate is calculated in the kinematic region where chiral perturbation theory is valid. It is remarkable that these symmetries combine to constrain the Lagrangian so that at leading order there is only one unknown coupling  $g$  independent of the heavy quark flavor and spin. This decay could be used to probe the heavy flavor dependence of  $g$ . Concluding remarks are made in Section 4.4.

### 4.2. KINEMATICAL ANALYSIS

In this section, the kinematical framework for decays of the form given by eq. (4.1.1) is presented. For definiteness, we consider the decay  $B \rightarrow D^* X \ell \bar{\nu}_\ell$  where  $X$  is a pseudo-Goldstone boson; however, this formalism is more generally applicable to any decay of the form given by eq. (4.1.1). If  $p_B, p_{D^*}, p_X, p_\ell, p_{\bar{\nu}}$  are the four-momenta of the  $B, D^*$  (which also has a polarization vector  $\varepsilon$ ),  $X, \ell, \bar{\nu}_\ell$ , respectively, then the

---

<sup>3</sup>Based on C.L.Y. Lee, *Phys. Rev.* **D48**, 2121 (1993).<sup>[38]</sup>

kinematics of the decay can be more conveniently expressed in terms of quantities involving the following combinations of these four-momenta.

$$P = p_{D^*} + p_X \quad (4.2.1a)$$

$$Q = p_{D^*} - p_X \quad (4.2.1b)$$

$$L = p_\ell + p_{\bar{\nu}} \quad (4.2.1c)$$

$$N = p_\ell - p_{\bar{\nu}} \quad (4.2.1d)$$

Apart from spin, four-body decay is kinematically parameterized by five variables. By choosing these variables appropriately, one can express the distribution for the decay in a form where the dependence of the angular distribution on the hadronic and leptonic currents factorizes. This can be achieved by the choice<sup>[23]</sup>

- i.  $s_H = P^2$ , the effective mass of the hadron pair,  $D^*$  and  $X$ ;
- ii.  $s_L = L^2$ , the effective mass of the lepton pair,  $\ell$  and  $\bar{\nu}_\ell$ ;
- iii.  $\theta_H$ , the angle between the  $D^*$  three-momentum in the  $D^*X$  rest frame and the line of flight of the  $D^*X$  in the rest frame of the  $B$ ;
- iv.  $\theta_L$ , the angle between the  $\ell$  three-momentum in the  $\ell\bar{\nu}_\ell$  rest frame and the line of flight of the  $\ell\bar{\nu}_\ell$  in the rest frame of the  $B$ ;
- v.  $\phi$ , the angle from the normal of the plane formed by the hadron pair to the normal of the plane formed by the lepton pair.

In the following analysis, one finds that over much of the available phase space including the region where chiral perturbation theory is valid, terms that depend on the mass of the lepton are suppressed by  $m_\ell/s_L \ll 1$ , so that the lepton mass may be neglected. With  $m_\ell = 0$ ,

$$Q^2 = 2(m_{D^*}^2 + m_X^2) - s_H = (\chi^2 - U^2)s_H, \quad (4.2.2a)$$

$$N^2 = -s_L, \quad (4.2.2b)$$

$$P \cdot L = V = \frac{m_B^2 - s_H - s_L}{2}, \quad (4.2.2c)$$

$$P \cdot Q = m_{D^*}^2 - m_X^2 = \chi s_H, \quad (4.2.2d)$$

$$P \cdot N = W \cos \theta_L, \quad (4.2.2e)$$

$$L \cdot N = 0, \quad (4.2.2f)$$

$$Q \cdot L = \chi V + UW \cos \theta_H, \quad (4.2.2g)$$

$$Q \cdot N = (\chi W + UV \cos \theta_H) \cos \theta_L - U \sqrt{s_H s_L} \sin \theta_H \sin \theta_L \cos \phi, \quad (4.2.2h)$$

$$\epsilon_{\mu\nu\rho\sigma} P^\mu Q^\nu L^\rho N^\sigma = -UW \sqrt{s_H s_L} \sin \theta_H \sin \theta_L \sin \phi, \quad (4.2.2i)$$

(where the convention for the anti-symmetric tensor is  $\epsilon^{0123} = +1$ .) In eqs. (4.2.2)

$$\chi = \frac{m_{D^*}^2 - m_X^2}{s_H}, \quad (4.2.3a)$$

$U$  is the magnitude of the  $D^*$  three-momentum in the  $D^*X$  rest frame,

$$U = (s_H^2 + m_{D^*}^4 + m_X^4 - 2s_H m_{D^*}^2 - 2s_H m_X^2 - 2m_{D^*}^2 m_X^2)^{1/2} / s_H, \quad (4.2.3b)$$

and

$$W = (V^2 - s_H s_L)^{1/2}. \quad (4.2.3c)$$

The invariant transition amplitude for the decay  $B \rightarrow D^* X \ell \bar{\nu}_\ell$  is given by

$$\mathcal{M}_{fi} = \frac{G_F}{\sqrt{2}} V_{cb}^* \langle X(p_X) D^*(p_{D^*}, \varepsilon) | \bar{c} \gamma_\mu (1 - \gamma_5) b | B(p_B) \rangle \bar{u}(p_\ell) \gamma^\mu (1 - \gamma_5) v(p_{\bar{\nu}}), \quad (4.2.4)$$

where  $G_F$  is the Fermi constant and  $V_{cb}^*$  is the Cabibbo-Kobayashi-Maskawa matrix element for  $b \rightarrow c$  transitions. The hadronic matrix element can be expressed in terms of fifteen form factors:

$$\begin{aligned} & \langle X(p_X), D^*(p_{D^*}, \varepsilon) | \bar{c} \gamma_\mu (1 - \gamma_5) b | B(p_B) \rangle \\ &= \left[ i(a_+ \varepsilon^* \cdot P + b_+ \varepsilon^* \cdot p_B) + \frac{w_+}{2} \epsilon_{\alpha\beta\gamma\delta} L^\alpha P^\beta Q^\gamma \varepsilon^{*\delta} \right] P_\mu \\ &+ \left[ i(a_- \varepsilon^* \cdot P + b_- \varepsilon^* \cdot p_B) + \frac{w_-}{2} \epsilon_{\alpha\beta\gamma\delta} L^\alpha P^\beta Q^\gamma \varepsilon^{*\delta} \right] Q_\mu \\ &+ \left[ i(c \varepsilon^* \cdot P + d \varepsilon^* \cdot p_B) + \frac{w}{2} \epsilon_{\alpha\beta\gamma\delta} L^\alpha P^\beta Q^\gamma \varepsilon^{*\delta} \right] L_\mu \\ &+ i t \varepsilon^*_\mu \\ &+ g_+ \epsilon_{\mu\alpha\beta\gamma} L^\alpha P^\beta \varepsilon^{*\gamma} + g_- \epsilon_{\mu\alpha\beta\gamma} L^\alpha Q^\beta \varepsilon^{*\gamma} + r \epsilon_{\mu\alpha\beta\gamma} P^\alpha Q^\beta \varepsilon^{*\gamma} \\ &+ (u_1 \varepsilon^* \cdot P + u_2 \varepsilon^* \cdot p_B) \epsilon_{\mu\alpha\beta\gamma} L^\alpha P^\beta Q^\gamma, \end{aligned} \quad (4.2.5)$$

where the form factors  $a_\pm, b_\pm, c, d, g_\pm, \tilde{r}, t, u_1, u_2, w$ , and  $w_\pm$  are functions of  $s_H, s_L$ , and  $\theta_H$ . The absolute value of the transition amplitude squared when summed over the vector meson and lepton polarizations is then

$$\sum_{\text{spins}} |\mathcal{M}_{fi}|^2 = \frac{G_F^2}{2} |V_{cb}|^2 H_{\mu\nu} L^{\mu\nu}, \quad (4.2.6)$$

where

$$H_{\mu\nu} = \langle X(p_X), D^*(p_{D^*}, \varepsilon) | \bar{c} \gamma_\mu (1 - \gamma_5) b | B(p_B) \rangle \\ \times \langle X(p_X), D^*(p_{D^*}, \varepsilon) | \bar{c} \gamma_\nu (1 - \gamma_5) b | B(p_B) \rangle^*, \quad (4.2.7a)$$

$$L^{\mu\nu} = 4(L^\mu L^\nu - N^\mu N^\nu - s_L g^{\mu\nu} - i \epsilon^{\alpha\mu\beta\nu} L_\alpha N_\beta). \quad (4.2.7b)$$

Using eqs. (4.2.2a-i), the differential decay rate can then be written in the form

$$d^5\Gamma = \frac{G_F^2 |V_{cb}|^2}{(4\pi)^6 m_B^3} UWI(s_H, s_L, \theta_H, \theta_L, \phi) ds_H ds_L d \cos \theta_H d \cos \theta_L d\phi, \quad (4.2.8)$$

with

$$I = I_1 + I_2 \cos 2\theta_L + I_3 \sin^2 \theta_L \cos 2\phi + I_4 \sin 2\theta_L \cos \phi + I_5 \sin \theta_L \cos \phi \\ + I_6 \cos \theta_L + I_7 \sin \theta_L \sin \phi + I_8 \sin 2\theta_L \sin \phi + I_9 \sin^2 \theta_L \sin 2\phi \quad (4.2.9)$$

where  $I_j$ ,  $1 \leq j \leq 9$ , are functions of  $s_H, s_L, \theta_H$  only. As we alluded to earlier, the separation of the variables  $s_H, s_L, \theta_H$  from  $\theta_L, \phi$  in eq. (3.3.11) is a direct consequence of this particular choice for the five variables parameterizing four-body decay. The distribution functions  $I_j$  can be written in a compact form by introducing the following combinations of kinematic factors and form factors.

$$G_1 = \frac{1}{2m_{D^*}} \left\{ \lambda s_H [W a_+ + (\chi W + UV \cos \theta_H) a_-] \right. \\ \left. + \left( \frac{m_B^2 + s_H - s_L}{2} \lambda + UW \cos \theta_H \right) [W b_+ + (\chi W + UV \cos \theta_H) b_-] \right. \\ \left. + (\lambda W + UV \cos \theta_H) t \right\} \quad (4.2.10a)$$

$$G_2 = \frac{U \sqrt{s_H s_L}}{2m_{D^*}} \left[ (\lambda s_H) a_- + \left( \frac{m_B^2 + s_H - s_L}{2} \lambda + UW \cos \theta_H \right) b_- + t \right] \quad (4.2.10b)$$

$$G_3 = \sqrt{s_H} \left\{ [W a_+ + (\chi W + UV \cos \theta_H) a_-] \right. \\ \left. + \frac{m_B^2 + s_H - s_L}{2s_H} [W b_+ + (\chi W + UV \cos \theta_H) b_-] + \frac{W}{s_H} t \right\} \quad (4.2.10c)$$

$$G_4 = U s_H \sqrt{s_L} \left( a_- + \frac{m_B^2 + s_H - s_L}{2s_H} b_- \right) \quad (4.2.10d)$$

$$G_5 = \frac{1}{\sqrt{s_H}} [W^2 b_+ + W(\chi W + UV \cos \theta_H) b_- + Vt] \quad (4.2.10e)$$

$$G_6 = UW \sqrt{s_L} b_- \quad (4.2.10f)$$

$$G_7 = \sqrt{s_L} t \quad (4.2.10g)$$

$$G_8 = \frac{UW\sqrt{s_H s_L}}{2m_{D^*}} \left[ g_+ - g_- + (\lambda s_H) u_1 + \left( \frac{m_B^2 + s_H - s_L}{2} \lambda + UW \cos \theta_H \right) u_2 \right] \quad (4.2.10h)$$

$$G_9 = \sqrt{s_L} [W g_+ + (\chi W + UV \cos \theta_H) g_- + (U s_H \cos \theta_H) r] \quad (4.2.10i)$$

$$G_{10} = U \sqrt{s_H} (s_L g_- + V r) \quad (4.2.10j)$$

$$G_{11} = UW \sqrt{s_L} \left[ g_- - \left( s_H u_1 + \frac{m_B^2 + s_H - s_L}{2} u_2 \right) \right] \quad (4.2.10k)$$

$$G_{12} = UV \sqrt{s_L} (g_- - V u_2) \quad (4.2.10l)$$

$$G_{13} = U \sqrt{s_H} s_L (g_- - V u_2) \quad (4.2.10m)$$

$$G_{14} = UV \sqrt{s_H} (r + s_L u_2) \quad (4.2.10n)$$

$$G_{15} = U s_H \sqrt{s_L} (r + s_L u_2) \quad (4.2.10o)$$

$$G_{16} = UW \sqrt{s_H} [W w_+ + (\chi W + UV \cos \theta_H) w_-] \quad (4.2.10p)$$

$$G_{17} = U^2 W s_H \sqrt{s_L} w_- \quad (4.2.10q)$$

In these equations,  $\lambda = 1 + \chi$ .

Then

$$\begin{aligned} I_1 = & \frac{1}{4} (|G_1|^2 - |G_3|^2 + |G_5|^2) + \frac{3}{4} |G_7|^2 + \frac{3}{8} |G_9|^2 \\ & + \frac{3}{8} (|G_2|^2 - |G_4|^2 + |G_6|^2 + |G_8|^2 + |G_{10}|^2 \\ & - |G_{11}|^2 + |G_{12}|^2 - |G_{13}|^2 - |G_{14}|^2 + |G_{15}|^2) \sin^2 \theta_H \\ & + \frac{1}{4} |G_{10} + G_{16}|^2 \sin^2 \theta_H + \frac{3}{8} |G_9 - G_{17}|^2 \sin^2 \theta_H \end{aligned} \quad (4.2.11a)$$

$$\begin{aligned} I_2 = & -\frac{1}{4} (|G_1|^2 - |G_3|^2 + |G_5|^2) + \frac{1}{4} |G_7|^2 + \frac{1}{8} |G_9|^2 \\ & + \frac{1}{8} (|G_2|^2 - |G_4|^2 + |G_6|^2 + |G_8|^2 + |G_{10}|^2 \\ & - |G_{11}|^2 + |G_{12}|^2 - |G_{13}|^2 - |G_{14}|^2 + |G_{15}|^2) \sin^2 \theta_H \\ & - \frac{1}{4} |G_{10} + G_{16}|^2 \sin^2 \theta_H + \frac{1}{8} |G_9 - G_{17}|^2 \sin^2 \theta_H \end{aligned} \quad (4.2.11b)$$

$$\begin{aligned} I_3 = & \frac{1}{4} (-|G_2|^2 + |G_4|^2 - |G_6|^2 + |G_8|^2 + |G_{10}|^2 \\ & - |G_{11}|^2 + |G_{12}|^2 - |G_{13}|^2 - |G_{14}|^2 + |G_{15}|^2) \sin^2 \theta_H \\ & - \frac{1}{4} |G_{17}|^2 \sin^4 \theta_H \end{aligned} \quad (4.2.11c)$$

$$I_4 = \frac{1}{2} \text{Re}(G_1 G_2^* - G_3 G_4^* + G_5 G_6^* - G_9 G_{10}^*) \sin \theta_H$$

$$+ \frac{1}{2} \text{Re}(G_{16}G_{17}^*) \sin^3 \theta_H \quad (4.2.11d)$$

$$I_5 = \text{Re}[G_1G_8^* + G_3G_{11}^* - G_5(G_{12} + G_{15})^* - G_7(G_{10} + G_{16})^*] \sin \theta_H \quad (4.2.11e)$$

$$I_6 = \text{Re}\{[G_2G_8^* + G_4G_{11}^* - G_6(G_{12} + G_{15})^*] \sin^2 \theta_H + 2G_7G_9^* - G_7G_{17}^* \sin^2 \theta_H\} \quad (4.2.11f)$$

$$I_7 = \text{Im}(G_1G_2^* - G_3G_4^* + G_5G_6^* + G_9G_{10}^*) \sin \theta_H \quad (4.2.11g)$$

$$I_8 = \frac{1}{2} \text{Im}[G_1G_8^* + G_3G_{11}^* - G_5(G_{12} + G_{15})^* + G_7(G_{13} + G_{14})^*] \sin \theta_H \quad (4.2.11h)$$

$$I_9 = -\frac{1}{2} \text{Im}[G_2G_8^* + G_4G_{11}^* - G_6(G_{12} + G_{15})^*] \sin^2 \theta_H \quad (4.2.11i)$$

Eqs.(4.2.11) indicates that the partial wave expansions for the  $G_i$  in eqs.(4.2.10) are of the form

$$G_i(s_H, s_L, \cos \theta_H) = \sum_{\ell=0}^{\infty} \tilde{G}_{i,\ell}(s_H, s_L) P_{\ell}(\cos \theta_H), \quad (4.2.12a)$$

for  $i = 1, 3, 5, 7, 9,$

$$G_i(s_H, s_L, \cos \theta_H) = \sum_{\ell=1}^{\infty} \frac{\tilde{G}_{i,\ell}(s_H, s_L)}{\sqrt{\ell(\ell+1)}} \frac{d}{d \cos \theta_H} P_{\ell}(\cos \theta_H), \quad (4.2.12b)$$

for  $i = 2, 4, 6, 8, 10, 11, 12, 13, 14, 15, 16,$  and

$$G_{17}(s_H, s_L, \cos \theta_H) = \sum_{\ell=1}^{\infty} \frac{\tilde{G}_{17,\ell}(s_H, s_L)}{\sqrt{(\ell-1)\ell(\ell+1)(\ell+2)}} \frac{d^2}{d^2 \cos \theta_H} P_{\ell}(\cos \theta_H). \quad (4.2.12c)$$

The form of the distribution given by eq.(4.2.8-4.2.12), where the dependence on the lepton angles  $(\theta_L, \phi)$  is explicit, is ideally suited for the determination of the  $I_j$ 's and hence the form factors from angular distribution measurements.

Implementing eqs. (4.2.9,4.2.11,4.2.12) in eq. (4.2.8) and integrating over the angles yields

$$d^2\Gamma = \frac{G_F^2 |V_{cb}|^2}{3(4\pi)^5 m_B^3} UW \sum_{\ell} \frac{2}{2\ell+1} \left[ |\tilde{G}_{1,\ell}|^2 - |\tilde{G}_{3,\ell}|^2 + |\tilde{G}_{5,\ell}|^2 + 2|\tilde{G}_{7,\ell}|^2 + |\tilde{G}_{9,\ell}|^2 + |\tilde{G}_{9,\ell} - \tilde{G}_{17,\ell}|^2 + |\tilde{G}_{2,\ell}|^2 - |\tilde{G}_{4,\ell}|^2 + |\tilde{G}_{6,\ell}|^2 + |\tilde{G}_{8,\ell}|^2 + |\tilde{G}_{10,\ell}|^2 - |\tilde{G}_{11,\ell}|^2 + |\tilde{G}_{12,\ell}|^2 - |\tilde{G}_{13,\ell}|^2 - |\tilde{G}_{14,\ell}|^2 + |\tilde{G}_{15,\ell}|^2 + |\tilde{G}_{10,\ell} + \tilde{G}_{16,\ell}|^2 \right]; \quad (4.2.13)$$

and the total decay rate is

$$\Gamma = \int_{(m_{D^*} + m_X)^2}^{m_B^2} \left[ \int_0^{(m_B - \sqrt{s_H})^2} \left( \frac{d^2\Gamma}{ds_H ds_L} \right) ds_L \right] ds_H. \quad (4.2.14)$$

The simplicity of the limits in the integration over phase space in eq. (4.2.14) is another advantage of our choice of the five variables describing four body decay.

### 4.3. $B \rightarrow D^* X \ell \bar{\nu}_\ell$ DECAY

All weak  $b \rightarrow c$  transitions like the decay  $B \rightarrow D^* X \ell \bar{\nu}_\ell$  are effected by the current operator  $\bar{c}\gamma_\mu(1 - \gamma_5)b$ . The form of this current in the heavy meson chiral perturbation theory is given by eq. (3.3.1) of the previous chapter. At leading order in this effective theory,  $\pi, K, \eta$  fields are absent in the operator of eq. (3.5.1), and hence the matrix element for  $B \rightarrow D^* X \ell \bar{\nu}_\ell$  decay is dominated by the tree-level pole-type Feynman graphs in Fig. 9. The Feynman rules for these diagrams are obtained by expanding out eq. (3.2.4) and (3.5.1) in powers of the pseudo-Goldstone boson fields and the heavy meson fields  $P_a$  and  $P_{a\mu}^*$ .

Calculating the Feynman diagrams for the case  $X = \pi^\pm$  gives the following predictions for the form factors.

$$a_+ = A \left( \frac{1}{2m_{D^*}} + \frac{1}{m_B} \right) \left( \frac{1}{v' \cdot p_\pi + \Delta_D} - \frac{1}{v \cdot p_\pi + \Delta_B} \right) \quad (4.3.1a)$$

$$a_- = \frac{A}{2m_{D^*}} \left( \frac{1}{v' \cdot p_\pi + \Delta_D} - \frac{1}{v \cdot p_\pi + \Delta_B} \right) \quad (4.3.1b)$$

$$b_+ = \frac{A}{2m_B} \left[ \frac{1}{m_{D^*}} \left( 1 + \frac{v \cdot p_\pi}{v \cdot p_\pi + \Delta_B} \right) + \left( \frac{1}{v \cdot p_\pi + \Delta_B} - \frac{1}{v' \cdot p_\pi} \right) \right] \quad (4.3.1c)$$

$$b_- = \frac{A}{2m_B} \left[ \frac{1}{m_{D^*}} \left( 1 + \frac{v \cdot p_\pi}{v \cdot p_\pi + \Delta_B} \right) - \left( \frac{1}{v \cdot p_\pi + \Delta_B} - \frac{1}{v' \cdot p_\pi} \right) \right] \quad (4.3.1d)$$

$$c = \frac{A}{m_B} \left( \frac{1}{v' \cdot p_\pi + \Delta_D} - \frac{1}{v \cdot p_\pi + \Delta_B} \right) \quad (4.3.1e)$$

$$d = 0 \quad (4.3.1f)$$

$$t = A \left[ \frac{v' \cdot p_\pi - (v \cdot v')(v \cdot p_\pi)}{v \cdot p_\pi + \Delta_B} + \frac{v \cdot p_\pi - v \cdot v'}{v' \cdot p_\pi} \right] \quad (4.3.1g)$$

$$g_+ = -\frac{A}{2m_B} \left[ \frac{1}{m_{D^*}} \left( \frac{v \cdot p_\pi}{v \cdot p_\pi + \Delta_B} \right) + \frac{1}{v \cdot p_\pi + \Delta_B} \right] \quad (4.3.1h)$$

$$g_- = -\frac{A}{2m_B} \left[ \frac{1}{m_{D^*}} \left( \frac{v \cdot p_\pi}{v \cdot p_\pi + \Delta_B} \right) - \frac{1}{v \cdot p_\pi + \Delta_B} \right] \quad (4.3.1i)$$

$$\begin{aligned} \tilde{r} = & -\frac{A}{2} \left\{ \frac{1}{m_B} \left[ \frac{1}{m_{D^*}} \left( \frac{v \cdot p_\pi}{v \cdot p_\pi + \Delta_B} \right) - \frac{1}{v \cdot p_\pi + \Delta_B} \right] \right. \\ & \left. + \frac{1}{m_{D^*}} \left( \frac{1 + v \cdot v'}{v' \cdot p_\pi} - \frac{1}{v \cdot p_\pi + \Delta_B} \right) \right\} \quad (4.3.1j) \end{aligned}$$

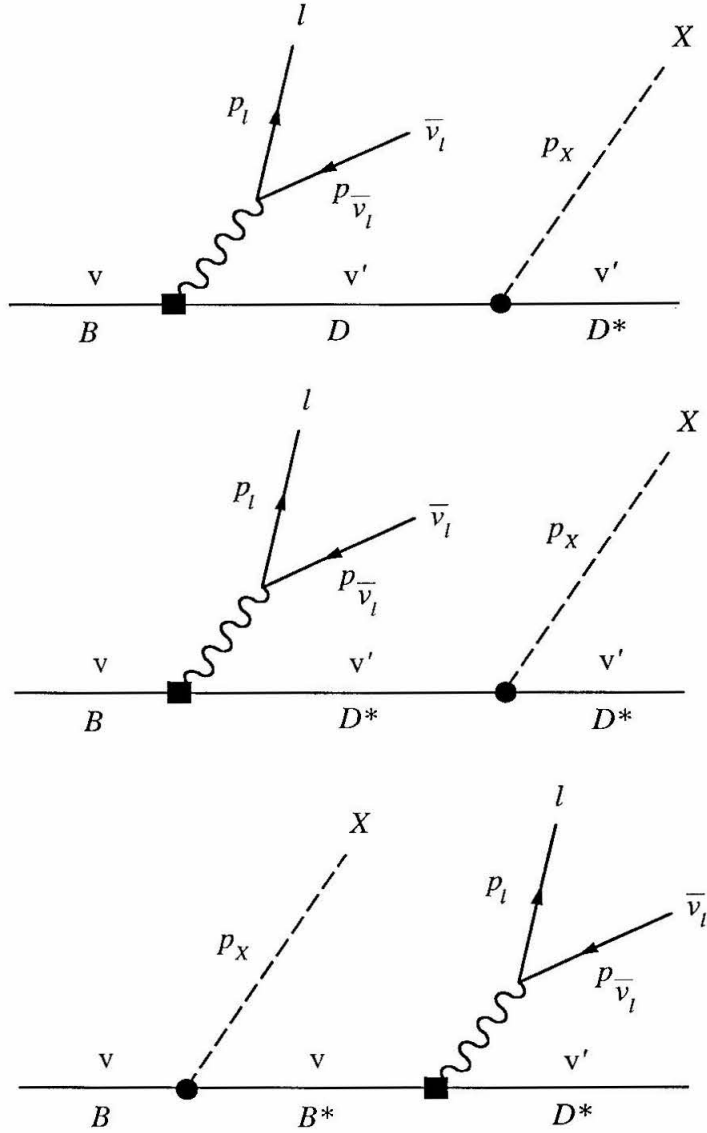


Fig. 9: Leading order Feynman diagrams for  $B \rightarrow D^* X l \bar{\nu}_l$  decay. The shaded circle represents an interaction term coming from the heavy meson chiral Lagrangian of eq. (3.2.4), and the shaded box denotes an insertion of the weak current given by eq. (3.5.1).

$$u_1 = 0 \quad (4.3.1k)$$

$$u_2 = 0 \quad (4.3.1l)$$

$$w = 0 \quad (4.3.1m)$$

$$w_+ = w_- = \frac{A}{2 m_B m_{D^*}^2 v' \cdot p_\pi} \quad (4.3.1n)$$

In these equations,

$$A = \sqrt{m_{D^*} m_B} g \eta(v \cdot v')/f \quad (4.3.2a)$$

$$\Delta_D = m_{D^*} - m_D \approx 142 \text{ MeV}, \quad (4.3.2b)$$

$$\Delta_B = m_{B^*} - m_B \approx 46 \text{ MeV}. \quad (4.3.2c)$$

Multiplying the above expressions by the factor  $\pm 1/\sqrt{2}$  gives the corresponding form factors for a neutral pion.

The above results are generally applicable when  $X$  is any of the pseudo-Goldstone bosons with appropriate modifications to take into account isospin factors. However, the large masses of the kaon and eta compared to the chiral symmetry breaking scale ( $\Lambda_\chi \sim 1 \text{ GeV}$ ) may render leading order chiral perturbation theory inadequate, so in the remainder of this analysis we will continue to take  $X$  to be a pion.

Since the masses of the heavy mesons are so much greater than that of the pseudo-Goldstone bosons, it is appropriate to make the dependence on the heavy masses manifest and to neglect terms that are suppressed by factors of  $m_\pi/m_B$  and  $m_\pi/m_{D^*}$ . The pertinent formulae in Section 4.2 can be written in this form by expressing the pion's four-momentum in terms of its four-velocity  $v_\pi^\mu = p_\pi^\mu/m_\pi$  and by changing variables from  $s_H$  and  $s_L$  to  $v \cdot v'$  and  $v' \cdot v_\pi$  so that the integration measure in eq. (4.2.8) becomes

$$ds_H ds_L \approx 4 m_B m_{D^*}^2 m_\pi d(v \cdot v') d(v' \cdot v_\pi). \quad (4.3.3)$$

Now we introduce the dimensionless quantities  $\hat{G}_j$  which are defined in terms of the  $G_j$  by

$$G_j = \frac{m_B^{3/2} m_{D^*}^{1/2} g \eta(v \cdot v')}{f} \hat{G}_j \quad (4.3.4)$$

into eq. (4.2.8). Substituting

$$U \approx \frac{2 m_\pi}{m_{D^*}} [(v' \cdot v_\pi)^2 - 1]^{1/2},$$

$$W \approx m_B m_{D^*} [(v \cdot v')^2 - 1]^{1/2},$$

and performing the integrations over  $\theta_L$  and  $\phi$  in the differential decay rate in eq. (4.2.8) yields

$$d^3\Gamma = \frac{8G_F^2 m_B^2 m_{D^*}^3 |V_{cb}|^2}{3(4\pi)^5} \left(\frac{m_\pi}{f}\right)^2 g^2 \eta(v \cdot v')^2 [(v \cdot v')^2 - 1]^{1/2} [(v' \cdot v_\pi)^2 - 1]^{1/2}$$

$$\begin{aligned}
& [ (|\hat{G}_1|^2 - |\hat{G}_3|^2 + |\hat{G}_5|^2 + 2|\hat{G}_7|^2 + |\hat{G}_9|^2 + |\hat{G}_9 - \hat{G}_{17} \sin^2 \theta_H|^2) \\
& + (|\hat{G}_2|^2 - |\hat{G}_4|^2 + |\hat{G}_6|^2 + |\hat{G}_8|^2 + |\hat{G}_{10}|^2 \\
& \quad - |\hat{G}_{11}|^2 + |\hat{G}_{12}|^2 - |\hat{G}_{13}|^2 - |\hat{G}_{14}|^2 \\
& \quad + |\hat{G}_{15}|^2 + |\hat{G}_{10} + \hat{G}_{16}|^2) \sin^2 \theta_H ] d(v \cdot v') d(v' \cdot v_\pi) d \cos \theta_H, \quad (4.3.5)
\end{aligned}$$

where

$$v \cdot v_\pi = (v \cdot v')(v' \cdot v_\pi) - [(v \cdot v')^2 - 1]^{1/2} [(v' \cdot v_\pi)^2 - 1]^{1/2} \cos \theta_H. \quad (4.3.6)$$

A source of uncertainty in eq. (4.3.5) is the Isgur-Wise function  $\eta(v \cdot v')$  since its value is only known at the zero recoil point given by  $\eta(v \cdot v' = 1) = 1$ . However, the quantity  $v \cdot v'$  is unconstrained, so this dependence on  $\eta$  can be removed by normalizing this decay rate to that for the corresponding semi-leptonic transition without the emission of pseudo-Goldstone bosons:

$$B \rightarrow D^* \ell \bar{\nu}_\ell. \quad (4.3.7)$$

This transition was considered in Section 2.4 and is mediated by the current in eq. (3.5.1).d The hadronic matrix element was determined to be

$$\begin{aligned}
& \langle D^*(v', \epsilon) | \bar{c} \gamma_\mu (1 - \gamma_5) b | B(v) \rangle \\
& = \sqrt{m_B m_{D^*}} \eta(v \cdot v') [ -(1 + v \cdot v') \epsilon_\mu^* + (\epsilon^* \cdot v) v'_\mu + i \epsilon_{\mu\alpha\beta\gamma} \epsilon^{*\alpha} v'^\beta v^\gamma ], \quad (4.3.8)
\end{aligned}$$

Then the rate could be studied away from the zero recoil point.

Since the above rate involves the ratio  $m_\pi/f$  which is close to unity, and is not suppressed by heavy quark masses, the rate for the decay as given by eq. (4.3.5) is appreciable in the region of phase space where chiral perturbation theory is valid. To show this, we introduce a scaled decay rate  $d^3 \hat{\Gamma}$  defined by

$$d^3 \Gamma = \frac{G_F^2 m_B^5}{192 \pi^3} |V_{cb}|^2 g^2 \eta(v \cdot v')^2 d^3 \hat{\Gamma}, \quad (4.3.9)$$

where  $\frac{G_F^2 m_B^5}{192 \pi^3} |V_{cb}|^2$  is the usual factor which appears in three-body decays. The differential rate  $d^2 \hat{\Gamma} / d(v \cdot v') d(v' \cdot v_\pi)$  is calculated for various values of  $v \cdot v'$  and  $v' \cdot v_\pi$  in Table 2.

**Table 2.** Scaled Decay Rate for  $B \rightarrow D^* \pi \ell \bar{\nu}_\ell$   
 $d^2 \hat{\Gamma} / d(v \cdot v') d(v' \cdot v_\pi)$  at different values of  $v \cdot v'$  and  $v' \cdot v_\pi$ .

$v \cdot v'$	$v' \cdot v_\pi$	$d^2 \hat{\Gamma} / d(v \cdot v') d(v' \cdot v_\pi)$
1.2	1.1	0.0022
1.4	1.1	0.0037
1.2	1.2	0.0033
1.4	1.2	0.0057
1.2	1.3	0.0043
1.4	1.3	0.0074
1.1	1.4	0.0022
1.2	1.4	0.0052
1.4	1.4	0.0090
1.2	1.5	0.0061
1.4	1.5	0.011

Table 2 shows that the differential rate for  $B \rightarrow D^* \pi \ell \bar{\nu}_\ell$  decay is smaller than the corresponding rate for  $B \rightarrow D \pi \ell \bar{\nu}_\ell$  decay given in Table 1 of the previous chapter. This enhancement for  $B \rightarrow D \pi \ell \bar{\nu}_\ell$  can be attributed in part to the  $D^*$  propagator in Fig. 8 which becomes on-shell as its pole is approached. However, the presence of the  $D^*$  in the decay  $B \rightarrow D^* \pi \ell \bar{\nu}_\ell$  allows this process to be selected experimentally with much better signal to background (because of the small amount of phase space available for  $D^* \rightarrow D \pi$  decay) as compared to the decay mode  $B \rightarrow D \pi \ell \bar{\nu}_\ell$ . Moreover, the decay rate for the former channel increases much more rapidly with  $v \cdot v'$  than in the latter channel. So an experimental study of  $B \rightarrow D^* \pi \ell \bar{\nu}_\ell$  decay would complement a similar study of  $B \rightarrow D \pi \ell \bar{\nu}_\ell$ . A measurement of this decay rate could be used to test heavy quark flavor symmetry: if this symmetry were violated, there would be different couplings  $g_c$  and  $g_b$  for the  $D^* D \pi$  and  $B^* B \pi$  vertices in Fig. 9 which would result in different expressions for the form factors in eqs. (4.3.1) and hence in a different decay rate.

The value that the differential decay rate takes is determined by the contributions

coming from the pole-type graphs in Fig. 9. In order for these pole diagrams to be the dominant contribution to the perturbative chiral expansion, the pseudo-Goldstone boson must be emitted with low momentum. Or equivalently, the chiral expansion parameters  $v \cdot p_\pi / \Lambda_\chi$  and  $v' \cdot p_\pi / \Lambda_\chi$  should be small — with  $v \cdot p_\pi$  and  $v' \cdot p_\pi$  on the order of a few hundred MeV. An attempt to estimate the regime where chiral perturbation theory is valid for the decay  $B \rightarrow D\pi\ell\bar{\nu}_\ell$  was made in the last chapter where it was found that predictions of next-to-leading order effects in chiral perturbation theory could not be made because there were too many new higher dimension operators with unknown coefficients. A similar study here yields the same result, but the predictions made in this chapter on the basis of leading order chiral perturbation theory may well be valid over a kinematic range much larger than that exhibited in Table 2. An experiment would ultimately establish the region of phase space where our results are valid.

#### 4.4. CONCLUDING REMARKS

In this chapter, a complete kinematical analysis for  $B \rightarrow D^*X\ell\bar{\nu}_\ell$  decay is presented. The constraints that the heavy quark and chiral symmetries impose on this decay are found to considerably simplify the dynamics and are used to determine the decay rate for this process. A number of extensions to this work can be pursued. For instance, it is interesting to determine how large symmetry-breaking effects are by calculating sub-leading  $\Lambda_{\text{QCD}}/m_c$  corrections. Decays in which more than one pseudo-Goldstone boson is emitted can also be considered.

## 5. ONE-LOOP EFFECTIVE ACTION AT ZERO AND FINITE TEMPERATURE

### 5.1. INTRODUCTION

The evaluation of quantum corrections to classical solutions is an important problem which pervades much of modern theoretical physics.<sup>4</sup> However, while effective potentials have been studied extensively, methods for determining the effective action are less well-developed. Moreover, the actual evaluation of such effects for realistic systems has often been hampered by their general intractability to analytical solution and the lack of efficient computational methods, although there have been efforts to address this problem.<sup>[39–43]</sup>

In the effective potential approximation to the effective action, quantum fluctuations are integrated out about a constant classical field — but this is not expected to be adequate because the classical field is generally an inhomogeneous configuration. The derivative expansion<sup>[44]</sup> improves on this by accounting for spatially varying background fields; its leading term is the effective potential. The expansion is a perturbative approximation which extracts the dominant contribution of short-distance quantum effects on long-distance physics. When it converges, it provides an efficient means for performing calculations. However, when it diverges, one must often resort to brute-force techniques which entail an explicit, computationally-intensive evaluation. Furthermore, the derivative expansion fails whenever the potential  $V$  is non-convex ( $V'' < 0$ ) in some region of space, which includes an important class of perturbatively calculated potentials which includes those considered in the next chapter.<sup>[45]</sup> It is clear that a general method, which is also applicable to such cases, is needed.

In this chapter, a method for calculating the quantum effects arising from the effective action is presented. The next section contains the general formalism for evaluating the effective action. Section 5.3 discusses the exact formulation of the computational method as well as extrapolation techniques which improve its convergence properties. This formalism is applied to the analysis of phase transitions in Section 5.4 and the next chapter.<sup>[45]</sup>

---

<sup>4</sup>This chapter is based on C.L.Y. Lee, *Phys. Rev.* **D49**, 4101 (1994).

Consider a scalar field theory with the Lagrangian density

$$\mathcal{L}(\phi) = \frac{1}{2} \partial_\mu \phi \partial^\mu \phi - V(\phi), \quad (5.1.1)$$

where  $V$  is the tree-level potential which has a (classical) vacuum at  $\phi_v$ . In 1+1 dimensions, the one-loop effective action for a  $\phi^4$  potential is given by an exact analytical expression presented in the next chapter.<sup>[39]</sup> In general, exact analytical solutions exist whenever the potential is reflectionless. So this chapter considers 3+1 dimensions exclusively, and renormalizability constrains  $V$  to have no polynomials in  $\phi$  of higher power than a quartic. The classical field  $\tilde{\phi}$  is determined by the equation

$$\partial_\mu \partial^\mu \tilde{\phi} = -V'(\tilde{\phi}). \quad (5.1.2)$$

The contribution of one-loop quantum effects to the effective action can be written as

$$\text{Tr} \mathcal{L}^{(1)} = \frac{i}{2} \text{Tr} \ln \left| \frac{\partial^2 + V''(\tilde{\phi})}{\partial^2 + \mu^2} \right|,$$

where  $\mu^2 = V''(\phi_v)$  and the trace runs over space-time coordinates.<sup>5</sup> Part of this trace can be evaluated as  $\text{Tr} \mathcal{L}^{(1)} = \text{Tr}' \int \langle t | \mathcal{L}^{(1)} | t \rangle dt$ , where  $\text{Tr}'$  runs over the remaining spatial degrees of freedom. Since this chapter deals only with time-independent  $\tilde{\phi}$  fields, specializing to this case means that states in the energy basis  $|\omega\rangle$  are eigenstates of the operator in  $\mathcal{L}^{(1)}$ . So inserting a complete set of such states and performing a partial integration yields

$$\text{Tr} \mathcal{L}^{(1)} = -i \int \text{Tr}' \int \left[ \frac{1}{-\omega^2 - \nabla^2 + V''(\tilde{\phi})} - \frac{1}{-\omega^2 - \nabla^2 + \mu^2} \right] \omega^2 \frac{d\omega}{2\pi} dt.$$

Observe the non-locality of this expression; this generic feature of loop corrections makes exact analytical treatments difficult. The remaining trace can be conveniently performed over the eigenstates of the operators in  $\mathcal{L}^{(1)}$ : if  $\psi_j^0$  and  $\psi_j$  are chosen such that

$$[-\nabla^2 + \mu^2] \psi_j^0 = (\omega_j^0)^2 \psi_j^0, \quad (5.1.3)$$

$$[-\nabla^2 + V''(\tilde{\phi})] \psi_j = (\omega_j)^2 \psi_j, \quad (5.1.4)$$

---

<sup>5</sup>The trace excludes possible negative and zero modes of the operator  $\partial^2 + V''(\tilde{\phi})$ . When such modes arise, they must be explicitly removed and treated differently as shown in the following chapter.<sup>[45]</sup>

where the subscript  $j$  indexes the eigenstates, then

$$\text{Tr}\mathcal{L}^{(1)} = -\frac{1}{2} \int \sum_j (\omega_j - \omega_j^0) dt.$$

Hence the one-loop effective action can be written as

$$S_{\text{eff}}(\tilde{\phi}) = \int \left[ \mathcal{L}(\tilde{\phi}) - \mathcal{L}(\phi_v) \right] d^4x + \int \left[ -\frac{1}{2} \sum_{\omega_j^0 < \Lambda} (\omega_j - \omega_j^0) + \int \mathcal{L}_{\text{ct}}(\tilde{\phi}, \Lambda) d^3x \right] dt. \quad (5.1.5)$$

The bare sum in  $\text{Tr}\mathcal{L}^{(1)}$  is divergent; it is regulated in eq. (5.1.5) by a momentum cut-off  $\Lambda$ , and a counterterm  $\mathcal{L}_{\text{ct}}(\tilde{\phi}, \Lambda)$  has been added to render it finite.

For time-independent fields  $\tilde{\phi}$ , it is more convenient to focus on the energy  $E$  of the system which is related to  $S_{\text{eff}}$  through

$$S_{\text{eff}}(\tilde{\phi}) = -E(\tilde{\phi}) \int dt.$$

Then

$$E(\tilde{\phi}) = E_{\text{cl}}(\tilde{\phi}) + E^{(1)}(\tilde{\phi}, \Lambda) + E_{\text{ct}}(\tilde{\phi}, \Lambda), \quad (5.1.6)$$

where  $E_{\text{cl}}$  is the energy of the classical field configuration

$$E_{\text{cl}}(\tilde{\phi}) = - \int \left[ \mathcal{L}(\tilde{\phi}) - \mathcal{L}(\phi_v) \right] d^3x, \quad (5.1.7)$$

$E^{(1)}$  is the one-loop contribution

$$E^{(1)}(\tilde{\phi}, \Lambda) = \frac{1}{2} \sum_{\omega_j^0 < \Lambda} (\omega_j - \omega_j^0), \quad (5.1.8)$$

and  $E_{\text{ct}}$  is the energy due to the one-loop counterterms

$$E_{\text{ct}}(\tilde{\phi}, \Lambda) = - \int \mathcal{L}_{\text{ct}}(\tilde{\phi}, \Lambda) d^3x. \quad (5.1.9)$$

At finite temperature  $T$ , the free energy  $F$  replaces  $E$ :<sup>[46]</sup>

$$F_{\text{cl}} \rightarrow E_{\text{cl}}, \quad \Delta F_1 \rightarrow E^{(1)}, \quad F^{\text{ct}} \rightarrow E_{\text{ct}}; \quad (5.1.10)$$

for bosons,  $\tilde{\phi}(\vec{x}, \tau)$  is periodic in Euclidean time  $\tau$  with period  $T^{-1}$ , and there is an additional contribution due to one-loop effects:<sup>[45]</sup>

$$\Delta F_T = T \sum_j \ln \left( \frac{1 - e^{-\omega_j/T}}{1 - e^{-\omega_j^0/T}} \right). \quad (5.1.11)$$

Observe that no additional counterterms need to be added to  $F^{\text{ct}}$  because finite temperatures do not change the short-distance behavior of the theory.

In the following section, we describe the method developed to evaluate the quantum corrections,  $\Delta F_1$  and  $\Delta F_T$ , formally given by eq. (5.1.8) and (5.1.11). While for some special situations, the  $\omega_j$  can be obtained analytically, this is unfortunately not possible for a general potential  $V''(\tilde{\phi})$ . Instead the eigenvalues must be found numerically, then for  $\Delta F_1$ , the bare sum  $\sum_{\omega_j^0 < \Lambda} (\omega_j - \omega_j^0)$  is computed explicitly, and finally the counterterm subtracted; for  $\Delta F_T$ , the sum in eq. (5.1.11) must be performed term-by-term. To attain reasonable accuracy this subtraction has to be done at a large cut-off  $\Lambda$  (to achieve convergence) when both the bare sum and the counterterm (which individually diverge as a function of the cut-off) are numerically very large. Since the final result is much smaller, each term has to be determined very precisely, resulting in a heavy computational burden. Furthermore, the straight-forward approach of evaluating the free energy by a “brute-force” term-by-term summation of the expressions in eq. (5.1.8) and (5.1.11) until convergence is reached is also computationally inefficient.

## 5.2. METHOD OF COMPUTATION

To circumvent the above-described problem of having to compute both the regulated bare sum and its counterterm to very high numerical accuracy, the three-dimensional problem is first decomposed into channels of definite angular momentum. Then for each channel, the divergent part of the bare sum is analytically removed through subtraction with the corresponding divergence in the counterterm, leaving a much smaller finite piece. Since the contribution of higher partial-wave channels decrease rapidly, this procedure overcomes the problem.

An improved computational method is then presented. It is based in part on the observation that the higher-energy modes in the spectrum of eq. (5.1.4) are less perturbed by the potential  $V''(\tilde{\phi})$  due to the non-uniform background field  $\tilde{\phi}$  than the lower-energy ones. This allows us to formulate an approximation method which accounts for the contribution of the high-energy modes accurately (where the accuracy of the approximation increases with the energy) so that only some of the lower-energy modes need to be treated exactly.<sup>[40]</sup>

## Exact Formulation

The difference in the eigenenergies  $\omega_j$  and  $\omega_j^0$  of the unbound states ( $\omega > \mu$ ) can be characterized by the phase shift between the (asymptotic forms) of the corresponding continuum state eigenfunctions  $\psi_j$  and  $\psi_j^0$ , as was first shown in one dimension.<sup>[39]</sup> Since the phase shift is generally a well-behaved, smoothly-varying function of the energy, it is relatively easy to calculate. Hence it is convenient to express the free energy in terms of this quantity. To determine the phase shift, we consider eq. (5.1.4) which determines the fluctuations about the classical field configuration.

Since most classical solutions  $\tilde{\phi}$  exhibit spherical symmetry ( $\tilde{\phi} = \tilde{\phi}(r)$ ), we will restrict our analysis to such systems. Then the solution to eq. (5.1.4) can be separated into radial and angular parts by choosing an eigenfunction of the form

$$\psi_{nlm}(r, \theta, \phi) = \frac{1}{r} u_{nl}(r) Y_{lm}(\theta, \phi), \quad (5.2.1)$$

where the radial wavefunction is determined by

$$\left[ -\frac{d^2}{dr^2} + \frac{l(l+1)}{r^2} + V''(\tilde{\phi}(r)) - \omega_{n,l}^2 \right] u_{n,l}(r) = 0 \quad (5.2.2)$$

with the boundary condition  $u_{n,l}(0) = 0$ . The  $Y_{lm}$  are the spherical harmonics corresponding to a state with total angular momentum  $l$  and  $z$ -component  $m$ .

The corresponding equation for  $u_{n,l}^0$  where  $V''(\tilde{\phi})$  is replaced by  $\mu^2$ ,

$$\left[ -\frac{d^2}{dr^2} + \frac{l(l+1)}{r^2} + \mu^2 - (\omega_{n,l}^0)^2 \right] u_{n,l}^0(r) = 0, \quad (5.2.3)$$

has an exact analytical solution:

$$u_{nl}^0(r) = \sqrt{2} k_n r j_l(k_n r) \quad (5.2.4)$$

where  $j_l$  is the  $l$ -th order spherical Bessel function of the first kind and  $k_n^2 = \omega_n^2 - \mu^2$ . These solutions have the asymptotic form

$$u_{nl}^0(r) \rightarrow \sqrt{2} \sin(k_n r - \frac{l\pi}{2}), \quad r \rightarrow \infty. \quad (5.2.5)$$

The potentials we consider behave asymptotically as  $V''(\tilde{\phi}(r)) \rightarrow \mu^2$  when  $r \rightarrow \infty$  (which corresponds to those with finite action). For such potentials, the asymptotic behavior of the solution to eq. (5.2.2) will be

$$u_{nl}(r) \rightarrow \sqrt{2} \sin(k_n r - \frac{l\pi}{2} + \delta_l(k_n)), \quad r \rightarrow \infty. \quad (5.2.6)$$

These equations serve to define the phase shift  $\delta_l$  for each angular momentum channel  $l$ . Note also that both  $u_{n,l}$  and  $u_{n,l}^0$  are  $(2l+1)$ -fold degenerate.

To facilitate the counting of states, it is convenient to discretize the eigenvalue spectrum. This procedure can be achieved by enclosing the system in a box of radius  $L$  (where  $L$  is much greater than the range of the potential  $V''$ ) and imposing the boundary condition

$$u_{n,l}(L) = 0 \quad (5.2.7)$$

which requires that

$$k_n L - \frac{l\pi}{2} + \delta_l(k_n) = n\pi. \quad (5.2.8)$$

Note that such a discretization is implicit in the formal sums in eq. (5.1.8) and (5.1.11). The values attained by  $\omega^0$  (before discretization) as defined by the energy eigenvalue of eq. (5.2.3) is a continuous spectrum ranging from an energy of  $\mu$  to infinity. The corresponding spectrum for  $\omega$  determined by eq. (5.2.2) will generally consist of some discrete bound states with energies  $\omega_j^2 < \mu^2$  and a continuous spectrum with energies  $\omega_j^2 > \mu^2$ . The difference in structure between the continuum spectra of the two systems manifests in a difference in the respective density of states. Hence it is appropriate to express the sum over eigenenergies for the states in the continuum as an integral over the density of states:

$$\sum_j \omega_j^0 = \sum_l (2l+1) \int_\mu^\infty \omega n_l^0(\omega) d\omega \quad (5.2.9)$$

$$\sum_j \omega_j = \sum_{\omega_{nl}^2 < \mu^2} (2l+1)\omega_{nl} + \sum_l (2l+1) \int_\mu^\infty \omega n_l(\omega) d\omega \quad (5.2.10)$$

where  $(2l+1)n_l(\omega)$  is the density of states of angular momentum  $l$  for the potential  $V''(\tilde{\phi})$  with an analogous definition for  $n_l^0$ . On taking the continuum limit ( $L \rightarrow \infty$ ), it follows from eq. (5.2.8) that the densities of states are related to the continuum phase shift through

$$n_l(\omega) = n_l^0(\omega) + \frac{1}{\pi} \frac{d\delta_l(\omega)}{d\omega}. \quad (5.2.11)$$

Now if eq. (5.1.4) has  $N$  bound states, then since eq. (5.1.4) and eq. (5.1.3) must have the same total number of states,

$$N + \sum_l (2l+1) \int_\mu^\infty n_l(\omega) d\omega = \sum_l (2l+1) \int_\mu^\infty n_l^0(\omega) d\omega. \quad (5.2.12)$$

For a finite potential, this implies  $N\pi = \delta(\mu)$  (by Levinson's theorem).

It is convenient to define the free energy in each angular momentum channel such that

$$\Delta F_1(\Lambda) = \sum_l (2l+1) \Delta F_1^l(\Lambda), \quad (5.2.13)$$

$$\Delta F_T = \sum_l (2l+1) \Delta F_T^l, \quad (5.2.14)$$

and to similarly partition the counterterm energy as

$$F^{\text{ct}}(\Lambda) = \sum_l (2l+1) F_l^{\text{ct}}(\Lambda), \quad (5.2.15)$$

then from the above equations

$$\Delta F_1^l(\Lambda) = \frac{1}{2} \sum_{\omega_{nl}^2 < \mu^2} (\omega_{nl} - \mu) - \frac{1}{2\pi} \sum_l \int_{\mu}^{\Lambda} \delta_l(\omega) d\omega, \quad (5.2.16)$$

and

$$\Delta F_T^l = T \sum_{\omega_{nl}^2 < \mu^2} \ln \left( \frac{1 - e^{-\omega_{nl}/T}}{1 - e^{-\mu/T}} \right) - \frac{1}{\pi} \int_{\mu}^{\infty} \frac{\delta_l(\omega)}{e^{\omega/T} - 1} d\omega. \quad (5.2.17)$$

In Appendix B the renormalization of the Lagrangian given by eq. (5.1.1) discussed. It is shown there that the contribution of the counterterms to the energy are of the general form

$$\int \left[ g(\omega^2 - p^2 - \mu^2) \int h(x) d^3x \right] \frac{d^3p}{(2\pi)^3} \frac{d\omega}{2\pi} \equiv \int_{-\infty}^{\infty} \text{Tr}'(gh) \frac{d\omega}{2\pi}, \quad (5.2.18)$$

where  $g$  is a power of the propagator,  $h$  is a function of  $\phi$  and its derivatives, and  $\text{Tr}'$  is a trace over the spatial variables. The partial wave decomposition of these contributions is achieved by taking the trace with respect to the eigenstates of eq. (5.1.3) denoted here by  $|nlm\rangle$ :

$$\begin{aligned} \text{Tr}'(gh) &= \sum_{nlm} \sum_{n'l'm'} \langle nlm | g(\omega^2 + \nabla^2 - \mu^2) | n'l'm' \rangle \langle n'l'm' | h(r) | nlm \rangle \\ &= \frac{1}{\pi} \sum_l (2l+1) \int_0^{\infty} \left[ g(\omega^2 - p^2 - \mu^2) \int_0^{\infty} h(r) |u_{pl}^0(r)|^2 dr \right] dp. \end{aligned} \quad (5.2.19)$$

From Appendix B, the counterterm contribution to the free energy is

$$F^{\text{ct}}(\Lambda) = -\frac{i}{2} \int_{-\infty}^{\infty} \text{Tr}' \left\{ \Delta_0(\omega, p) [m^2(r) - \mu^2] + \frac{1}{2} \Delta_0(\omega, p)^2 [m^2(r) - \mu^2]^2 \right\} \frac{d\omega}{2\pi}, \quad (5.2.20)$$

where

$$\Delta_0(\omega, p) = \frac{1}{\omega^2 - p^2 - \mu^2 + i\epsilon},$$

and  $m^2(r) = V''(\tilde{\phi}(r))$ . Evaluating the trace using eq. (5.2.19) yields

$$F_l^{\text{ct}}(\Lambda) = \int_0^{\Lambda_p} \left\{ -\frac{1}{4\pi} \frac{1}{(p^2 + \mu^2)^{1/2}} \int_0^\infty |u_{pl}^0(r)|^2 [m^2(r) - \mu^2] dr \right. \\ \left. + \frac{1}{16\pi} \frac{1}{(p^2 + \mu^2)^{3/2}} \int_0^\infty |u_{pl}^0(r)|^2 [m^2(r) - \mu^2]^2 dr \right\} dp, \quad (5.2.21)$$

where  $\Lambda_p = \sqrt{\Lambda^2 - \mu^2}$  is a three-momentum cut-off.

This completes the formulation of the method for the exact calculation of the free energy. However, as we have remarked above, the convergence of such an exact computation can be sufficiently slow so that extrapolation techniques can be useful. Amongst the various such procedures, we consider in particular the WKB approximation, which provides an analytic expression for the phase shift that is valid at high energies and hence can significantly reduce the effort required to evaluate the phase shift integral.<sup>[40]</sup>

### WKB-Improved Method

A differential equation of the form

$$\left[ \frac{d^2}{dx^2} + k^2(x) \right] f(x) = 0 \quad (5.2.22)$$

has an approximate WKB solution given by

$$f_{WKB}(x) = \frac{\exp \left[ i \int_0^x k(\omega, y) dy \right]}{\sqrt{k(\omega, x)}} \quad (5.2.23)$$

which is valid when the wavelength is much less than the distance scale over which  $k$  varies:

$$\frac{1}{k^2} \frac{dk}{dx} \ll 1$$

where  $k(\omega, x)$  is the local wavenumber

$$k(\omega, x) = \sqrt{\omega^2 - V''(\tilde{\phi}(x))}.$$

Hence the accuracy of the WKB approximation increases with energy. The phase shift for such solutions is given by

$$\delta^{\text{WKB}}(\omega) = \int_{-\infty}^{\infty} \left[ k(\omega, x) - \lim_{y \rightarrow \infty} k(\omega, y) \right] dx. \quad (5.2.24)$$

Explicitly,

$$\delta_l^{\text{WKB}}(\omega) = \int_{a(\omega)}^{\infty} \sqrt{\omega^2 - m^2(r) - \frac{l(l+1)}{r^2}} dr - \int_{a_0(\omega)}^{\infty} \sqrt{\omega^2 - \mu^2 - \frac{l(l+1)}{r^2}} dr, \quad (5.2.25)$$

where  $a$  and  $a_0$  denote the classical turning points defined by

$$\omega^2 - m^2(a) - \frac{l(l+1)}{a^2} = 0, \quad \text{and} \quad \omega^2 - \mu^2 - \frac{l(l+1)}{a_0^2} = 0.$$

Applying this method to eq. (5.2.2) yields an analytic expression for the energy integral of the phase shift:

$$\begin{aligned} \int_{\mu}^{\Lambda} \delta_l^{\text{WKB}}(\omega) d\omega = \int_0^{\infty} \left[ \int_{\Omega(r)}^{\Lambda} \sqrt{\omega^2 - m^2(r) - \frac{l(l+1)}{r^2}} \theta(\Lambda - \Omega(r)) d\omega \right. \\ \left. - \int_{\Omega_0(r)}^{\Lambda} \sqrt{\omega^2 - \mu^2 - \frac{l(l+1)}{r^2}} \theta(\Lambda - \Omega_0(r)) d\omega \right] dr \end{aligned} \quad (5.2.26)$$

with

$$\Omega(r) = \sqrt{m^2(r) + \frac{l(l+1)}{r^2}}, \quad \Omega_0(r) = \sqrt{\mu^2 + \frac{l(l+1)}{r^2}},$$

and  $\theta(x)$  is the unit step-function. Observe that since the high-energy behavior of the phase shift is independent of the angular momentum, the energy of each angular momentum channel is logarithmically divergent:

$$\Delta F_1^l(\Lambda) = \frac{1}{4\pi} \ln\left(\frac{\Lambda}{\mu}\right) \int_0^{\infty} [m^2(r) - \mu^2] dr + \mathcal{O}(\Lambda^0). \quad (5.2.27)$$

Now the divergent piece in  $\Delta F_1^l$  can be analytically combined with the infinite part of  $F_l^{\text{ct}}$  in eq. (5.2.21) to leave only finite terms. Performing this subtraction and taking the limit  $\Lambda \rightarrow \infty$  gives the final expression for the WKB-improved, temperature-independent renormalized free energy:

$$\begin{aligned} \Delta F_{1,\text{ren}}^l &= \lim_{\Lambda \rightarrow \infty} [\Delta F_1^l(\Lambda) + F_l^{\text{ct}}(\Lambda)] \\ &= \frac{1}{2} \sum_{\omega_{nl}^2 < \mu^2} (\omega_{nl} - \mu) - \frac{1}{2\pi} \int_{\mu}^{\Lambda_{\text{WKB}}} \delta_l(\omega) d\omega \\ &\quad - \frac{1}{2\pi} \int_0^{\infty} \left\{ \chi_l(\Lambda_{\text{WKB}}, r) + \kappa_l(r) [m^2(r) - \mu^2] + \rho_l(r) [m^2(r) - \mu^2]^2 \right\} dr. \end{aligned} \quad (5.2.28)$$

In this equation,  $\chi_l$  is the contribution from the WKB phase shift above  $\Lambda_{\text{WKB}}$ ,

$$\begin{aligned} \chi_l(r) = & \frac{m_l^0(r)^2 - m_l(r)^2}{4} - \frac{1}{2}\Lambda_{\text{eff}}(r)\sqrt{\Lambda_{\text{eff}}(r)^2 - m_l(r)^2} \\ & + \frac{1}{2}\Lambda_{\text{eff}}^0(r)\sqrt{\Lambda_{\text{eff}}^0(r)^2 - m_l^0(r)^2} \\ & + \frac{1}{2}m_l(r)^2 \ln \frac{\Lambda_{\text{eff}}(r) + \sqrt{\Lambda_{\text{eff}}(r)^2 - m_l(r)^2}}{\mu} \\ & - \frac{1}{2}m_l^0(r)^2 \ln \frac{\Lambda_{\text{eff}}^0(r) + \sqrt{\Lambda_{\text{eff}}^0(r)^2 - m_l^0(r)^2}}{\mu}, \end{aligned} \quad (5.2.29)$$

where

$$m_l^0(r)^2 = \mu^2 + \frac{l(l+1)}{r^2}, \quad m_l(r)^2 = m^2(r) + \frac{l(l+1)}{r^2},$$

$$\Lambda_{\text{eff}}^0(r) = \max(\Lambda_{\text{WKB}}, \Omega_0(r)), \quad \Lambda_{\text{eff}}(r) = \max(\Lambda_{\text{WKB}}, \Omega(r)),$$

and  $\Lambda_{\text{WKB}}$  denotes the energy above which the phase shift is computed by the WKB method. The remaining terms in the last integral come from finite parts of the counterterm with

$$\kappa_l(r) = \int_0^\infty \frac{s^2 |j_l(s)|^2 - \frac{1}{2}}{\sqrt{s^2 + (\mu r)^2}} ds, \quad (5.2.30)$$

and

$$\rho_l(r) = -\frac{r^2}{4} \int_0^\infty \frac{s^2 |j_l(s)|^2}{(s^2 + (\mu r)^2)^{3/2}} ds. \quad (5.2.31)$$

Equation (5.2.28) indicates that  $\Delta F_{1,\text{ren}}^l$  can now be computed by first summing over the bound state energies, then the continuum state contributions can be evaluated by explicitly computing the exact phase shift only up to  $\Lambda_{\text{WKB}}$ , beyond which the WKB method provides an analytical expression that accounts for contributions at higher energies. Note that while the WKB procedure entails an approximation, its accuracy can be made such that the difference between the exact and the WKB results is smaller than the desired precision. Finally, summation over  $l$  yields

$$\Delta F_{1,\text{ren}} = \sum_l (2l+1) \Delta F_{1,\text{ren}}^l. \quad (5.2.32)$$

Since  $\Delta F_T$  is not divergent, it can be computed exactly using eq. (5.2.14) and (5.2.16), or by replacing the exact phase shift  $\delta_l$  above a certain energy scale by the approximate WKB phase shift  $\delta_l^{\text{WKB}}$  given by eq. (5.2.25).

### 5.3. APPLICATION AND DISCUSSION

In the next chapter these methods are used to calculate the free energy of an instanton configuration which determines the decay rate in a first order phase transition. The computation of  $\Delta F_1$  will be described first. It is found that the accuracy available on conventional computers prevents a precise determination of this quantity when it is straight-forwardly evaluated as in eq. (5.1.8) — that is, by doing the bare sum and subtracting the counterterm, without a decomposition into partial waves. When  $\Delta F_1$  is computed exactly, by utilizing such a decomposition, very high numerical accuracy is still required because for each  $l$  the bare sum and  $F_l^{\text{ct}}(\Lambda)$  must be evaluated at a large value of the cut-off  $\Lambda$ . But since both quantities diverge as a function of  $\Lambda$ , we find that convergence with reasonable accuracy is still difficult to attain. In contrast, evaluation of  $\Delta F_{1,\text{ren}}$  using the WKB-improved method consisting of eq. (5.2.28) and (5.2.32) converges rapidly for much lower values of the cut-off  $\Lambda_{\text{WKB}}$  and typically only the first fifty partial waves need to be summed; the parameters required for convergence are very much dependent on the nature  $V''(\tilde{\phi}(r))$  and the values we have quoted come from the potentials we have examined.

The exact computation of  $\Delta F_T$  can be performed by evaluating eq. (5.2.14) and (5.2.17), but at high temperatures it is found that several hundred partial waves must be summed to attain convergence. When the exact phase shift is replaced by the approximate WKB expression at high energies, there is a reduction in the computational burden but the same number of angular momentum channels must be summed. The improvement is not marked as it was for  $\Delta F_{1,\text{ren}}$  in part because  $\Delta F_T$  is not renormalized. The results of these computations are summarized in Tables 6 and 7 of the following chapter.

In summary, we have elucidated a method for the exact evaluation the effective action to one-loop. The WKB extrapolation scheme was devised to reduce the computational effort. These methods enable an efficient calculation of the free energy associated with a phase transition, as detailed above. However, the applicability of this method is not limited to this example. Rather, it can be utilized in a broader variety of problems involving the non-perturbative evaluation of observables in a non-uniform background in quantum field theory<sup>[47]</sup> as well as in classical systems.<sup>[48]</sup> It can also be generalized to encompass theories with fermions.<sup>[49]</sup>

## 6. EFFECTIVE ACTIONS, EFFECTIVE POTENTIALS AND FIRST-ORDER PHASE TRANSITIONS

### 6.1. INTRODUCTION

#### Thermal Tunneling and the Critical Bubble Free Energy

A scalar field theory whose potential  $V$  has two local minima may tunnel out of the false vacuum ( $\phi_f$ ) by the nucleation and subsequent growth of bubbles of true vacuum ( $\phi_t$ ).<sup>6</sup> While we will refer to  $V$  as the “classical” potential, it may arise in part from integrating out other particles in the theory, *e.g.*, gauge bosons,<sup>[50]</sup> so  $V$  may have implicit temperature ( $T$ ) dependence. The nucleation rate per unit volume in the static limit ( $RT \gg 1$ ) is calculated in the Gaussian approximation (*i.e.*, to 1-loop order) to be<sup>[51–53]</sup>

$$\frac{\Gamma}{\mathcal{V}} = \frac{1}{\mathcal{V}} \frac{|\omega_-|}{\pi T} \frac{1}{2} T \left| \frac{\det[\partial^2 + V''(\bar{\phi})]}{\det[\partial^2 + \mu^2]} \right|^{-1/2} e^{-E_c/T} \quad (6.1.1)$$

where  $\mu^2 = V''(\phi_f)$ .  $E_c$  is the classical energy of the critical bubble, a static and spherically symmetric field configuration  $\bar{\phi}(r)$ , of radius  $R$ , which extremizes the classical action<sup>[54]</sup> subject to periodic boundary conditions in Euclidean time. The determinants range over a complete basis of fluctuations about the classical solution ( $\bar{\phi}(r)$  or  $\phi_f$ ), subject to the same boundary conditions.  $\omega_-^2 < 0$  is the eigenvalue of the “breathing” mode about  $\bar{\phi}(r)$ . The second term on the RHS of Eq. (6.1.1) is from Affleck,<sup>[52]</sup> and the  $\frac{1}{2}$  is from analytically continuing the breathing mode integration.<sup>[51]</sup>

With the periodic boundary conditions,

$$\det[\partial^2 + V''(\bar{\phi})] = \exp \left\{ \sum_{n=-\infty}^{\infty} \sum_j \ln [(2\pi nT)^2 + \omega_j^2] \right\}, \quad (6.1.2)$$

where the  $\omega_j^2$  are eigenvalues of  $[-\nabla^2 + V''(\bar{\phi})]$ , and the  $(\omega_j^0)^2$  are eigenvalues of  $[-\nabla^2 + \mu^2]$ . We use the identity<sup>[55]</sup>

$$\frac{T}{2} \sum_n \ln [(2\pi nT)^2 + \omega^2] = \frac{\omega}{2} + T \ln(1 - e^{-\omega/T}) + \mathcal{C} = T \ln \left[ 2 \sinh \left( \frac{\omega}{2T} \right) \right] + \mathcal{C}. \quad (6.1.3)$$

---

<sup>6</sup>This chapter is based on D.E. Brahm and C.L.Y. Lee, *Phys. Rev.* **D49**, 4094 (1994).

The constants  $\mathcal{C}$  cancel out in Eq. (6.1.1). The  $\omega_-$  contribution is then traditionally pulled back into the prefactor. The 3 “translation” modes ( $n=0$  and  $\omega_0=0$ ) are not treated correctly above; they actually give  $\mathcal{V}(E_c/2\pi T)^{3/2}$  in the prefactor,<sup>[51]</sup> and the remaining  $\omega_0$  contribution (from  $n \neq 0$  modes) gives  $T^3$  in the prefactor. This gives

$$\frac{\Gamma}{\mathcal{V}} = \frac{T^4}{2\pi} \left( \frac{E_c}{2\pi T} \right)^{3/2} \frac{|\omega_-|/2T}{\sin(|\omega_-|/2T)} e^{-F_c^{trad}/T} \quad (6.1.4)$$

where the “traditional” bubble free energy

$$F_c^{trad} \equiv E_c + \Delta F_{1+T}^{trad} \equiv E_c + \Delta F_1^{trad} + \Delta F_T^{trad}, \quad (6.1.5)$$

$$\Delta F_1^{trad} = \sum_j' \frac{\omega_j - \omega_j^0}{2} + F^{ct}, \quad \Delta F_T^{trad} = \sum_j' T \ln \left( \frac{1 - e^{-\omega_j/T}}{1 - e^{-\omega_j^0/T}} \right). \quad (6.1.6)$$

Primes on the sums in Eq. (6.1.6) indicate omission of the translation and breathing modes ( $\omega_j$ ,  $j = 1-4$ ). Counterterms  $F^{ct}$  are discussed below.

We now define<sup>7</sup>

$$F_c^{sub} \equiv E_c + \Delta F_{1+T}^{sub} \equiv E_c + \Delta F_1^{sub} + \Delta F_T^{sub}, \quad (6.1.7)$$

$$\Delta F_1^{sub} \equiv \Delta F_1^{trad}, \quad \Delta F_T^{sub} \equiv \Delta F_T^{trad} - 4T \ln(T/\mu). \quad (6.1.8)$$

Now Eq. (6.1.4) becomes

$$\frac{\Gamma}{\mathcal{V}} = \frac{\mu^4}{2\pi} \left( \frac{E_c}{2\pi T} \right)^{3/2} \frac{|\omega_-|/2T}{\sin(|\omega_-|/2T)} e^{-F_c^{sub}/T}. \quad (6.1.9)$$

We will find that the effective potential approximation most closely approximates  $F_c^{sub}$ .

---

<sup>7</sup>This is somewhat like removing the lowest 4  $\omega_j^0$ 's from the sums in Eq. (6.1.6), in addition to the lowest 4  $\omega_j$ 's, since their contribution to  $F_c^{trad}$  is  $-4[\frac{\mu}{2} + T \ln(1 - e^{-\mu/T})] \approx 4T \ln(T/\mu)$ .

## The Effective Potential

The sums in Eq. (6.1.6) are often approximated by treating the fluctuations locally as plane waves to get an effective potential  $V_{1+T} = V_1 + V_T$ , then integrating  $[V_{1+T}(\bar{\phi}) - V_{1+T}(\phi_f)]$  over all space. No attempt is made to remove the 4 translation and breathing modes. In Eq. (6.1.6) one substitutes

$$\sum_j \rightarrow \int d^3\mathbf{x} \int_0^\Lambda \frac{d^3\mathbf{k}}{(2\pi)^3}, \quad \omega_j \rightarrow \sqrt{\mathbf{k}^2 + V''(\bar{\phi})}, \quad \omega_j^0 \rightarrow \sqrt{\mathbf{k}^2 + \mu^2}, \quad (6.1.10)$$

and one finds, with  $m^2 \equiv V''(\phi)$ ,

$$V_1(\phi) = \frac{1}{64\pi^2} \left\{ m^4 \ln\left(\frac{m^2}{\mu^2}\right) - \frac{3}{2}m^4 + 2m^2\mu^2 - \frac{1}{2}\mu^4 \right\}, \quad (6.1.11)$$

$$V_T(\phi) = \frac{T^4}{2\pi^2} I(m/T), \quad I(y) \equiv \int_0^\infty dx x^2 \ln\left(1 - e^{-\sqrt{x^2+y^2}}\right). \quad (6.1.12)$$

The expansion of  $I(y)$  for real  $y < 2\pi$  is<sup>[55,56]</sup>

$$I(y) = \frac{-\pi^4}{45} + \frac{\pi^2}{12}y^2 - \frac{\pi}{6}y^3 - \frac{y^4}{32} \left[ \ln y^2 - c_3 + \sum_{k=1}^{\infty} \frac{4(2k)! \zeta(2k+1)}{k!(k+2)!} \left(\frac{-y^2}{16\pi^2}\right)^k \right] \quad (6.1.13)$$

where  $c_3 = \frac{3}{2} + 2\ln(4\pi) - 2\gamma \approx 5.4076$ . We choose a renormalization scheme in which all divergent graphs are precisely cancelled by counterterms so that at zero external momenta,  $V_1(\phi_f) = V_1'(\phi_f) = V_1''(\phi_f) = 0$  (and there is no wavefunction renormalization),<sup>[57]</sup> specifically:

$$F^{\text{ct}} = \frac{-1}{64\pi^2} \int d^3\mathbf{x} \left\{ [4\Lambda^4 + \frac{1}{2}\mu^4] + m^2[4\Lambda^2 - 2\mu^2] + m^4 \left[ 2 - \ln\left(\frac{4\Lambda^2}{\mu^2}\right) \right] \right\} \Big|_{m^2=\mu^2}^{m^2=V''}. \quad (6.1.14)$$

In the region  $m^2 < 0$ , we must modify these results to give a real answer. For  $V_1$  we will always take the real part of Eq. (6.1.11). For  $V_T$  let us keep the first equation of Eq. (6.1.12), but replace  $I(m/T)$  by  $I^{(\text{neg})}(|m|/T)$  where

$$I^{(\text{neg})}(Y) \equiv \frac{-\pi^4}{45} - \frac{\pi^2}{12}Y^2 + Y^3 [a + b \ln(Y^2)] - \frac{Y^4}{32} [\ln(Y^2) - c_3 + c] + \dots \quad (6.1.15)$$

Methods we consider are then parametrized by  $\{a, b, c\}$ . The most common and obvious method (A) is to take the real part of Eq. (6.1.13), corresponding to  $\{a = b = c = 0\}$ . Another method (B), proposed in ref. [58], replaces the lower limit of integration in Eq. (6.1.10) by  $k = \text{Im}\{m\}$  (eliminating fluctuations with wavelengths longer than the bubble thickness), and corresponds to  $\{a = \frac{4}{9} - \frac{1}{3}\ln(2), b = \frac{1}{6}, c = 0\}$ .

## The Derivative Expansion

For configurations  $\bar{\phi}(\mathbf{x})$  which vary slowly, the effective potential approximation is the leading term in a derivative expansion of the free energy. The next term (at high  $T$ ) is<sup>[59,60]</sup>

$$\Delta F_T^{der} - \Delta F_T^{pot} = \frac{T}{192\pi} \int d^3\mathbf{x} m^{-1} \nabla^2(m^2), \quad (6.1.16)$$

and again we take the real part (Method A) when necessary. More terms are given explicitly in ref. [60]; they become increasingly divergent at  $m^2 = 0$ , where the derivation breaks down (because an integration by parts becomes invalid). Also, no attempt is made to omit modes. The usefulness of Eq. (6.1.16) is thus highly suspect, but we note that derivative corrections are predicted to be  $\mathcal{O}(T^1)$ .

## Scales, Approximations, and Goals

Our generic tree-level potential will be quartic in  $\phi$  with  $\phi_f = 0$ ,  $V''(0) = \mu^2$ , and  $\phi_t = \sigma$ . By rescaling<sup>[61]</sup>  $\phi = \sigma\tilde{\phi}$ ,  $x = \tilde{x}/\mu$ , and  $T = \mu\tilde{T}$ , we can rewrite the 4-action  $S_0$  as

$$S_0 = \frac{E_c}{T} = \left(\frac{\sigma}{\mu}\right)^2 \frac{1}{\tilde{T}} \int d^3\tilde{\mathbf{x}} \left\{ \frac{1}{2} \left(\frac{d\tilde{\phi}}{d\tilde{r}}\right)^2 - \left[ \frac{1}{2}\tilde{\phi}^2 - \frac{2\kappa+1}{3}\tilde{\phi}^3 + \frac{\kappa}{2}\tilde{\phi}^4 \right] \right\}. \quad (6.1.17)$$

$\kappa \geq 1$  is a dimensionless parameter;  $\kappa \rightarrow 1$  (degenerate minima) is the thin-wall limit, while larger  $\kappa$  gives thicker bubbles. With tildes indicating dimensionless results,

$$E_c = (\sigma^2/\mu) \tilde{E}_c, \quad \Delta F_{1,T} = \mu \Delta \tilde{F}_{1,T}. \quad (6.1.18)$$

The loop expansion<sup>[62]</sup> is an expansion in  $(\mu/\sigma)^2$  and  $\tilde{T}$ . It is sometimes claimed that higher loops should eliminate the complex terms in  $F_c^{pot}$ , but this cannot be generally true since the higher-loop contributions are suppressed by these arbitrary parameters. Henceforth we will drop the tildes and work in the rescaled theory (*i.e.*, set  $\mu = \sigma = 1$ ).

We always use the static approximation<sup>[63]</sup> ( $RT \gg 1$ ) and the 1-loop approximation. In Section 6.3 we will use the thin-wall approximation,  $R \gg 1$ . At times we will make high-temperature expansions, requiring  $T \geq 1$  (note the thin-wall and high-temperature limits together imply the static limit). We are examining the validity of the effective potential approximation.

In this chapter we will study several systems: the 1-dimensional (1D) kink, the thin-wall bubble, and two thick-wall bubbles. We will calculate  $\Delta F_1$  and  $\Delta F_T$  for each system exactly [ $F_c^{sub}$  in Eq. (6.1.8)], in the effective potential approximation [ $F_c^{pot}$  from Eqs. (6.1.11-6.1.12), using different methods to calculate  $I^{(neg)}$  in Eq. (6.1.15)], and using the next term of the derivative expansion [ $F_c^{der}$  from Eq. (6.1.16)].

## 6.2. THE ONE-DIMENSIONAL KINK

### Classical Results

We warm up by calculating the free energy of a kink in 1 spatial dimension:<sup>[64]</sup>

$$\frac{d^2\bar{\phi}}{dx^2} = V'(\bar{\phi}), \quad \frac{d\bar{\phi}}{dx} = -\sqrt{2V(\bar{\phi})}, \quad V(\phi) = \frac{1}{2}\phi^2(1-\phi)^2. \quad (6.2.1)$$

The potential is that of Eq. (6.1.17) with  $\kappa = 1$ . The kink solution is (up to an arbitrary shift in coordinate)

$$\bar{\phi}(x) = \frac{1}{2}[1 - \tanh(\frac{1}{2}x)], \quad V''(\bar{\phi}(x)) = 1 - \frac{3}{2}\text{sech}^2(\frac{1}{2}x). \quad (6.2.2)$$

Eq. (6.2.1) allows us to convert integrals over  $x$  into integrals over  $\phi$ :

$$\int_{-\infty}^{\infty} dx \rightarrow \int_0^1 \frac{d\phi}{\phi(1-\phi)}. \quad (6.2.3)$$

For example, the classical energy is

$$E_c^{1D} = \int_0^1 \frac{d\phi}{\phi(1-\phi)} \phi^2(1-\phi)^2 = \frac{1}{6}. \quad (6.2.4)$$

Note that in 1D [compare to Eq. (6.1.18)]  $E_c = \mu\sigma^2 \tilde{E}_c$  and  $\Delta F_{1,T} = \mu \Delta \tilde{F}_{1,T}$ , so with scales restored  $E_c^{1D} = \mu\sigma^2/6$ .

### Exact Results from the Eigenvalue Sum

The solutions to the eigenvalue equations (setting  $\mu = 1$ ) are known:<sup>[64-66]</sup>

$$\omega_s^0 = \sqrt{(k_s^0)^2 + 1}, \quad \omega_1 = 0, \quad \omega_2 = \sqrt{3}/2, \quad \omega_{s>2} = \sqrt{(k_s)^2 + 1},$$

$$k_s^0 = \frac{\pi s}{L}, \quad k_s = \frac{\pi s - \delta(k_s)}{L}, \quad \delta(k) = 2\pi - 2 \tan^{-1}(k) - 2 \tan^{-1}(2k), \quad (6.2.5)$$

where we have imposed vanishing boundary conditions on a box of length  $L$ , so  $s$  is a positive integer. We drop the translation mode eigenvalue  $\omega_1$ ; there is no negative eigenvalue in 1D. In the continuum limit,

$$\Delta F_1^{trad} = \frac{\sqrt{3}}{4} + \int_0^\Lambda \frac{dk}{\pi} \frac{d\delta}{dk} \frac{\sqrt{k^2+1}}{2} - \frac{3}{2\pi} + F^{ct},$$

$$\Delta F_T^{trad} = T \ln \left( 1 - e^{-\sqrt{3}/2T} \right) + \int_0^\infty \frac{dk}{\pi} \frac{d\delta}{dk} T \ln \left( 1 - e^{-\sqrt{k^2+1}/T} \right). \quad (6.2.6)$$

In our renormalization scheme the 1D counterterms analogous to Eq. (6.1.14) are

$$F^{ct} = \frac{-1}{16\pi} \int dx \left\{ [4\Lambda^2 + 1] + m^2 [2 + 2 \ln(4\Lambda^2)] - m^4 \right\} \Big|_{m^2=1}^{m^2=V''} = \frac{1}{8\pi} [3 + 6 \ln(4\Lambda^2)]. \quad (6.2.7)$$

(This differs from ref. [64] by  $3/8\pi$  due to different renormalization schemes; also note their  $m^2 \equiv \mu^2/2$ .) We define  $\Delta F_1^{sub} \equiv \Delta F_1^{trad}$  and  $\Delta F_T^{sub} \equiv \Delta F_T^{trad} - T \ln(T/\mu)$ , and find

$$\Delta F_1^{sub} = \frac{1}{4\sqrt{3}} - \frac{9}{8\pi} = -.2138. \quad (6.2.8)$$

$$\Delta F_{1+T}^{sub} = -(\ln \sqrt{12}) T + \frac{3}{2\pi} \ln(T) + \frac{6c_1 - 3}{8\pi} + \frac{3\zeta(3)}{32\pi^3} T^{-2} + \dots \quad (6.2.9)$$

where  $c_1 = 1 + 2 \ln(4\pi) - 2\gamma \approx 4.9076$ , and  $\zeta(3) \approx 1.2021$ . These results are in the row marked “sub” of Table 3.

Method	$\Delta F_1$	$\Delta F_{1+T}$					
		$T \ln(T)$	$T$	$\ln(T)$	1	$T^{-1}$	$T^{-2}$
sub	-.2138	0	-1.2425	.4775	1.0522	0	.0036
pot(A)	-.0916	0	-2.1145	.4775	1.0522	0	.0036
der(A)	-.0916	0	-2.1730	.4775	1.0522	0	.0036
pot(B)	-.0916	0.4495	-1.7222	.4775	1.0522	.0045	.0036

**Table 3: Kink free energy in low- and high-T regimes.**

## 1D Effective Potential and Derivative Expansion Results

The 1D effective potential for real  $m$  is<sup>[56]</sup>

$$V_1 = \frac{-m^2}{8\pi} \ln(m^2) + \frac{m^4 - 1}{16\pi}, \quad V_T = \frac{T^2}{\pi} \hat{I}(m/T) \quad (6.2.10)$$

$$\hat{I}(y) = \frac{-\pi^2}{6} + \frac{\pi y}{2} + \frac{y^2}{8} [\ln(y^2) - c_1] - \frac{\zeta(3)y^4}{64\pi^2} + \dots \quad (6.2.11)$$

For  $m^2 < 0$  we replace  $\hat{I}(m/T)$  by  $\hat{I}^{(neg)}(|m|/T)$  where

$$\hat{I}^{(neg)}(Y) = \frac{-\pi^2}{6} + Y [\hat{a} + \hat{b} \ln(Y^2)] - \frac{Y^2}{8} [\ln(Y^2) - c_1 + \hat{c}] + \dots \quad (6.2.12)$$

Method A gives  $\{\hat{a} = \hat{b} = \hat{c} = 0\}$ , and Method B gives  $\{\hat{a} = 1 - \ln(2), \hat{b} = -\frac{1}{2}, \hat{c} = 0\}$ .

We integrate (the real part of)  $V_1$  from Eq. (6.2.10) over all space, using Eq. (6.2.3), to get  $\Delta F_1^{pot(A)} = -.0916$ , which differs significantly from  $\Delta F_1^{sub} = -.2138$  (note each result is renormalization-dependent, but the difference is not). This difference, which was calculated in ref. [64], dominates the low-T regime.

A similar integral for the high-T expansion gives

$$\Delta F_{1+T}^{pot(A)} = \ln[2(\sqrt{3}-\sqrt{2})^{\sqrt{6}}] T + \frac{3}{2\pi} \ln(T) + \frac{6c_1 - 3}{8\pi} + \frac{3\zeta(3)}{32\pi^3} T^{-2} + \dots, \quad (6.2.13)$$

as shown in the line marked “pot(A)” of Table 3. Note that the difference between the true result and the potential approximation no longer lies in the constant term, but only (as far as we have taken the expansion) in the  $T$  term! It is

$$\Delta F_{1+T}^{sub} - \Delta F_{1+T}^{pot(A)} = -\ln [4\sqrt{3}(\sqrt{3}-\sqrt{2})^{\sqrt{6}}] T = .8720 T. \quad (6.2.14)$$

The next term of the derivative expansion [analogous to Eq. (6.1.16)] is

$$\Delta F_T^{der} - \Delta F_T^{pot} = \frac{T}{96} \int dx m^{-3} \nabla^2(m^2) = \frac{\sqrt{6}}{48} \ln(\sqrt{3} - \sqrt{2}) T = -.0585 T \quad (6.2.15)$$

as incorporated in the third line of Table 3. It is a very poor approximation to Eq. (6.2.14)!

Results from Method B are given in the fourth line of Table 3; these are also unsatisfactory. In fact, the choice  $\{\hat{a} = 1.940, \hat{b} = \hat{c} = 0\}$  in Eq. (6.2.12) would give the correct (“sub”) results, but it is not clear if there is any physics in this choice.

### 6.3. THE THIN-WALL CRITICAL BUBBLE

#### Classical Results

For  $\kappa$  close to (but larger than) unity in Eq. (6.1.17), the solution to

$$\nabla^2 \bar{\phi} = V'(\bar{\phi}) \quad (6.3.1)$$

is a thin-wall bubble, given approximately by the kink solution in the radial coordinate, Eq. (6.2.2) with  $x = r - R$  and  $R \gg 1$ .<sup>[51]</sup> The tree-level critical bubble energy has volume and surface terms:

$$E_c = 4\pi \int r^2 dr \left[ \frac{1}{2} \left( \frac{d\bar{\phi}}{dr} \right)^2 + V(\bar{\phi}(r)) \right] \approx -\frac{4}{3}\pi R^3 |V(1)| + 4\pi R^2 E_c^{1D}, \quad (6.3.2)$$

where  $E_c^{1D} = \frac{1}{6}$  was given in Eq. (6.2.4), and  $|V(1)| = (\kappa - 1)/6$ . We extremize to find the bubble radius  $R$  and energy  $E_c$ ,

$$R = \frac{2}{\kappa - 1}, \quad E_c = \frac{8\pi}{9(\kappa - 1)^2} = \frac{2\pi R^2}{9}. \quad (6.3.3)$$

The wall thickness is  $\mathcal{O}(1)$  (*i.e.*,  $\mu^{-1}$ ). It can also be shown<sup>[51]</sup> that  $\omega_-^2 \approx -2/R^2$ , so the static and thin-wall limits imply that the third factor of Eq. (6.1.4) is near unity.

#### Exact Results for a Domain Wall

In the thin-wall limit, the surface free-energy density  $f_{1,T} = \Delta F_{1,T}/(4\pi R^2)$  of the bubble wall equals that of a planar domain wall<sup>[67]</sup>. We can thus solve the eigenvalue equation in Cartesian coordinates, using Eq. (6.2.5) for the radial wavenumber  $k_r$ , and plane waves for the tangential  $k_t$ , to get

$$\begin{aligned} f_1^{sub} &= \int_0^\Lambda \frac{k_t dk_t}{2\pi} \left\{ \frac{k_t}{2} + \frac{\sqrt{k_t^2 + 3/4}}{2} - \frac{\sqrt{\Lambda^2 + 1}}{2\pi} \delta(\sqrt{\Lambda^2 - k_t^2}) \right. \\ &\quad \left. + \int_0^{\sqrt{\Lambda^2 - k_t^2}} \frac{dk_r}{\pi} \left( \frac{-2}{k_r^2 + 1} + \frac{-4}{4k_r^2 + 1} \right) \frac{\sqrt{k_t^2 + k_r^2 + 1}}{2} \right\} + \frac{3\Lambda^2}{8\pi^2} - \frac{3}{32\pi^2} \ln(4\Lambda^2) \\ &= \frac{-1}{32\pi^2} \left( \frac{\pi}{\sqrt{3}} + 6 \right) = -.02474, \\ f_T^{sub} &= T \int_0^\infty \frac{k_t dk_t}{2\pi} \left\{ \ln [1 - e^{-k_t/T}] + \ln \left[ 1 - e^{-\sqrt{k_t^2 + 3/4}/T} \right] + \int_0^\infty \frac{dk_r}{\pi} \right. \\ &\quad \left. \times \left( \frac{-2}{k_r^2 + 1} + \frac{-4}{4k_r^2 + 1} \right) \ln \left[ 1 - e^{-\sqrt{k_t^2 + k_r^2 + 1}/T} \right] \right\}. \end{aligned} \quad (6.3.4)$$

We have performed the  $f_T$  integral numerically, and fit to an expansion in  $T^{-1}$ ; the results are shown in Table 4 in the row marked “sub”.<sup>8</sup>

Method	$f_1$	$f_{1+T}$						
		$T^2$	$T \ln(T)$	$T$	$\ln(T)$	1	$T^{-1}$	$T^{-2}$
sub	−.02474	−1/4	0	.15215	−.01900	−.03712	0	−.00012
pot(A)	−.00661	−1/4	0	.15452	−.01900	−.05612	0	−.00012
der(A)	−.00661	−1/4	0	.15187	−.01900	−.05612	0	−.00012
pot(B)	−.00661	−1/4	.00864	.16409	−.01900	−.05612	.00006	−.00012

**Table 4:** Thin-wall bubble free energy density for low- and high- $T$ .

### Effective Potential and Derivative Expansion Results

Results from integrating the effective potential, and the next term of the derivative expansion, over the bubble [again using Eq. (6.2.3)] are shown in the rest of Table 4. Using the general  $I^{(neg)}$  of Eq. (6.1.15) gives

$$f_{1+T}^{pot} = -\frac{1}{4}T^2 - (.0518 b) T \ln(T) + (.1545 + .0259 a - .0242 b) T - (.0190) \ln(T) + (-.05612 - .000514 c) \quad (6.3.5)$$

Matching this to the true  $f_{1+T}^{sub}$  gives the coefficients  $\{a, b, c\}$  shown in the first line ( $\kappa = 1$ ) of Table 5.<sup>9</sup>

We see “derivative corrections” are  $\mathcal{O}(T)$ . The derivative expansion prediction,  $f_{1+T}^{der}$  from Eq. (6.1.16), is a reasonable approximation to them in this case.

<sup>8</sup>These results are also useful for the study of second-order phase transitions, in which the domain wall free energy density is set to zero.<sup>[67]</sup> Restoring units,

$$f[\bar{\phi}^{wall}] = \mu \left[ \frac{\sigma^2}{6} - \frac{T_c^2}{4} + .15215 \mu T_c - .01900 \mu^2 \ln(T_c/\mu) - \dots \right] = 0$$

giving, for  $\mu \ll \sigma$ ,  $T_c = \sqrt{2/3} \sigma + 0.3\mu + \dots$ . That is, the critical temperature is a bit higher than the leading result which is in the literature.

<sup>9</sup>First subtracting the derivative correction of Eq. (6.1.16) from  $\Delta F_{1+T}^{sub}$  would give  $a$  values of .0109, .3877, and .5128, respectively. For the kink it gives  $\hat{a} = 2.070$ . These results are no more enlightening.

$\kappa$	$a$	$b$	$c$
1	-.0913	0	-36.974
1.5	.2834	0	- 1.424
2.5	.4188	0	- 0.180

Table 5:  $I^{(neg)}$  parameters that make  $\Delta F_{1+T}^{pot} = \Delta F_{1+T}^{sub}$ .

## 6.4. THICK WALL CRITICAL BUBBLES

### Classical Results

From Eq. (6.1.17), the (scaled) potential (Fig. 10) is

$$V = \frac{1}{2}\phi^2 - \frac{2\kappa + 1}{3}\phi^3 + \frac{\kappa}{2}\phi^4. \quad (6.4.1)$$

Larger  $\kappa > 1$  gives thicker bubbles. The minima are at  $\phi = 0$  and  $\phi = 1$ , with  $V''(0) = 1$  and  $V''(1) = 2\kappa - 1$ . The bubble profile is the solution to

$$\bar{\phi}'' + 2\bar{\phi}'/r = \bar{\phi}(1 - \bar{\phi})(1 - 2\kappa\bar{\phi}). \quad (6.4.2)$$

Fig. 11 and 12 plots  $\bar{\phi}(r)$  and  $V''(r)$  for  $\kappa = 1.5$  and  $\kappa = 2.5$ . From ref. [61], the classical energy is approximately

$$E_c \approx \frac{4.85\alpha}{\kappa} \left[ 1 + \frac{\alpha}{4} \left( 1 + \frac{2.4}{1 - \alpha} + \frac{.26}{(1 - \alpha)^2} \right) \right], \quad \alpha \equiv \frac{9\kappa}{(1 + 2\kappa)^2}. \quad (6.4.3)$$

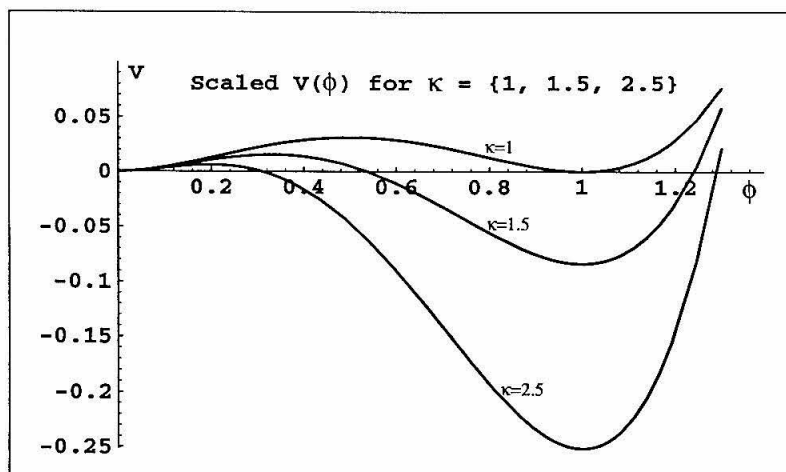


Fig. 10: The potential  $V(\phi)$  for several values of  $\kappa$ .

## Exact, Effective Potential, and Derivative Expansion Results

Our method of calculating the exact free energy  $F_c^{sub}$ , formally given by Eq. (6.1.7), is described in ref. [57]. The results for  $\kappa = 1.5$  are in Table 6, and for  $\kappa = 2.5$  in Table 7<sup>10</sup>, along with effective potential and derivative expansion approximations. Thin-wall predictions are also shown for two values of  $R$ : one chosen to give the correct  $T^2$  coefficient (“thin-1”), and one given by Eq. (6.3.3) (“thin-2”). Finally, the parameters in  $I^{(neg)}$  needed to match the effective potential approximation to the exact result are given in Table 5.

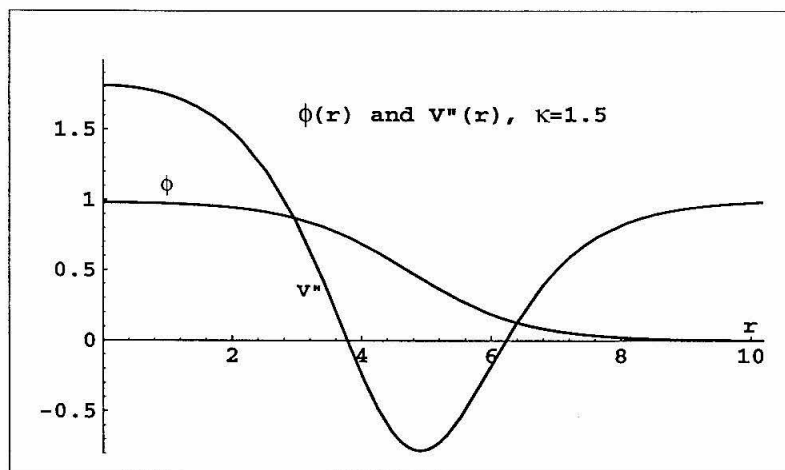


Fig. 11: Thick-wall bubble profiles for  $\phi(r)$  and  $V''(r)$  when  $\kappa = 1.5$ .

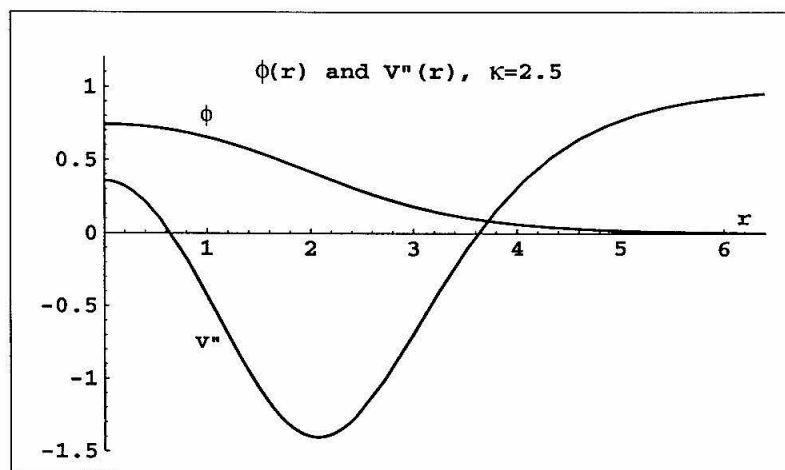


Fig. 12: Thick-wall bubble profiles for  $\phi(r)$  and  $V''(r)$  when  $\kappa = 2.5$ .

<sup>10</sup>In our fit to the data, we allowed a  $T^{-2}$  term, not shown, and constrained the  $T^2$ ,  $T \ln(T)$ , and  $\ln(T)$  terms.

Method	$\Delta F_1$	$\Delta F_{1+T}$				
		$T^2$	$T \ln(T)$	$T$	$\ln(T)$	1
sub	-2.13	-78.61	0	49.52	-5.193	-15.64
pot(A)	-2.65	-78.61	0	45.47	-5.193	-16.12
der(A)	-2.65	-78.61	0	43.98	-5.193	-16.12
pot(B)	-2.65	-78.61	4.76	49.73	-5.193	-16.12
thin-1	-1.81	-78.61	0	47.84	-5.974	-17.65
thin-2	-4.97	-50.27	0	30.59	-3.820	-7.46

Table 6: Thick-wall bubble free energy for  $\kappa = 1.5$ .

Method	$\Delta F_1$	$\Delta F_{1+T}$				
		$T^2$	$T \ln(T)$	$T$	$\ln(T)$	1
sub	-1.34	-24.90	0	17.17	-1.408	-4.60
pot(A)	-1.009	-24.90	0	14.05	-1.408	-4.64
der(A)	-1.009	-24.90	0	13.35	-1.408	-4.64
pot(B)	-1.009	-24.90	2.48	15.60	-1.408	-4.64
thin-1	-0.572	-24.90	0	15.15	-1.892	-5.59
thin-2	-0.553	-5.59	0	3.40	-0.424	-0.83

Table 7: Thick-wall bubble free energy for  $\kappa = 2.5$ .

## 6.5. CONCLUSIONS: A New Prefactor, and Derivative Corrections

We have tested the effective potential approximation to the critical bubble free energy. The agreement is best if one pulls a factor of  $\mu^4/T^4$  into the decay rate prefactor, Eq. (6.1.9), and takes the real part of the effective potential in the region  $V'' < 0$  (Method A). That is,  $F_c^{pot(A)}$  closely approximates  $F_c^{sub} \equiv F_c^{trad} - 4T \ln(T/\mu)$ . Table 5 shows that no single set of  $I^{(neg)}$  parameters  $\{a, b, c\}$  does consistently better than Method A. With scales restored,  $E_c = \mathcal{O}(\sigma^2/\mu)$ ,  $\Delta F_{1+T}^{sub} = \mathcal{O}(T^2/\mu)$ , and “derivative corrections” are

$$\Delta F_{1+T}^{sub} - \Delta F_{1+T}^{pot(A)} = \mathcal{O}(T). \quad (6.5.1)$$

This difference is numerically fairly small, and very poorly predicted by the derivative expansion [Eq. (6.1.16)]. In summary,

$$\frac{\Gamma}{\mathcal{V}} = X \frac{\mu^4}{2\pi} \left( \frac{E_c}{2\pi T} \right)^{3/2} \frac{|\omega_-|/2T}{\sin(|\omega_-|/2T)} e^{-F_c^{pot(A)}/T}, \quad (6.5.2)$$

where  $X$  is a dimensionless number representing derivative corrections, typically  $10^{-2}$  to  $10^2$ .

In 1D, where  $\Delta F_{1+T}^{sub}$  is only  $\mathcal{O}(T)$ , derivative corrections [still  $\mathcal{O}(T)$ , and numerically larger] are much more significant than in 3D.

## APPENDIX A: Calculation of Loop Momentum Integrals in HQEFT

The calculation of the loop momentum integrals arising from the Green functions is complicated by the unusual heavy quark propagators of the form  $\frac{i}{v \cdot q}$  given by Eq. (2.3.1) which have the dimensions of inverse mass. This causes the evaluation of certain Feynman graphs to become quite involved. The generic method developed to evaluate such loop integrals will now be outlined.

- (a) Combine the various denominator factors, arising from propagators, of the loop integral into one expression using the usual Feynman parametrization

$$\frac{1}{A^a B^b} = \frac{\Gamma(a+b)}{\Gamma(a)\Gamma(b)} \int_0^1 \frac{\alpha^{a-1}(1-\alpha)^{b-1}}{[A\alpha+B(1-\alpha)]^{a+b}} d\alpha,$$

or the identity

$$\frac{1}{a^\ell b^n} = \frac{\Gamma(\ell+n)}{\Gamma(\ell)\Gamma(n)} \int_0^\infty \frac{\lambda^{n-1} d\lambda}{(a+b\lambda)^{\ell+n}},$$

where  $\lambda$  is a parameter with the dimensions of mass.

- (b) Regularize the ultraviolet divergences using dimensional regularization and then integrate over the internal loop momenta using dimensional regularization formulae.
- (c) Integrate over the dimensional  $\lambda$  parameters using the formula

$$\int_0^\infty \frac{\lambda^a d\lambda}{(\lambda^2 + c\lambda)^b} = \frac{\Gamma(a+1-b)\Gamma(-a-1+2b)}{\Gamma(b)} c^{a+1-2b}.$$

- (d) Finally integrate over the usual dimensionless Feynman-type parameters.

## Appendix B: One-loop Renormalization of the Scalar Field Theory

This Appendix discusses the one-loop and renormalization of the scalar field theory described by Eq. (5.1.1). The classical vacuum  $\phi_v$  satisfies

$$V'(\phi_v) = 0 \text{ and } \mu^2 = V''(\phi_v) > 0. \quad (B.1)$$

At one-loop the only divergent graphs are those with one and two vertices corresponding to quadratic and logarithmic divergences, respectively.

It is convenient to adopt a renormalization scheme where the counterterms are chosen to exactly cancel the divergent graphs as shown in Figs. 13 and 14. These conditions are imposed at zero external momenta; this choice has the advantage that the one-loop contribution to the effective potential  $V_1$  satisfies

$$V_1(\phi_v) = V_1'(\phi_v) = V_1''(\phi_v) = 0, \quad (B.2)$$

so that Eq. (B.1) is unchanged at one-loop. Then the counterterm Lagrangian to be added to Eq. (5.1.1) is

$$\mathcal{L}_{ct} = \alpha [V''(\phi) - \mu^2] + \frac{1}{2}\beta [V''(\phi) - \mu^2]^2, \quad (B.3)$$

where

$$\alpha = \frac{1}{2} \int \frac{i}{k^2 - \mu^2 + i\epsilon} \frac{d^4k}{(2\pi)^4},$$

and

$$\beta = \frac{1}{2} \int \frac{i}{(k^2 - \mu^2 + i\epsilon)^2} \frac{d^4k}{(2\pi)^4}.$$

The terms in Eq. (B.3) involving  $\alpha$  and  $\beta$  renormalize the graphs with one and two external vertices, respectively. These divergent integrals can be suitably regularized by imposing a momentum cut-off  $\Lambda$ .

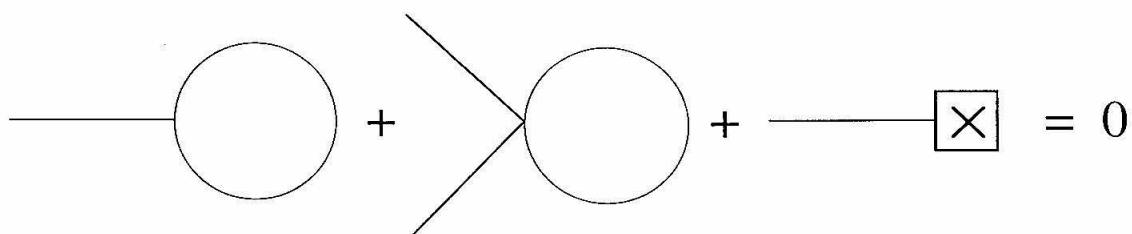


Fig. 13: Renormalization scheme for the divergent one-loop graphs with one vertex.

A box with a cross denotes a counterterm insertion.

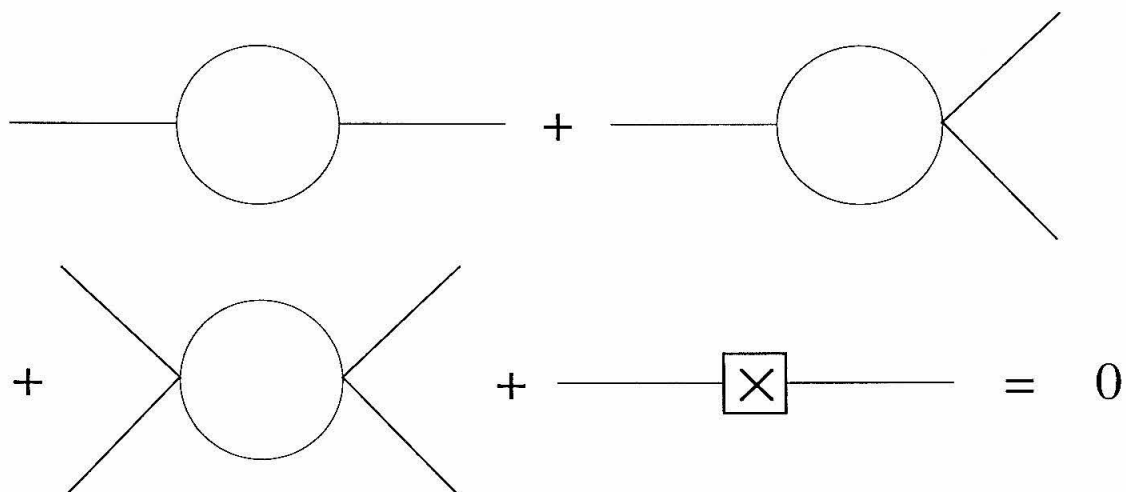


Fig. 14: Renormalization scheme for the divergent graphs at one-loop order with two vertices.

## REFERENCES

1. N. Isgur and M.B. Wise, *Phys. Lett.* **B232** (1989) 113;  
N. Isgur and M.B. Wise, *Phys. Lett.* **B237** (1990) 527.
2. H. Georgi, *Phys. Lett.* **B240**(1990) 447.
3. S. Coleman and J. Mandula, *Phys. Rev.* **159**(1967) 1251.
4. C.L.Y. Lee, unpublished.
5. T. Mannel, W. Roberts, and Z. Ryzak, *Nucl. Phys.* **B368** (1992) 204.
6. M.B. Wise, Heavy Flavor Theory: Overview, Talk given at the 1993 Lepton-Photon Conference, CALT-68-1901.
7. M.E. Luke, *Phys. Lett.* **B252**(1990) 447.
8. N. Isgur and M.B. Wise, *Nucl. Phys.* **B348**(1991) 276;  
H. Georgi, *ibid.*B348(1991)293.
9. L.F. Abbott, *Nucl. Phys.* **B185**(1981)189.
10. A. F. Falk, B. Grinstein, and M. E. Luke, *Nucl. Phys.* **B357** (1991) 185.
11. E. Eichten and B. Hill, *Phys. Lett.* **B234**(1990) 511.
12. G.P. Lepage and B.A. Thacker, *Nucl. Phys.* **B4** (Proc. Supp.)(1988) 199.
13. J.M. Flynn and B.R. Hill, FERMILAB-PUB-91/82-T (1991).
14. Particle Data Group, *Phys. Lett.* **B247**(1990) 1.
15. D. S. Akerib *et al.*, *Phys. Rev. Lett.* **67** (1991) 1692.
16. E. Eichten, *Nucl. Phys.* **B20** (Proc. Supp.) (1991) 475.
17. M.B. Wise, *Phys. Rev. D* **45**(1992) R2188.
18. G. Burdman and J.F. Donoghue, *Phys. Lett.* **B280**(1992) 287.
19. T.-M. Yan, H.-Y. Cheng, C.-Y. Cheung, G.-L. Lin, Y.C. Lin, and H.-L. Yu, *Phys. Rev. D* **46**(1992) 1148.
20. ACCMOR Collaboration, S. Barlag *et al.*, *Phys. Lett.* **B278**(1992) 480.
21. H. Georgi, *Weak Interactions and Modern Particle Theory*,  
Benjamin/Cummings Publishing Co., Inc., Menlo Park, CA (1984);  
A. Manohar and H. Georgi, *Nucl. Phys.* **B234**, (1984) 189.
22. G.L. Kane, K. Stowe, and W.B. Rolnick, *Nucl. Phys.* **B152**, (1979) 390.
23. N. Cabibbo and A. Maksymowicz, *Phys. Rev.* **137** (1965) B438; A. Pais and  
S.B. Treiman, *ibid.* **168**(1968) 1858.
24. M.B. Voloshin and M.A. Shifman, *Sov. J. Nucl. Phys.* **45**, (1987) 292.

24. M.B. Voloshin and M.A. Shifman, *Sov. J. Nucl. Phys.* **45**, (1987) 292.
25. H.D. Politzer and M.B. Wise, *Phys. Lett.* **B208** (1988) 504.
26. S. Nussinov and W. Wetzel, *Phys. Rev.* **D36**, (1987) 130.
27. M.B. Voloshin and M.A. Shifman, *Sov. J. Nucl. Phys.* **47**, 199 (1988).
28. A. Ali and T.C. Yang, *Phys. Lett.* **65B**, 275 (1976); S.C. Chao, G. Kramer, W.F. Palmer and S. Pinsky, *Phys. Rev.* **D30**, 1916 (1984); S.C. Chao, R. Kass, G. Kramer, W.F. Palmer and S. Pinsky, *Phys. Rev.* **D31**, 1756 (1985); J. Cline, W.F. Palmer and G. Kramer, *Phys. Rev.* **D40**, 793 (1989).
29. S. Stone, talk presented at the Heavy Quark Symmetry Conference, Santa Barbara, CA., Feb. (1992).
30. N. Isgur and M.B. Wise, *Phys. Rev. Lett.* **66**, 1130 (1991); M. Lu, M.B. Wise and N. Isgur, *Phys. Rev.* **D45**, 1553 (1992).
31. S. Sharpe, *Nucl. Phys.* **B17** (Proc. Suppl.) 146 (1990); C. Bernard, C. Heard, J. Labrenz and A. Soni, Proceedings of Lattice 91, Tsukuba Japan (1991); A. Abada, C.R. Allton, Ph. Boucaud, D.B. Carpenter, M. Crisafulli, J. Galand, S. Gusken, G. Martinelli, O. Pène, C.T. Sachrajda, R. Sarno, K. Schilling and R. Sommer, *Nucl. Phys.* **B376**, 172 (1992).
32. M. Neubert, *Phys. Rev.* **D45** 2451, (1992).
33. B. Grinstein and P.F. Mende, SSCL-64 (1992).
34. C.L.Y. Lee, *Phys. Rev.* **D48** (1993) 2121.
35. A. Falk, B. Grinstein, H. Georgi and M.B. Wise, *Nucl. Phys.* **B343**, 1 (1990).
36. A. Falk and B. Grinstein, *Phys. Lett.* **B247**, 406 (1990); *Phys. Lett.* **B249**, 314 (1990); G.P. Korchemsky and A.V. Radyushkin, *Nucl. Phys.* **B283**, 342 (1987); X. Ji and M.J. Musolf, *Phys. Lett.* **B257**, 409 (1991).
37. For a compilation of the  $\alpha_s(m_c)$  and  $\alpha_s(m_b)$  corrections to the weak currents see: M. Neubert, *Phys. Rev.* **D46**, 2212 (1991).
38. This decay has also been considered by H.-Y. Cheng, C.-Y. Cheung, W. Dimm, G.-L. Lin, Y.C. Lin, T.-M. Yan, and H.-L. Yu, CNLS-93-1204.
39. R. F. Dashen, B. Hasslacher & A. Neveu, *Phys. Rev.* **D10**:4130 (1974).
40. D. A. Wasson, Ph.D. thesis, California Institute of Technology, 1990.
41. M. Li & R. J. Perry, *Phys. Rev.* **D37**:1670 (1988).
42. J. Baacke, *Z. Phys.* **C47**:263 (1990).

43. J. Baacke & V. G. Kiselev, *Phys. Rev.* **D48**, 5648 (1993).
44. See for example, L.-H. Chan, *Phys. Rev. Lett.* **54**:1222 (1985); *Phys. Rev. Lett.* **56**:404(E) (1986).
45. D. E. Brahm & C. L. Y. Lee, *Phys. Rev.* **D49**, 4094 (1994).
46. J. I. Kapusta, *Finite-temperature field theory*, Cambridge University Press, 1989.
47. A detailed discussion can be found in R. Rajaraman, *Solitons and Instantons*, North-Holland Press, Amsterdam, 1982.
48. For a survey, see *Phase Transitions and Critical Phenomena*, (Academic Press, London, 1983), Vol. 8, edited by C. Dom & J. L. Lebowitz.
49. C. L. Y. Lee, CALT-68-1925.
50. Errors that arise when particles are naively integrated out are discussed (at  $T = 0$ ) by E. Weinberg, *Phys. Rev.* **D47**:4614 (1993).
51. S. Coleman, *Phys. Rev.* **D15**:2929 (1977), **16**:1248(E) (1977);  
C.G. Callan & S. Coleman, *Phys. Rev.* **D16**:1762 (1977);  
S. Coleman, "The Uses of Instantons," *Proc. 1977 Int. School of Subnuclear Physics, Ettore Majorana*, ed. A. Zichichi (Plenum, New York, 1979); reprinted in *Aspects of Symmetry* (Cambridge University Press, 1985).
52. I. Affleck, *Phys. Rev. Lett.* **46**:388 (1981).
53. J.W. Cahn & J.E. Hilliard, *J. Chem. Phys.* **31**:688 (1959);  
J.S. Langer, *Ann. Phys.* **41**:108 (1967); *ibid.* **54**:258 (1969);  
M.B. Voloshin, I.Y. Kobzarev & L.B. Okun', *Yad. Fiz.* **20**:1229 (1974) [*Sov. J. Nucl. Phys.* **20**:644 (1975)];  
P.H. Frampton, *Phys. Rev.* **D15**:2922 (1977);  
A.D. Linde, *Phys. Lett.* **70B**:306 (1977); *ibid.* **100B**:37 (1981); *Nucl. Phys.* **B216**:421 (1983); *ibid.* **B223**:544 (1983)(E);  
O.J.P. Éboli & G.C. Marques, *Rev. Bras. Fis.* **16**:147 (1986).
54. M. Gleiser, G.C. Marques & R.O. Ramos, *Phys. Rev.* **D48**:1571 (1993).
55. L. Dolan & R. Jackiw, *Phys. Rev.* **D9**:3320 (1974).
56. H. Haber & H.A. Weldon, *J. Math. Phys.* **23**, 1852 (1982).
57. C.L.Y. Lee, *Phys. Rev.* **D49**, 4101 (1993).
58. C.G. Boyd *et al.*, *Phys. Rev.* **D48**:4952 (1993).
59. L.-H. Chan, *Phys. Rev. Lett.* **54**:1222 (1985); *Phys. Rev. Lett.* **56**:404(E) (1986).

60. I. Moss, D. Toms & A. Wright, *Phys. Rev.* **D46**:1671 (1992).
61. M. Dine *et al.*, *Phys. Rev.* **D46**:550 (1992); *ibid.*, *Phys. Lett.* **283B**:319 (1992).
62. T.-P. Cheng & L.-F. Li, *Gauge Theory of Elementary Particle Physics* (Oxford U. Press, 1984), eq. (6.133).
63. Andrei Linde, private communication.
64. S. Dodelson & B. Gradwohl, *Nucl. Phys.* **B400**:435 (1993).
65. R. F. Dashen, B. Hasslacher & A. Neveu, *Phys. Rev.* **D10**:4114 (1974); *ibid.* **D10**:4130 (1974).
66. See ref. [47], secs. 5.3–5.4.
67. I. Ventura, *Phys. Rev.* **B24**:2812 (1981);  
C. Aragão de Carvalho *et al.*, *Phys. Rev.* **D31**:1411 (1985);  
C. Aragão de Carvalho *et al.*, *Nucl. Phys.* **B265**:45 (1986);  
D. Bazeia *et al.*, *Z. Phys.* **C46**:457 (1990).